MRI-GUIDED NON-INVASIVE EPICARDIAL MAPPING IN PATIENTS WITH IMPLANTED PACING DEVICES

MAURITS VAN DER GRAAF

MRI-GUIDED NON-INVASIVE EPICARDIAL MAPPING IN PATIENTS WITH **IMPLANTED PACING DEVICES**

MAURITS VAN DER GRAAF

An electronic version of this thesis is accessible at:
http://www.publicatie-online.nl/publicaties/m-vd-graaf

Cover design and layout:	Design Your Thesis (www.designyourthesis.com)
Printing:	Ridderprint (www.ridderprint.nl)
ISBN:	978-94-6299-726-4

MRI-GUIDED NON-INVASIVE EPICARDIAL MAPPING IN PATIENTS WITH IMPLANTED PACING DEVICES

MRI GESTUURD NIET-INVASIEF LOKALISEREN VAN ELEKTRISCHE STIMULI IN PATIËNTEN MET EEN PACEMAKER

PROEFSCHRIFT

ter verkrijging van de graad van doctor aan de
Erasmus Universiteit Rotterdam
op gezag van de
rector magnificus
Prof.dr. H.A.P. Pols
en volgens besluit van het College voor Promoties.
De openbare verdediging zal plaatsvinden op
donderdag 9 november 2017 om 09:30 uur

door

Abraham Willem Maurits van der Graaf
geboren te Voorburg

Promotor:	Prof.dr. F. Zijlstra
Overige leden:	Prof.dr. A.C. van Rossum Prof.dr. H.J.G.M. Crijns Dr. R.P.J. Budde
Copromotoren:	Dr. M.J.W. Götte Dr. N.M.S. de Groot

Financial support by the Dutch Heart Foundation for the publication of this thesis is gratefully acknowledged.

CONTENTS

01

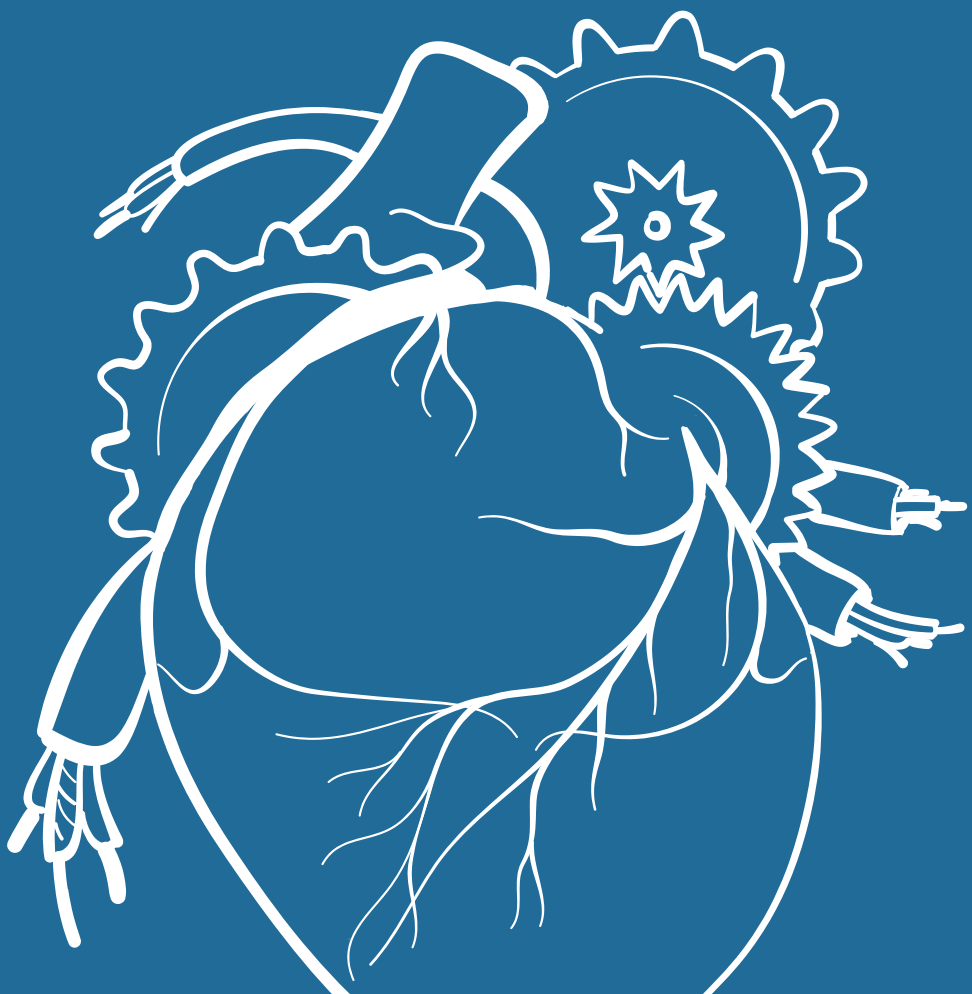

GENERAL INTRODUCTION

NON-INVASIVE IMAGING

Non-invasive imaging of the heart has become the cornerstone of modern day cardiology. Non-invasive imaging of the heart can relate to the 12-lead electrocardiogram (ECG) that provides rapid information about the electrical processes in the heart, or to transthoracic echocardiography (TTE), magnetic resonance imaging (MRI) or computed tomography (CT), to evaluate the mechanical function of the heart. Research described in this thesis focusses on the development of a novel *non-invasive* imaging method through which electrical processes in the heart and thorax can be analysed.

BODY SURFACE POTENTIALS

The cardiac cells contract after stimulation by automatically generated electrical impulses. Potentials resulting from these electrical impulses can be recorded from the body surface. In 1887, a British physician named Augustus D. Waller published the first recording of human body potentials after numerous experiments on his dog Jimmy [1]. Later, the Dutch physician and physiologist Willem Einthoven developed a standardised 12-lead ECG method that is indispensable for the evaluation of cardiac status in clinical practice to this day [2].

When more detailed information about the electrical processes in the heart is desired, an invasive electrophysiological study (EPS) can be performed. During an EPS, several recording catheters are inserted into the heart through veins or arteries. In this way, local depolarisation or repolarisation processes can be recorded and analysed in order to identify an arrhythmogenic substrate for ablation. An EPS is associated with exposure to radiation and risks of bleeding or stroke.

For years, clinicians and researchers have sought a non-invasive electrophysiological alternative that would provide more detailed information than the standard 12-lead ECG and would be applicable in routine daily clinical practice. Recording multiple potentials on the body surface using more than 12-leads, i.e. Body Surface Potential Mapping (BSPM), was explored by several research groups [3-5]. The resulting potential maps could be used to indicate regions of ischemia [6] or sources of arrhythmia [7], but the application of the individual torso electrodes (up to 252 in number) and processing of the data was very cumbersome and time consuming.

Subsequently, researchers discovered that potentials recorded on the body surface could be related to the potentials on the surface of the heart using a mathematical equation termed the Laplace equation [8]. This equation describes the relationship

between potentials on two surfaces separated by regions that are electrically neutral. Patient-specific anatomy, in order to visualise the exact position of the two surfaces (body surface and cardiac surface) was obtained using CT. Rudy et al. performed numerous experiments and published several papers on the clinical application of this technique [9-12]. Using an electrode vest to record the body surface potentials, this technique is now commercially available and has been used in various hospitals throughout the world. Despite the favourable reports, the fact that CT (exposing the patient to radiation) was used to obtain anatomical information and doubts regarding the validity of assuming the region between the body surface and the cardiac surface is electrically neutral, prompted researchers to investigate alternative methods.

DEVELOPING A NOVEL MRI-BASED NON-INVASIVE MAPPING METHODOLOGY

The research in this thesis focusses on the development and application of a novel non-invasive mapping approach. Since this approach is based on anatomical information obtained using MRI, it is not associated with exposure to radiation. MRI offers the advantage of obtaining detailed anatomical and functional information. In this way, the anatomy of a patient and the position of every electrode on the body surface could be observed on the MRI images. Regional differences in cardiac wall motion could be assessed thoroughly. Unlike CT, MRI can characterise local differences in the myocardium. Hence, the location and size of inflamed, infarcted or hypertrophic cardiac muscle as a arrhythmogenic substrate can be distinguished from normal cardiac tissue [13]. These features make MRI a very potent tool to guide clinical interventions.

The first step in the development of a novel non-invasive mapping methodology was the design of a software program that would allow analyses of both the MRI images and the potentials recorded from the body surface. Besides processing recorded human data, computer simulations could be carried out with the software. In this way, various experiments could be performed before the technique was tested in real humans (in-vivo). Numerous body surface electrode layouts were tested using the simulation software in order to find an optimal electrode configuration. After deciding on a definitive electrode layout, the technique was applied in volunteers and later in patients to record potentials from the body surface.

Using the software, personalised three dimensional (3D) models of the torso and the inner organs could be reconstructed from MRI images for every patient. Later, data obtained through body surface potential mapping was used to calculate the distribution of potentials inside the torso and on the surface of the heart. Eventually, the results of this calculation could be visualised in the 3D model of the heart and torso.

Instead of using the Boundary Element Method (BEM), used by most research group to calculate epicardial potentials from the recorded body surface potentials, the Finite Element Method (FEM) was applied. Unlike the BEM, the FEM enables the incorporation of volume information [14]. Using the FEM, experiments could be performed to investigate the impact of including or excluding electrical information from different thoracic organs between the body surface and the cardiac surface.

In order to investigate the localisation accuracy of the novel mapping technique, it was applied in patients with an implanted MRI-conditional cardiovascular implantable electronic device (CIED). In this patient category, the pacing site is fixed and can therefore serve as a reference point. The location of the tip of the pacing lead could be identified on the MRI images. In this way, the site of earliest activation as identified by the non-invasive mapping system could be correlated to the location of the tip of the pacing lead. Hence, a single MRI investigation provided information about the anatomy of the patient, the position of the recording body surface electrodes, the mechanical function and tissue characterics of the heart and the location of the pacemaker lead tip. In patients suffering from premature ventricular contractions scheduled for ablation, the site of earliest activation as identified by the non-invasive mapping system was compared to the site of ablation.

AIMS

The aims of this thesis are to 1) investigate the safety of using MRI in patients with implanted pacing devices, 2) develop software through which the electrical activity inside the heart and thorax can be realistically modelled, 3) perform simulation studies to investigate the impact on the end-result of using different torso electrode layouts for the recording of body surface potentials, 4) investigate the validity of the simulation studies by performing non-invasive mapping in volunteers using different torso electrode layouts, 5) apply the novel non-invasive mapping technique in patients with an implanted pacing devices and in patients suffering from premature ventricular contractions and 6) investigate the localisation accuracy and reproducibility of the results in these patients.

OUTLINE OF THIS THESIS

At the time the research described in this thesis was initiated, MRI-conditional CIEDs were only recently introduced. For this reason, the first part of this thesis discusses the possibility and safety of using MRI in patients with a CIED.

Chapter 2 focusses on the feasibility and potential hazards of performing MRI in patients with a CIED. A safety protocol was developed and proposed in order to minimise the chance of adverse events. **Chapter 3** evaluates the use of MRI in patients after implantation of an MRI-conditional CIED, both pacemakers and internal cardioverter defibrillators (ICDs). Since implantation of MRI-conditional devices is not available for all patients, patient selection prior to implantation is a relevant topic. Ideally, MRI-conditional CIEDs would be implanted in patients with the highest chance of requiring an MRI during the lifetime of their device. **Chapter 4** illustrates that MRI can be used in patients with an MRI-conditional CIED to evaluate regional wall motion. Normally, global cardiac function is monitored using TTE in this patient category. However, global function measures are insensitive to early regional dysfunction. Therefore, it may be of advantage to evaluate local myocardial strain in these patients.

The second part of this thesis discusses the current status of non-invasive imaging of cardiac electrophysiology. **Chapter 5** provides an overview from the time of the first ECG recordings to the use of inverse procedures to non-invasively reconstruct (intra-) cardiac processes from potentials recorded on the thoracic surface. **Chapter 6** describes the first experiments using the in-house developed software. The advantage of using the Finite Element Method instead of the Boundary Element Method is illustrated by experiments performed in a plastic tank model filled with water. **Chapter 7** explores the possibility and the impact of including information on myocardial scar or oedema.

The third part of this thesis describes the application of the novel mapping technique in volunteers and patients. Computer simulations using various torso electrode layouts are described in **Chapter 8**. After deciding on a definitive electrode layout, it was applied in volunteers and later in patients to record potentials from the body surface. The localisation accuracy of the novel mapping technique is investigated in **Chapter 9**. The site of earliest activation as identified by the non-invasive mapping system was correlated to the actual location of the tip of the pacing lead on the MRI-images. In **Chapter 10**, the non-invasive mapping system was used to localise premature ventricular contractions in patients scheduled for ablation. The location of the identified

focus was subsequently compared to the ablation site on the electroanatomic maps. Finally, **Chapter 11** discusses the most important findings of this thesis, places these into the context of current knowledge and suggests directions of further research.

REFERENCES

1. Waller AD. A demonstration on man of electromotive changes accompanying the heart's beat. J Physiol. (Lond) 1887;8:227-34.
2. Einthoven W. Die galvanometrische Registerung des menschlichen Elektrokardiogram: Zugleich eine Beurtheilung der Anwendung des Capillar-Elektrometers in der Physiologie. Pflügers Arch ges Physiol. 1903;99:472-480.
3. Barr RC, Spach MS, Herman-Giddens S. Selection of the number and position of measuring locations for electrocardiography. IEEE Trans Biomed Eng. 1971;18(2);125-38.
4. Lux RL, Burgess MJ, Wyatt RF, et al. Clinically practical lead systems for improved electrocardiography: comparison with precordial grids and conventional lead systems. Circulation. 1979;59(2):256-63.
5. Donnelly MP, Finlay DD, Nugent CD, et al. Lead selection: old and new methods for locating the most electrocardiogram information. J Electrocardiol. 2008;41(3):257-63.
6. Kornreich F, Montague TJ, Rautaharju PM, et al. Identification of best electrocardiographic leads for diagnosing anterior and inferior myocardial infarction by statistical analysis of body surface potential maps. Am J Cardiol. 1986;58(10):863-71.
7. Peeters HA, SippensGroenewegen A, Wever EF, et al. Clinical application of an integrated 3-phase mapping technique for localisation of the site of origin of idiopathic ventricular tachycardia. Circulation. 1999;16;99(10):1300-11.
8. Gulrajani RM. The forward and inverse problems of electrocardiography. IEEE Eng Med Biol Mag. 1998;17(5):84-101.
9. Rudy Y. Noninvasive electrocardiographic imaging of arrhythmogenic substrates in humans. Circ Res. 2013;112(5):863-74.
10. Oster HS, Taccardi B, Lux RL, et al. Electrocardiographic imaging: Noninvasive characterisation of intramural myocardial activation from inverse-reconstructed epicardial potentials and electrograms. Circulation. 1998;21;97(15):1496-507.
11. Varma N, Jia P, Rudy Y. Electrocardiographic imaging of patients with heart failure with left bundle branch block and response to cardiac resynchronisation therapy. J Electrocardiol. 2007;40(6 Suppl):S174-8.
12. Zhang J, Cooper DH, Desouza KA, et al. Electrophysiologic Scar Substrate in Relation to VT: Noninvasive High-resolution Mapping and Risk Assessment with ECGI. Pacing Clin Electrophysiol. 2016;39(8):781-91.
13. Goenka AH, Flamm SD. Cardiac magnetic resonance imaging for the investigation of cardiovascular disorders. Part 1: current applications. Tex Heart Inst J. 2014;41(1):7-20.
14. Hunter P. FEM/BEM notes. CMISS Auckland Bioengineering Institute and Engineering Science, The University of Auckland, New Zealand. October 8, 2008:1-140.

PART 1
MRI & IMPLANTED PACING DEVICES

02

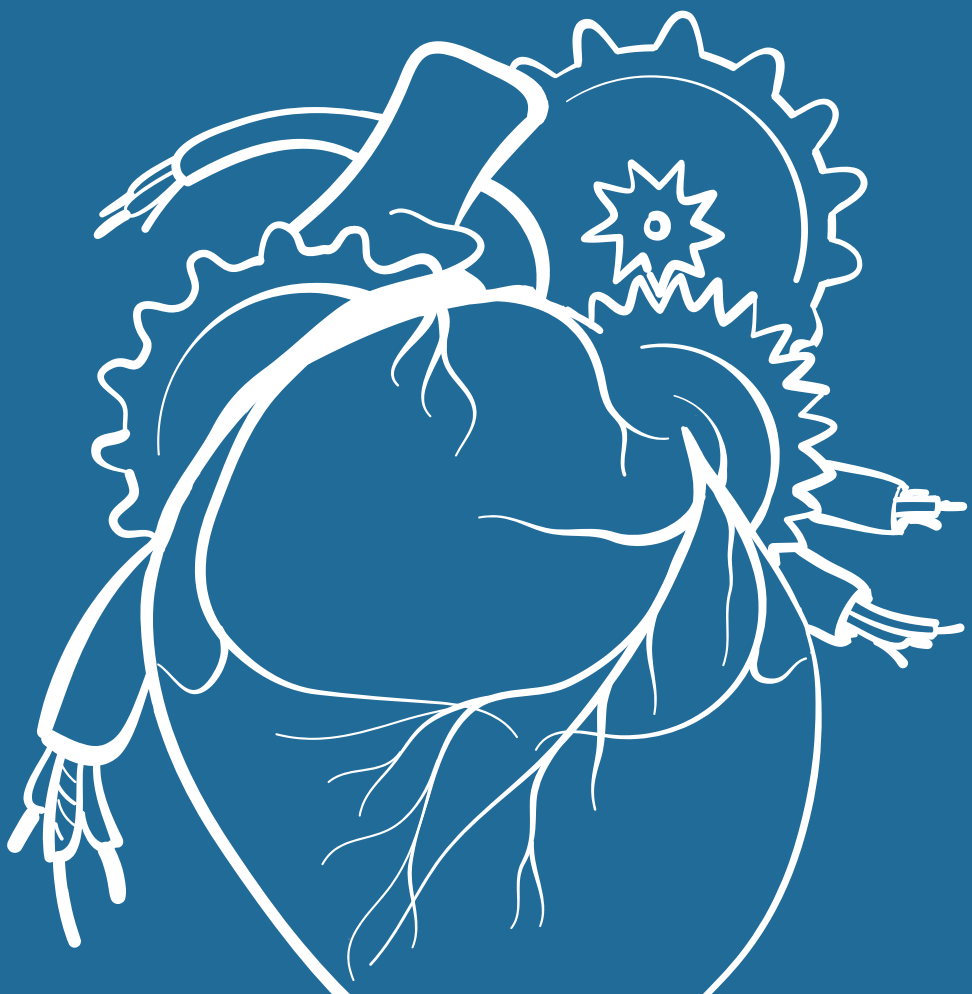

MRI AND CARDIAC IMPLANTABLE ELECTRONIC DEVICES; CURRENT STATUS AND REQUIRED SAFETY CONDITIONS

van der Graaf AW, Bhagirath P, Götte MJ.
Netherlands Heart Journal. 2014; 22(6);269-76.

ABSTRACT

Magnetic resonance imaging (MRI) has evolved into an essential diagnostic modality for the evaluation of all patient categories. This gain in popularity coincided with an increase in the number of implanted cardiac implantable electronic devices (CIEDs). Therefore, questions arose with regard to the MRI compatibility of these devices. Various investigators have reported the harmless performance of MRI in patients with conventional (non-MRI-conditional) devices. The recently published European Society of Cardiology (ESC) guidelines on cardiac pacing and cardiac resynchronisation therapy (CRT) indicate that MRI can be safely performed in patients with an implanted pacemaker or ICD (MRI-conditional or not), as long as strict safety conditions are met. This is a major modification of the former general opinion that patients with a pacemaker or ICD were not eligible to undergo MRI. This review paper attempts to elucidate the current situation for practising cardiologists by providing a clear overview of the potential life-threatening interactions and discuss safety measures to be taken prior to and during scanning. An overview of all available MRI-conditional devices and their individual restrictions is given. In addition, an up-to-date safety protocol is provided that can be used to ensure patient safety before, during and after the scan.

INTRODUCTION

Historically, magnetic resonance imaging (MRI) examination of patients with a cardiac implantable electronic device (CIED) has been considered hazardous due to potential life-threatening interaction between the MRI scanner and the pacemaker or internal cardioverter defibrillator (ICD) [1-2]. To increase patient safety and to anticipate the growing clinical need for MRI, an increasing number of MRI-conditional CIEDs have become available [3].

However, the recently published European Society of Cardiology (ESC) guidelines on cardiac pacing and cardiac resynchronisation therapy (CRT) [4] state that MRI can be safely performed in patients with an implanted pacemaker or ICD, irrespective of the MRI-conditional or non-specific MRI-conditional design, as long as strict safety conditions are met.

In order to clarify this somewhat confusing situation, this review paper provides an overview of the currently available data related to CIEDs and MRI, and attempts to offer an up-to-date and clinically useful summary for the practising cardiologist. In addition, a safety protocol applicable for patients with a CIED is provided that can be used to ensure a patient's safety before, during and after an MRI scan.

MRI SYSTEM

Technical background

The fundamental components of an MRI system are the main magnet coils, three gradient coils and an integral radiofrequency transmitter coil. The main magnet coils generate a strong, constant magnetic field. The strength of this magnetic field is expressed in Tesla.

Mounted inside the main magnet, three gradient coils generate gradient magnetic fields that are rapidly switched on and off. The integral radiofrequency transmitter coil produces a radiofrequency magnetic field, used to deliver energy to a population of protons. The static magnetic field and radiofrequency field combine to generate magnetic resonance signals that are spatially localised and encoded by the gradient magnetic fields [5].

Receiving coils capture the energy released by resonating hydrogen protons. Subsequent analysis results in high-grade tissue characterisation and reconstruction of a detailed image.

The amount of energy administered to an individual is expressed in SAR (specific absorption rate). SAR values vary from 2.0 to 4.0 W per kilogram (W/kg). For reference purposes, SAR values of a modern mobile telephone are approximately 0.9 W/kg [6].

Over time, the strength of the static magnetic field of MRI systems has increased from less than 0.5 T to clinical scanners operating at 7.0 T and even 9.4 T. Today, the vast majority of clinical MRI exams are performed using a 1.5 T system, while a rapid growth of 3.0 T systems is observed [7]. Since the SAR is proportional to the square of the static magnetic field strength, the amount of energy absorbed by a patient increases rapidly in a scanner operating at a higher field strength. Therefore, application of higher field strengths poses constraints on the total scan time or the imaging sequences used.

INTERACTION BETWEEN MRI SYSTEM AND CIEDS

Pavlicek et al. [8] were the first (1983) to discuss the potential interaction between pacing devices and the NMR (at that time nuclear magnetic resonance) environment using ex-vivo pacemakers of deceased patients. These interactions can be subdivided into three categories.

a. Mechanical forces

The constant static magnetic field strongly attracts different types of metal. Implantable devices usually contain a small amount of one or more of these metals and are considered to be ferromagnetic. Therefore, there is the possibility of movement of the implanted pacemaker.

A 6-week interval between implantation and MRI examination is advised in international guidelines in order to ensure sufficient encapsulation of the device [9].

b. Induction (antenna function)

The several electromagnetic components used in MRI may cause electrical or thermal induction in implanted leads. Inducted electrical currents could initiate arrhythmias or lead to oversensing or undersensing of the pacemaker or ICD with potentially fatal consequences. In addition, since tissue near the lead tip has limited conductivity, energy will be converted to heat at this location. Subsequent thermal damage around the lead tip includes oedema or formation of scar tissue. In both situations, an increase in pacing thresholds or even complete loss of capture may occur [10].

c. Defibrillators

The magnetic fields inside the MRI may have an unpredictable intermittent effect on the activity of the reed switch in a pacemaker or ICD. This may lead to either asynchronous pacing (reed switch closed) or unwanted inhibition of pacing in the presence of an open reed switch. In addition, the rapidly changing magnetic gradients can be registered as a life-threatening arrhythmia. The ICD can subsequently react with release of anti-tachycardia pacing (ATP) or shock [11]. In the presence of the main static magnetic field, the core of the transformer, necessary to charge the high-energy storage capacitor, tends to saturate. Thereby, the storage capacitor is prevented from charging. Although this reduces the risk for the deliverance of inappropriate shocks during the scan, the battery will lose life.

d. Software interaction

Exposure to the electromagnetic fields may also directly affect or modify the electronic circuits and functional settings of the CIED. Use of external programmers may become impossible due to damaged electrical circuits inside the CIED.

e. Implantable loop recorders (ILR)

Several studies have indicated that MRI scanning of ILR patients can be performed without harm to patient or device. However, signal artifacts that can be mistaken for a tachyarrhythmia are seen frequently [12-13]. Of course, image artifacts arising from the presence of an IPL can degrade the image quality.

REVIEW OF LITERATURE

Non-conditional pacemakers and ICDs

In 1984, Fetter et al. [14] investigated the potential interactions using four pacemakers in vivo. The asynchronous (VOO) pacing mode was activated during the scan in one patient. The authors concluded that patients with single-chamber implantable pacemakers may undergo scanning with MRI, provided the patient is monitored during scanning and the risks of asynchronous pacing are taken into account.

Gimbel et al. (1996) performed an MRI scan with a field strength of 0.5 T in five patients [15]. A 2-s pause was observed in one pacemaker-dependent patient. The other patients were asymptomatic and did not report any discomfort. Fontaine et al.

(1998) demonstrated the development of an irregular ventricular rhythm in a 69-year-old patient during RF pulsing on a 1.5 T scanner [16]. This rhythm terminated with the cessation of RF pulsing. The patient remained asymptomatic during the procedure.

In 2000, Sommer and co-workers examined 44 non-pacemaker-dependent patients 51 times in a 0.5 T MRI without any impairment of pacing function [17]. Vahlhaus (2001) and co-workers postulate in a paper that 'the general policy of never exposing a patient with a pacemaker to MRI should be revised' [18].

Bartsch et al. (2003) reported four MRI-associated deaths in paced patients undergoing MRI (1.5 T) assessment [19]. Importantly, none of these patients were pacemaker dependent and in some cases ventricular fibrillation was proven to be the cause of death.

In 2005, Irnich et al. questioned 30 legal medicine departments in Germany with respect to casualties with a fatal outcome of pacemaker patients during an MRI examination (0.5–1.5 T) between 1992 and 2001 [20]. Six fatal cases occurred, in three cases ventricular fibrillation (VF) was proven to be the cause of death. In the other three cases the pacemakers were removed from the deceased patient's body and introduced in the MRI scanner. The pacemaker showed a magnetic asynchronous rate of 100/min. It was suspected that the asynchronous pacing had induced VF in these patients.

In the following years, several investigators collected and published data on MRI examinations in patients with conventional (non-MRI-conditional) pacemakers and ICDs. Naehle et al. (2009) reported the safe scanning of 18 ICD patients at 1.5 T [21]. No significant change in pacing capture threshold, lead impedance or serum troponin I was observed. In two MRI examinations, oversensing of radiofrequency noise as ventricular fibrillation occurred. However, no attempt at therapy delivery was made.

More recently, Nazarian et al. (2011) published the most elaborate study [22]. A total of 555 MRI scans (1.5 T) were performed in 438 patients with a CIED (54 % pacemakers, 46 % defibrillators). Of the 555 MRI examinations, 222 (40 %) were of the brain, 122 (22 %) were of the spine, 89 (16 %) were of the heart, 72 (13 %) were of the abdomen or pelvis, and 50 (9 %) were of an extremity. Only small changes in programming, sensing and impedance were reported. The observed changes did not ever require device revision. Unfortunately, no data are available on the possible effects of repeated MRI examinations in individual patients. However, it must be noted that although a large

number of different models were studied, the numbers for each individual model were small. Patients were enrolled during a long period of time (from 2003 to 2010) and CIEDs were constantly evolving. Last but not least, a control group was lacking in this study.

Despite these limitations, it is only this paper that is exclusively referred to in the recently published ESC guidelines on cardiac pacing and CRT. MRI-conditional CIEDs were developed in order to decrease potential life-threatening hardware interactions.

MRI-conditional pacemakers and ICDs

These systems contain specially developed components, tested and approved for usage in an MRI environment. Improved lead design reduces the risk of complications, such as lead-tip heating. In addition to the modified hardware design, MRI-conditional pacemaker systems are provided with a special MRI software mode. Upon activation, the most appropriate settings are switched on automatically. These settings include bipolar stimulation instead of unipolar pacing and an increased electrical output. Specific filters inside the device prevent sensing of external non-cardiac signals. Furthermore, recording of arrhythmic episodes is temporarily disabled during the scan.

It must be noted that due to constant technological improvements the size of the available implantable pulse generators has substantially decreased and leads have become more sophisticated. Together with a reduction of ferromagnetic components in contemporary CIEDs, the chance of hardware interactions is therefore substantially diminished.

Medtronic commercialised the first MRI-conditional pacemaker system (Enrhythm MRI®) in 2008. Several trials reported the safe performance of MRI scans in patients with an implanted Enrhythm MRI system [23-24]. However, scanning of the thorax region was prohibited. Different manufacturers initiated comparable clinical trials to demonstrate the safety of their own MRI-conditional devices. Currently, several MRI-conditional pacemakers are commercially available that enable full body MRI examination. **Table 1** provides a complete overview of currently available MRI-conditional pacemakers and ICDs.

Table 1. Currently available MRI-conditional pacemakers and ICDs.

	Medtronic		St Jude Medical	Biotronik		Boston
	Enrhythm MRI / Revo MRI	**Advisa MRI**	**Accent MRI**	**Evia ProMRI**	**Lumax ProMRI / Iforia ProMRI / Ilesto ProMRI**	**Ingenio MRI**
Restrictions	Full body	Full body	Full body	No chest scans		Full body
MRI machine	Cylindrical bore magnet, clinical MRI systems with a static magnetic field of 1.5 T					
SAR limitation (whole-body)	≤ 2.0 W/kg	≤ 2.0 W/kg	≤ 4.0 W/kg	≤ 2.0 W/Kg		≤ 2.0 W/Kg
Maxixum number of scans	No	No	No	Yes: each scan ≤ 30 min Total scan time max: 10 hours		No
Published Clinical Trial evidence on MRI enviroment	Yes	Yes	No	No		No

Current clinical trials

An overview of clinical trials currently enrolling patients is given in **table 2**. Apart from demonstrating the safety of a device in an MRI environment, contemporary studies are more focused on the influence on image quality and artifacts caused by the CIED (**Figure 1**).

Table 2. An overview of currently enrolled clinical trials on MRI-conditional pacing devices.

	Medtronic	St Jude Medical	Biotronik	Boston
Study	Advisa II	Accent	ProMRI AFFIRM	Samurai
Number of participating sites	40	80	21	45
Estimated number of patients	270	800	245	363
Implantable Pulse Generator - Lead	Advisa - 5076	Accent - Tendril	Evia/Entovis - Safio S	Image Ready System
Estimated date of completion	October 2014	July 2014	December 2013	July 2014

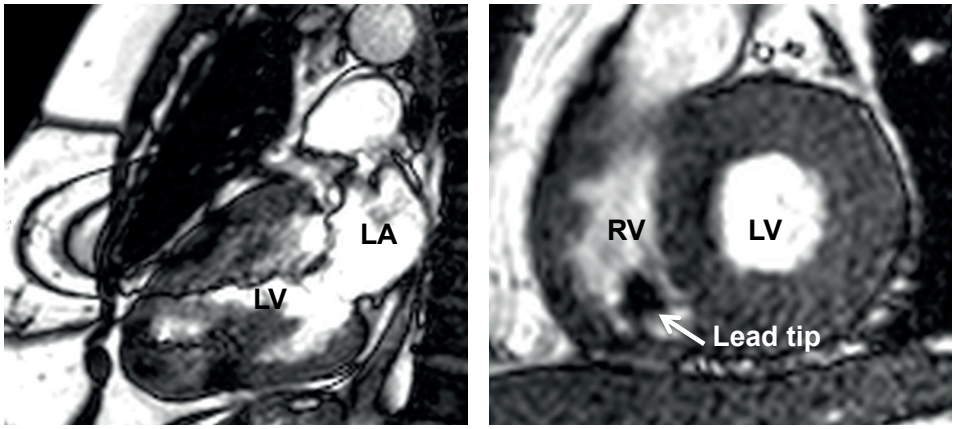

A B

Figure 1. Steady State Free Precession CINE images. Typical artifacts as can be observed in patients with an implanted impulse generator (**A**) and pacing leads (**B**). Note that the image quality in the short axis cine (**B)** is sufficient to allow reliable calculation of left ventricular ejection fraction.

Biventricular (CRT) devices

The presence of three leads in patients treated with biventricular (CRT) therapy increases the risk of interactions between MRI and the pacing system. Only a small and inconsistent amount of literature on MRI examinations in CRT patients is available at this time. The scanning of patients with an implanted biventricular pacing device is strongly discouraged.

RISK ASSESSMENT

Pacemaker dependent patients

Patients with an implanted pacemaker or ICD and an absent or insufficient intrinsic heart rhythm constitute a special group, because potential interaction between pacemaker and MRI can have life-threatening consequences. It must be ascertained that the potential benefit of an MRI examination outweighs the potential risks and no diagnostic alternative is available. Close monitoring of the patient using pulse oximetry is warranted.

MRI-conditional markers and MRI mode

Vendor-specific markers on CIEDs can facilitate the identification of MRI-conditional systems on routine chest X-rays (**Figure 2**). Certain CIEDs contain an optional MRI mode, which automatically activates the most appropriate settings. After the scan, the original settings can be reprogrammed easily. Other (non-conditional) CIEDs mandate a manual selection of some of these settings and reprogramming.

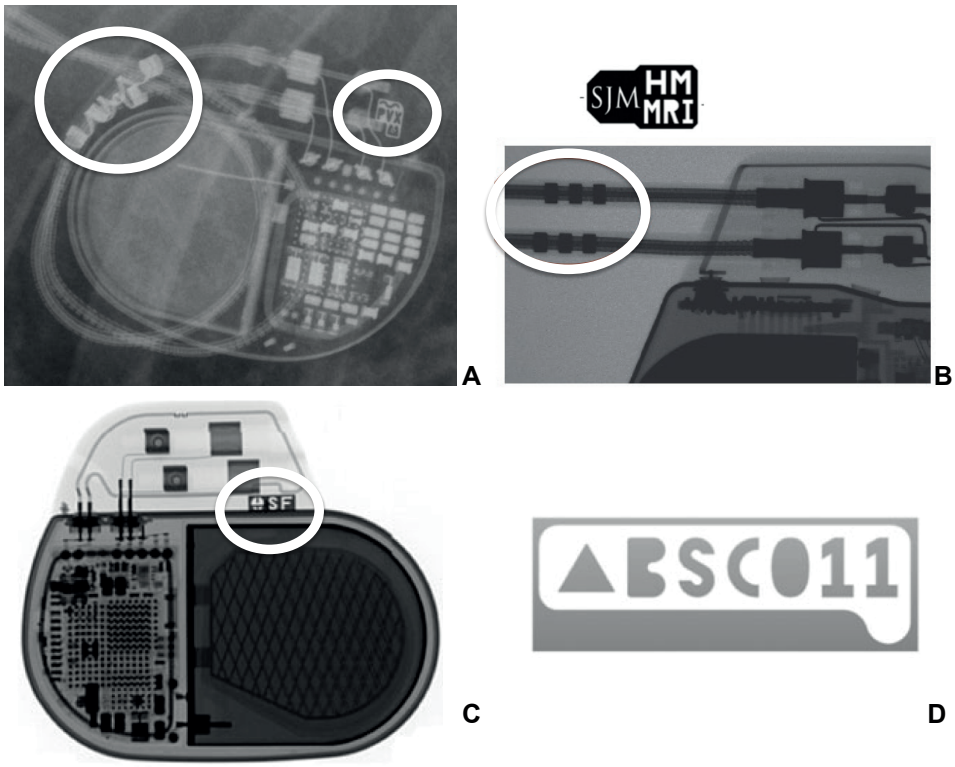

Figure 2. Vendor specific markers on MRI-conditional pacing systems as can be identified on routine X-rays. **A:** Medtronic, **B:** St. Jude Medical, **C:** Biotronik, **D:** Boston Scientific.

Various combinations of implantable pulse generators and leads

A more complex situation occurs when implantable pulse generators and leads from different vendors, each bearing their own MRI restrictions, are combined together in individual patients. In this case the MRI compatibility of all parts of the CIED needs to be ascertained. An individualised approach is mandatory in these patients. When

abandoned pacing leads are present, for example after recent coronary bypass grafting (CABG), scanning is strongly discouraged. The absence of an implantable pulse generator increases the chance of current induction in the leads of these patients.

PREPARATION AND MONITORING DURING MRI EXAMINATION

An MRI examination of a patient with a CIED is preferably performed exclusively in centers with extensive experience and expertise in this area. Written informed consent should be obtained from the patient after extensive notification of the procedural risks. Application of a safety protocol (Appendix 1) and appropriate monitoring are mandatory to perform an MRI scan in patients with a CIED.

Prior to the examination, proper functioning of the CIED needs to be assured. The pacing threshold is one of the most important issues and should always be determined. An already elevated stimulation threshold (>2.0 V) increases the risk of loss of capture during the examination. Pacemaker output should be increased and the examination should be suspended in case of a severely elevated threshold and/or deviated lead impedance <200 ohms or >1,500 ohms.

During the examination careful monitoring of the patient using a heart rate monitor and pulse oximetry is warranted. The recorded ECG signal in the scanner is subject to disturbances and therefore unreliable. Pulse oximetry is not affected by the MRI scanner and should always be used to monitor the patient. Cardiopulmonary resuscitation equipment including a cardiac defibrillator, along with staff experienced in resuscitation, should be available on site.

The nature of the cardiac MRI examination, especially in pacemaker patients, mandates routine verbal communication between operator and patient during the scan and is of vital importance. During and after the MRI examination, the patient should be asked about any discomfort or complaints. When the MRI examination is finished, the original settings of the CIED should be restored after confirming that these are still safe and provide adequate margins. In order to exclude any late side effects or symptoms, a control visit (3–6 months after the scan) to the outpatient department may be recommended [25].

DISCUSSION

The recently published ESC guidelines on cardiac pacing and CRT somewhat trivialised the absolute necessity of MRI-conditional CIEDs by stating that MRI can be safely performed in patients with an implanted pacemaker or ICD (MRI-conditional or not), as long as strict safety conditions are met.

Despite abundant literature [26–31] reporting the harmless performance of MRI investigations in patients with conventional (non-MRI-conditional) pacemakers and ICDs, it is still considered potentially hazardous. Only a limited number of prospective studies are available. Long-term studies are confounded by the use of several generations of CIEDs. The variety of tested devices in these studies affects the conclusions and decreases the clinical value.

Therefore, it remains difficult to state whether a specific conventional CIED can be introduced into the MRI room without possible consequences. For MRI-conditional CIEDs, the possibilities, limitations and required safety measures to be taken are more uniform and described in detail.

In daily practice, an increasing number of clinicians are confronted with questions on MRI compatibility of CIEDs. The value of a safety protocol, approved by the cardiology and radiology department, cannot be stressed enough.

It is expected that the role of MRI in clinical decision-making will gain even more clinical importance. There is an emerging role for MRI in identifying arrhythmogenic substrates and this modality has an expanding role in guiding electrophysiological therapies.

Now that the patient's safety seems to be conditionally guaranteed, a new challenge is the reduction of the impact of CIEDs on the image quality, especially with regard to the identification and modification of an arrhythmogenic substrate.

Finally, it is important to realise that almost all published data are only valid for scanning on 1.5 Tesla machines. The application of 3.0 Tesla machines is rapidly emerging, especially for orthopaedic and neurological patients, due to the higher signal-to-noise ratio (SNR). With the advance of 3.0 T machines, new technical challenges arise.

CONCLUSION

MRI-conditional CIEDs are designed to cope with the challenges introduced by the electromagnetic MRI environment. Various papers have demonstrated the safe and harmless performance of MRI examination in patients with CIEDs, MRI-conditional or not. With appropriate monitoring and application of a safety protocol, MRI can be safely performed in patients with CIEDs. For patients equipped with a conventional CIED or those who are pacing dependent it must be ascertained that the potential benefits of an MRI examination outweigh the potential risks.

REFERENCES

1. Kalin R, Stanton MS. Current clinical issues for MRI scanning of pacemaker and defibrillator patients. Pacing Clin Electrophysiol. 2005;28:326 –328.
2. Langman DA, Goldberg IB, Finn JP, Ennis DB. Pacemaker lead tip heating in abandoned and pacemaker-attached leads at 1.5 Tesla MRI. J Magn Reson Imaging. 2011;33:426–431.
3. Ahmed FZ, Morris GM, Allen S, Khattar R, Mamas M, Zaidi A. Not all pacemakers are created equal: MRI-conditional pacemaker and lead technology. J Cardiovasc Electrophysiol. 2013;24(9):1059-65.
4. Brignole M, Auricchio A, Baron-Esquivias G, et al. 2013 ESC guidelines on cardiac pacing and cardiac resynchronisation therapy: the task force on cardiac pacing and resynchronisation therapy of the European Society of Cardiology (ESC). Developed in collaboration with the European Heart Rhythm Association (EHRA). Europace 2013;15(8):1070-118.
5. Ridgway JP. Cardiovascular magnetic resonance physics for clinicians: part 1; J Cardiovasc Magn Reson. 2010;12:71.
6. Götte MJW, Rüssel IK, de Roest GJ, et al. Magnetic resonance imaging, pacemakers and implantable cardioverter-defibrillators: current situation and clinical perspective. Neth Heart J. 2010;18:31-7.
7. van der Wall EE. Crown years for non-invasive cardiovascular imaging (Part III): 30 years cardiovascular magnetic resonance. Neth Heart J. 2013;21(6):263-5.
8. Pavlicek W, Geisinger M, Castle L, et al. The effects of nuclear magnetic resonance on patients with cardiac pacemakers. Radiology 1983;147(1):149-53.
9. Luechinger R, Duru F, Scheidegger MB, Boesiger P, Candinas R. Force and torque effects of a 1.5 Tesla MRI scanner on cardiac pacemakers and ICD's. Pacing Clin Electrophysiol. 2001;24:199-205.
10. Luechinger R, Zeijlemaker VA, Pederson EM, et al. In vivo heating of pacemaker leads during magnetic resonance imaging. Eur Heart J. 2004;26:376-83.
11. Ainslie M, Miller C, Brown B, et al. Cardiac MRI of patients with implanted electrical cardiac devices. Heart 2014;100(5):363-9.
12. Gimbel JR, Zarghami J, Machado C, Wilkoff BL. Safe scanning, but frequent artifacts mimicking bradycardia and tachycardia during magnetic resonance imaging (MRI) in patients with an implantable loop recorder (ILR). Ann Noninvasive Electrocardiol. 2005;10(4):404-8.
13. Wong JA, Yee R, Gula LJ, Skanes AC, Ross IG, White JB, Klein GJ, Krahn AD. Feasibility of magnetic resonance imaging in patients with an implantable loop recorder. Pacing Clin Electrophysiol. 2008 Mar;31(3):333-7.
14. Fetter J, Aram G, Holmes DR, Gray JE, Hayes DL. The effects of nuclear magnetic resonance imagers on external and implantable pulse generators. Pacing Clin Electrophysiol. 1984;7:720e7.

15. Gimbel JR, Johnson D, Levine PA, Wilkoff BL. Safe performance of magnetic resonance imaging on five patients with permanent cardiac pacemakers. Pacing Clin Electrophysiol. 1996;19(6):913-9.

16. Fontaine JM, Mohamed FB, Gottlieb Ch, Callans DJ, Marchlinski FE. Rapid ventricular pacing in a pacemaker patient undergoing magnetic resonance imaging. Pacing Clin Electrophysiol. 1998;21:1336e9.

17. Sommer T, Vahlhaus C, Lauck G, et al. MRI and cardiac pacemakers: in-vitro evaluation and in vivo studies in 51 patients at 0.5T. Radiology 2000;215:869-79.

18. Vahlhaus Ch, Sommer T, Lewalter T, et al. Interference with cardiac pacemakers by magnetic resonance imaging: are there irreversible changes at 0.5 T? Pacing Clin Electrophysiol. 2001;24:489e95.

19. Bartsch C, Irnich W, Risse M, Weiler G. Unexpected sudden death of pacemaker patients during or shortly after magnetic resonance imaging [MRI]. In: XIX Congress of International Academy of Legal Medicine. Milan, Italy, 3–6 September 2003. 174, Abstract no. 114.

20. Irnich W, Irnich B, Bartsch C, Stertmann WA, Gufler H, Weiler G. Do we need pacemakers resistant to magnetic resonance imaging? Europace 2005;7(4):353-65.

21. Naehle CP, Strach K, Thomas D, et al. Magnetic resonance imaging at 1.5-T in patients with implantable cardioverter-defibrillators. J Am Coll Cardiol. 2009;4;54(6):549-55.

22. Nazarian S, Hansford R, Roguin A, et al. A Prospective Evaluation of a Protocol for Magnetic Resonance Imaging of Patients With Implanted Cardiac Devices. Ann Intern Med 2011;155:415-24.

23. Sutton R, Kanal E, Wilkoff BL, et al. Safety of magnetic resonance imaging of patients with a new Medtronic EnRhythm MRI SureScan pacing system: clinical study design. Trials. 2008;2;9:68.

24. Wilkoff BL, Bello D, Taborsky M, et al. Magnetic resonance imaging in patients with a pacemaker system designed for the magnetic resonance environment. Heart Rhythm 2011;8(1):65-73.

25. Nazarian S, Beinart R, Halperin HR. Magnetic resonance imaging and implantable devices. Circ Arrhythm Electrophysiol. 2013;6(2):419-28.

26. Cronin EM, Mahon N, Wilkoff BL. MRI in patients with cardiac implantable electronic devices. Expert Rev Med Devices 2012;9(2):139-46.

27. Cohen JD, Costa HS, Russo RJ. Determining the risks of magnetic resonance imaging at 1.5 tesla for patients with pacemakers and implantable cardioverter defibrillators. Am J Cardiol. 2012;110:1631–1636.

28. Boilson BA, Wokhlu A, Acker NG, et al. Safety of magnetic resonance imaging in patients with permanent pacemakers: a collaborative clinical approach. J Interv Card Electrophysiol. 2012;33:59–67.

29. Coman JA, Martin ET, Sandler DA, Thomas JR. Implantable cardiac defibrillator interactions with magnetic resonance imaging at 1.5 tesla. J Am Coll Cardiol. 2004;43:138A–138A.

30. Gimbel JR, Kanal E, Schwartz KM, Wilkoff BL. Outcome of magnetic resonance imaging (MRI) in selected patients with implantable cardioverter defibrillators (ICDs). Pacing Clin Electrophysiol. 2005;28:270–273.

31. Coman JA, Martin ET, Ramza BM, Margolis PD, Fair RD. Pacemaker safety during magnetic resonance imaging at 1.5 Tesla. J Am Coll Cardiol. 2001;37(Suppl. A):436.

APPENDIX 1.

CIED - MRI checklist

Patient ID: Date:	Device: Manufacturer:…… Type:…… Date of implant:……

Pre – MRI

CIED technician (name): ……

Only proceed when all conditions are met:

- Implant > 6 weeks? ☐
- MRI conditional device? ☐
- X-ray post implant available? ☐
- No abandoned (epicardial) leads? ☐

(√ when OK)

Measurements	Atrial	Ventricular
Pacing threshold < 2.0 V?	V @ ms	V @ ms
Lead impedance 200-1500 ohm	ohm	ohm
P/R wave amplitude in normal range?	mV	mV
Battery voltage?		V

- Activate MRI safe mode and print proof
- Is the patient pacing dependent? (consult cardiologist, if not sure)
  a. **Yes → VOO/DOO**
  b. **No → OVO/ODO**

CIED tech: *81 3471
MRI: tst 4915

- ICD: check whether tachycardia detection and therapies are deactivated

MRI - scan

MRI technician (name): ……

- No contraindications for MRI? ☐
- Resuscitation equipment available on site? ☐

(√ when OK)

- **During the scan: monitor ECG, pulse oximetry and symptoms** **SAR < 2.0 W.kg**

Post - MRI

CIED technician (name): ……

- Compare pre & post values:

Measurements	Atrial	Ventricular
Pacing threshold	V @ ms	V @ ms
Lead impedance	ohm	ohm
P/R wave amplitude	mV	mV
Battery voltage		V

- Deactivate MRI safe mode and restore original programming

Abnormalities
Yes ☐ **No** ☐

Visit after …… week(s)

HagaZiekenhuis + Hartcentrum

CIED_MRI protocol_v5_feb2015

03

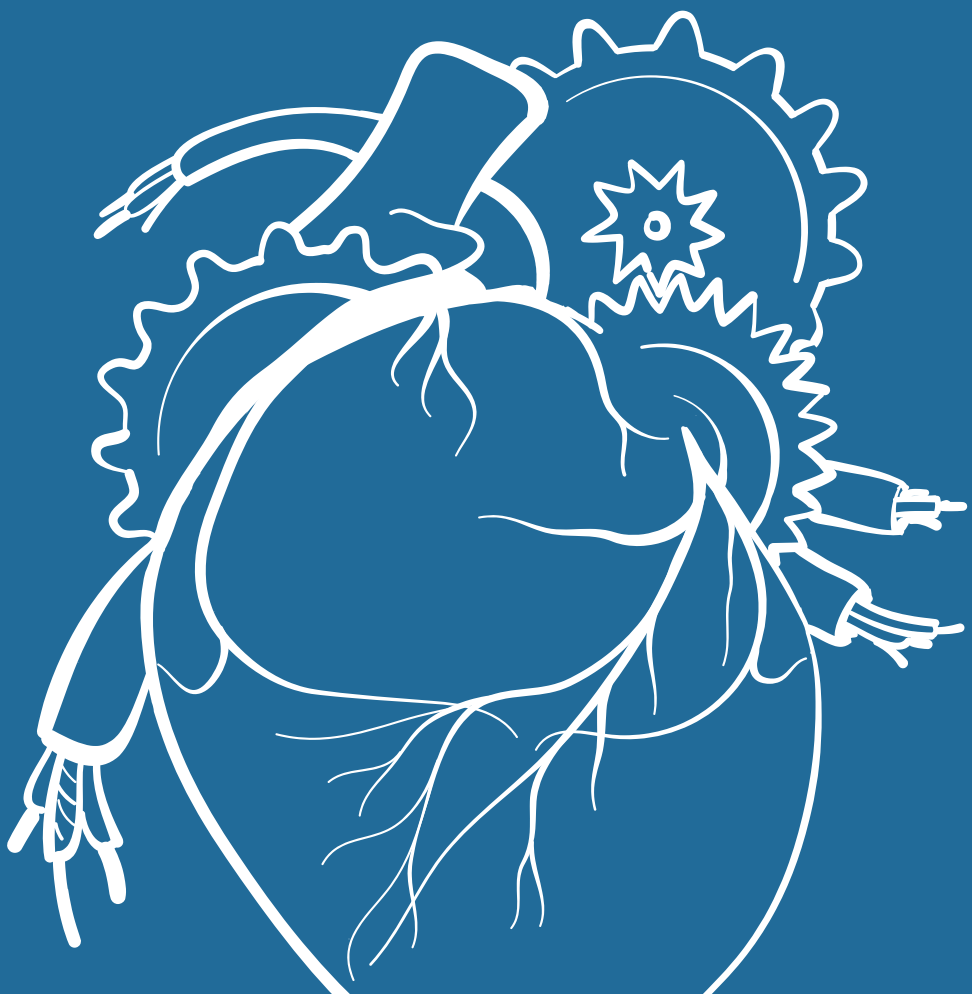

CLINICAL USE OF MRI IN PATIENTS WITH MRI-CONDITIONAL PACEMAKER SYSTEMS

van der Graaf AW, Bhagirath P, Götte MJ.
Submitted

ABSTRACT

Purpose: This study investigated the use and safety of Magnetic Resonance Imaging (MRI) for several pathologies in patients with an implanted MRI-conditional pacing system.

Methods: This was a retrospective, single center study. All patients with an MRI-conditional pacemaker or Internal Cardioverter Defibrillator (ICD) implanted in our center between June 2011 and March 2015 were enrolled. All MRI examinations performed in these patients were evaluated. For all patients, pacing thresholds, P- and R-wave amplitude, lead impedance and battery longevity were monitored during the entire follow-up.

Results: In total, 214 patients with an implanted MRI-conditional device (mean age 65 ± 14; 64% male; 138 pacemakers; 76 ICDs) were enrolled. At the time of implant, 94% of these patients suffered from a co-morbidity that may lead to a future indication for MRI. In 24 patients (11%), 36 MRI investigations were safely performed during a mean follow-up period of 406 days (51-1353 days).

Conclusion: The majority of the post-implant MRI scans (57%) were performed to confirm, exclude or follow-up on neurological disease. Further research is needed to facilitate the identification of patients with a high likelihood of requiring MRI investigations following implantation of a pacing device.

INTRODUCTION

Through recent years, Magnetic Resonance Imaging (MRI) has evolved into an important diagnostic modality for the evaluation of a wide variety of diseases. This increase in utilisation of MRI coincided with an increase in the number of implanted Cardiac Implantable Electronic Devices (CIEDs) [1]. To improve patient safety and to anticipate the growing clinical need for MRI, MRI-conditional CIEDs have been developed [2].

Currently, implantation of an MRI-conditional system is not (yet) the standard of care for all patients. Therefore, identification of suitable patients is mandatory. Based on earlier research, various patient characteristics indicating a higher probability of requiring an MRI examination during the lifespan of the device can be determined, including; age (above 65 years old); prior MRI examinations in life; desired follow-up on hereditary or congenital diseases [3-4]. The objective of this retrospective study was to evaluate whether these characteristics are indeed associated with a higher use of MRI in patients with an implanted CIED.

Therefore, the general clinical use of MRI in patients with an implanted MRI-conditional CIED was investigated. In addition, device parameters measured directly after MRI and during the follow-up period were compared to the device parameters of patients in whom no MRI was performed.

METHODS

Patient population

This was a retrospective, single center study. The study complies with the Declaration of Helsinki. The local medical ethical committee and the hospital scientific board approved this study. Only patients with an MRI-conditional pacemaker or ICD system implanted in our center were evaluated. Devices were implanted between June 2011 and December 2014.

MRI examinations

Only routine clinical MRI examinations were evaluated. Research scans were excluded from this study. MRI studies were performed between August 2011 and February 2015 on either a 1.5 Tesla Philips Intera system (Philips Healthcare, Best, The Netherlands) or a 1.5 Tesla Siemens Aera system (Siemens, Erlangen, Germany).

MRI scans were performed according to a standardised safety protocol [5]. The MRI compatibility of the devices was confirmed through patient records and chest radiography. Before entering the MRI room, pacing thresholds, P- and R-wave amplitude and lead impedances were determined and the CIED was programmed into the device manufacturer MRI compatible setting with an appropriate pacing mode; DOO/VOO for pacemaker dependent patients and VVI/DDI for non-pacemaker dependent patients [6-7]. During the MRI examination, patients were monitored using pulse-oximetry and verbal communication. In addition, when a cardiac MRI scan was performed, the ECG signal was also used for monitoring purposes.

After the examination, pacing thresholds, P- and R-wave amplitude and lead impedances were measured and compared to the initial values. Finally, original programming of the CIED was restored.

Statistical analysis

Statistical analysis was performed using IBM SPSS Statistics for Windows (version 20.0, Chicago, USA). Continuous variables were expressed as mean ± standard deviation (SD). Pacing thresholds, sensing amplitude, lead impedance and battery life were compared using a paired Student's t-test. All tests were two-tailed and a p-value <0.05 was considered significant.

RESULTS

Device implants

A complete overview of the patients enrolled in this study is provided in **figure 1**.

A total of 253 patients (mean age 66 ± 14; 64% male) with an implanted MRI-conditional impulse generator (165 pacemakers; 88 ICDs) were identified.

In 39 patients (mean age 75 ± 12, 62% male), an MRI-conditional impulse generator (27 pacemakers; 12 ICDs) was connected to previously implanted conventional leads (i.e. non-MRI-conditional). In these patients, the complete pacing system (impulse generator and leads) could not be classified as MRI-conditional. The remaining 214 patients (mean age 65 ± 14; 64% male; 138 pacemakers; 76 ICDs) were further analysed in this study.

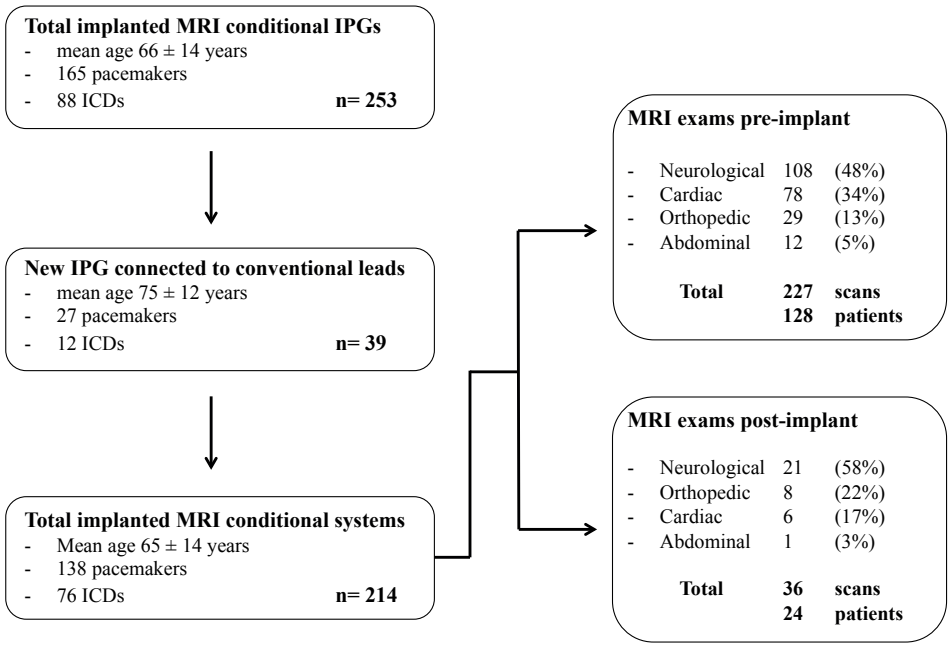

Figure 1. A complete overview of the patients enrolled in this study and the MRI exams performed prior to and after implantation of the device. Thirty-nine patients were excluded from the analysis, because an MRI-conditional impulse generator was connected to conventional (i.e. non-MRI-conditional) leads.

In the patients with an implanted pacemaker (n=138), the most common indication for pacing was complete heart block (54%). In the ICD group (n=76), primary prevention (61%) was the main reason for implantation. Baseline characteristics of the study population and the implanted devices are summarised in **table 1**.

MRI examinations

In 128 (60%) of the 214 patients with a complete MRI-conditional pacing system, 227 MRI examinations were performed prior to implantation. The majority of these scans (48%) was performed to confirm or rule out a neurological disorder. The complete distribution of scans per referring department is shown in **figure 1**.

The mean follow-up period for patients in this study was 406 ± 302 days (51-1353 days). The number of implants of conditional devices is shown in **figure 2**.

Table 1. Patient and device characteristics.

Patient characteristics	**N = 214**
Age (years)	65 ± 14
Male (% male)	138 (64%)
Indication for device	
- Pacemaker (n= 138)	
2nd degree / complete heart block	75
Sinus node dysfunction	48
Atrial fibrillation and bradycardia	15
- ICD (n= 76)	
Primary prevention	46
Secondary prevention	30
Relevant co-morbidity	**N = 202 (156 pts)**
Hemochromatosis	2
Sarcoid	1
Heart / vessel disease	43
CVA / TIA	28
Neurologic disorder	80
Orthopaedic	15
Urologic	17
Gastro-enteric	16
Device characteristics	
- Pacemaker (n= 138)	
Medtronic Advisa MRI / Evia	72
St Jude Accent MRI	45
Boston Ingenio MRI	21
- ICD (n= 76)	
Medtronic Evera ICD MRI	44
Biotronik Lumax ICD MRI	14
Biotronik Ilesto ICD MRI	18
- Leads	
Medtronic Capsure 5086/5076/6935	228
St Jude Tendril	84
Boston Fineline / Flextend	36
Biotronik Solia / Linox / Corox	67

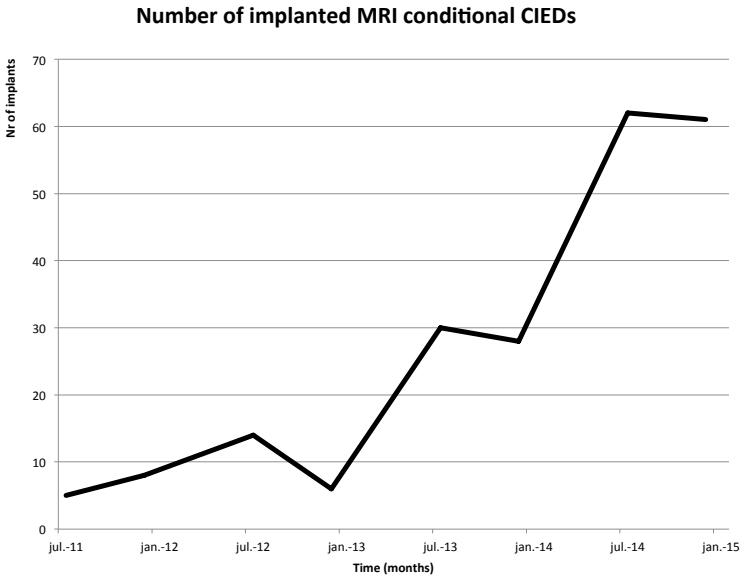

Figure 2. Increase in number of MRI-conditional pacing devices implanted through recent years.

In 24 (mean age 62 ± 12 years old) of the 214 patients who received a complete MRI-conditional pacing system, 36 MRI examinations were performed during follow-up. The mean time between CIED implantation and MRI was 222 ± 160 days (range: 50-572 days). The indication for the MRI scan was directly related to the pre-existent comorbidity in 19 of the 24 patients (76%) as can be observed in **table 2**.

Table 2. MRI examination and relation to co-morbidity.

Co-morbidity	**Nr of patients**	**Type of MRI examination(s)**
Hemochromatosis	1	Heart, Liver
Previous neurological disease/tumor	12	Cerebrum, Spine, Leg, Hip
Previous trauma	3	Spine, Knee, Ankle
Congenital heart defect	3	Heart, Aorta
Not related to co-morbidity	**Nr of patients**	**Type of MRI examination(s)**
Indication for MRI scan		
Myocarditis, follow-up on function	3	Heart
Diplopia, headache	2	Cerebrum

Safety

There were no significant changes in lead impedance or sensing threshold between the pre- and immediate post-procedural measurements. There was also no evidence of battery voltage depletion following MRI (**table 3**).

MRI studies were safely performed in all cases. There was no electrical pacemaker reset or any unexpected changes in heart rate or heart rhythm during the MRI scan. No patients reported pain or heating over the device site or symptoms that may indicate arrhythmia such as dizziness or palpitations. **Figure 3** shows typical artifacts that can be observed when performing cardiac MRI in patients with an implanted CIED.

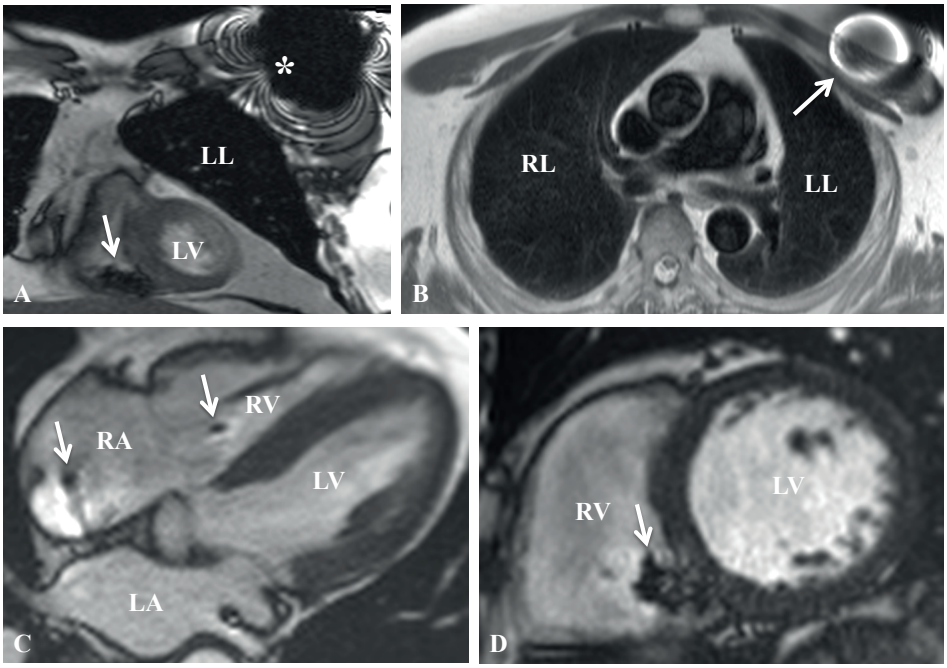

Figure 3. Typical artifacts that may be observed when performing cardiac MRI in patients with an implanted CIED. **A:** coronal T1 weighted sequence with artifact induced by the presence of the RV lead (white arrow) and artifact induced by the impulse generator in the pectoral region (asterisk). **B:** axial T1 weighted image with an artifact near in the area of the impulse generator. **C:** four/five chamber view with artifacts induced by the pacing leads in the right atrial and right ventricular. **D:** short axis image from a steady state free precession sequence with an artifact caused by the RV lead.

Device parameters during follow-up

Pacing thresholds, P- and R-wave amplitude and lead impedances were documented during long-term follow-up for all patients (**table 4**). There were no significant differences in device parameters between patients in whom an MRI examination was performed during follow up and those in whom no MRI was performed.

Table 3. Device parameters directly before and after MRI examination.

	Pre-MRI	Post-MRI	p-value
P-wave amplitude (mV)	2.9 ± 18	2.9 ± 1.8	0.71
Atrial lead impedance (Ohm)	476.1 ± 78.9	474.7 ± 92.7	0.36
Pacing threshold (V@0.4ms)	0.66 ± 0.2	0.7 ± 0.2	0.49
R-wave amplitude	13.5 ± 5.2	14.2 ± 5.2	0.55
Ventricular lead impedance	533.2 ± 96.6	536.4 ± 84.8	0.06
Pacing threshold	0.7 ± 0.2	0.7 ± 0.2	0.68
Battery life (months)	120.7 ± 19.9	113.6 ± 20.6	0.54

Table 4. Device parameters during follow-up.

	Clinical MRI scan(s) during follow-up (n=24 patients; 36 MRI exams)			
	Implant	3 months	12 months	18 months
P-wave amplitude (mV)	3.2 ± 1.6	3.1 ± 1.3	3.0 ± 1.4	2.8 ± 1.3
Atrial lead impedance (Ohm)	770.4 ± 204.8	500.1 ± 137.6	506.0 ± 127.2	537.2 ± 282.7
Pacing threshold (V@0.4ms)	0.9 ± 0.4	0.7 ± 0.3	0.6 ± 0.2	0.7 ± 0.3
R-wave amplitude	13.4 ± 5.5	13.0 ± 5.3	13.5 ± 5.5	13.2 ± 5.5
Ventricular lead impedance	904.0 ± 305.9	545.9 ± 93.6	545.8 ± 87.1	540.1 ± 78.3
Pacing threshold	0.8 ± 0.4	0.7 ± 0.2	0.7 ± 0.2	0.7 ± 0.3
Battery life (months)		103.5 ± 32.0	102.9 ± 27.2	95.5 ± 23.0
	No clinical MRI scan during follow-up (n=190 patients)			
	Implant	3 months	12 months	18 months
P-wave amplitude (mV)	3.2 ± 1.9	2.9 ± 18	2.9 ± 1.8	3.1 ± 1.9
Atrial lead impedance (Ohm)	645.7 ± 186.9	476.1 ± 78.9	474.7 ± 92.7	481.9 ± 83.5
Pacing threshold (V@0.4ms)	1.06 ± 0.6	0.66 ± 0.2	0.7 ± 0.2	0.7 ± 0.2
R-wave amplitude	13.1 ± 5.7	13.5 ± 5.2	14.2 ± 5.2	14.1 ± 5.2
Ventricular lead impedance	778.7 ± 249.8	533.2 ± 96.6	536.4 ± 84.8	527.5 ± 84.1
Pacing threshold	0.85 ± 1.1	0.7 ± 0.2	0.7 ± 0.2	0.7 ± 0.3
Battery life (months)		120.7 ± 19.9	113.6 ± 20.6	114.6 ± 20.2

DISCUSSION

Of the 214 patients analysed, the majority of the patients (n=128) had undergone a previous MRI scan. A total of 36 clinical MRI examinations (in 24 patients) were performed in the years following implantation. The majority of these scans were performed to confirm, exclude or follow-up a neurological disease. This is in accordance with previously published data.

In line with previously published reports, this data demonstrates MRI can be safely performed in patients with implanted (MRI-conditional) CIEDs [8-12]. MRI offers the advantage of radiation-free, clear anatomic imaging, soft tissue characterisation and functional assessment such as in cardiac MRI. Indications for MRI have expanded, particularly in the follow-up of chronic diseases or hereditary disorders.

Although it can be expected that all devices will be MRI-conditional in the future and limitations will only concern the applied field strength or scan duration, the current situation may be confusing for referring physicians. Despite the efforts to clearly indicate MRI compatibility of the device, e.g. on the patient's device card or by symbols that can be identified on chest radiography, it may be a challenging topic for non-cardiologists. In order to eliminate potential risks, current guidelines advise to adhere to a strict safety protocol when performing MRI scans in patients with implanted devices.

Image quality

The possible effects MR imaging may have on the function of the implanted device have been thoroughly investigated. Only when adhering to manufacturer's instructions, safe scanning of patients can be guaranteed.

In addition, the impact of the device on image quality has become an area of research [13-16]. In general, structures outside the thorax can be investigated without difficulties. Furthermore, recent studies have demonstrated the satisfactory performance of cardiac MRI in patients with implanted devices. Despite the presence of artifacts caused by the impulse generator and the pacing leads, biventricular volume and function assessment and late enhancement imaging was carried out with an acceptable image quality.

Study limitations

This is a single-center retrospective study in which the use of MRI in patients with implanted MRI-conditional pacemakers or ICDs was evaluated. Patients may have undergone MRI examinations in other centers. Therefore the number of scans after implantation may be underestimated.

The mean follow-up period in this study demonstrated a high variance. This is mainly due to the fact that implantation rates have increased dramatically in the year 2014, resulting in a relatively limited follow-up period in these patients.

MRI was only performed using a field strength of 1.5 Tesla. Therefore, the presented data regarding the safe performance of MRI cannot be translated to application of higher field strengths.

CONCLUSION

Patients with a high risk of requiring an MRI scan in the near future are eligible for implantation of an MRI-conditional pacing device. In this study, MRI-conditional pacing devices were implanted in 214 patients of whom 94% suffered from a co-morbidity that may lead to a future indication for MRI. During a mean follow-up period of 406 days (51-1353 days), 36 MRI investigations were safely performed in 24 (11%) patients. The diagnostic yield was not affected by the presence of the device.

REFERENCES

1. Kuck KH, Hindricks G, Padeletti L, Raatikainen P, Arnar DO. The EHRA White Book 2014: The Current Status of Cardiac Electrophysiology in ESC Member Countries. 2014.
2. Ferreira AM, Costa F, Tralhão A, Marques H, Cardim N, Adragão P.MRI-conditional pacemakers: current perspectives. Med Devices (Auckl). 2014 May 7;7:115-24.
3. Nordbeck P, Ertl G, Ritter O. Magnetic resonance imaging safety in pacemaker and implantable cardioverter defibrillator patients: how far have we come? Eur Heart J. 2015 Jun 21;36(24):1505-11.
4. Kalin R, Stanton MS. Current clinical issues for MRI scanning of pacemaker and defibrillator patients. Pacing Clin Electrophysiol. 2005;28:326–328.
5. van der Graaf AW, Bhagirath P, Götte MJ. MRI and cardiac implantable electronic devices; current status and required safety conditions. Neth Heart J. 2014 Jun;22(6):269-76.
6. Shenthar J, Milasinovic G, Al Fagih A, Götte M, Engel G, Wolff S, Tse HF, Herr J, Carrithers J, Cerkvenik J, Nähle CP. MRI scanning in patients with new and existing CapSureFix Novus 5076 pacemaker leads: Randomized trial results. Heart Rhythm. 2015 Apr;12(4):759-65.
7. Maglia G, Curnis A, Brieda M, Anaclerio M, Caccavo V, Bonfanti P, Melissano D, Caravati F, Giovene L, Gargaro A; the Really ProMRI Study Group. Assessing access to MRI of patients with magnetic resonance-conditional pacemaker and implantable cardioverter defibrillator systems: the Really ProMRI study design. J Cardiovasc Med (Hagerstown). 2015 Oct;16(10):715-20.
8. Wollmann CG, Thudt K, Kaiser B, Salomonowitz E, Mayr H, Globits S.Safe performance of magnetic resonance of the heart in patients with magnetic resonance conditional pacemaker systems: the safety issue of the ESTIMATE study. J Cardiovasc Magn Reson. 2014 May 6;16:30.
9. Muehling OM, Wakili R, Greif M, von Ziegler F, Morhard D, Brueckmann H, Becker A. Immediate and 12 months follow up of function and lead integrity after cranial MRI in 356 patients with conventional cardiac pacemakers. J Cardiovasc Magn Reson. 2014 Jun 5;16:39.
10. Ainslie M, Miller C, Brown B, Schmitt M. Cardiac MRI of patients with implanted electrical cardiac devices. Heart. 2014 Mar;100(5):363-9.
11. Marinskis G, Bongiorni MG, Dagres N, Dobreanu D, Lewalter T, Blomström-Lundqvist C; Scientific Initiative Committee, European Heart Rhythm Association. Performing magnetic resonance imaging in patients with implantable pacemakers and defibrillators: results of a European Heart Rhythm Association survey. Europace. 2012 Dec;14(12):1807-9.
12. Nazarian S, Beinart R, Halperin HR. Magnetic resonance imaging and implantable devices. Circ Arrhythm Electrophysiol. 2013 Apr;6(2):419-28.
13. Kaasalainen T, Kivistö S, Holmström M, Peltonen J, Pakarinen S, Hänninen H, Sipilä O. Cardiac MRI in patients with cardiac pacemakers: practical methods for reducing susceptibility artifacts and optimizing image quality. Acta Radiol. 2016 Feb;57(2):178-87.

14. Martinelli M. Magnetic resonance imaging and cardiac implantable electronic devices: safety barrier overtaken--is the image quality the current target? Heart Rhythm. 2013 Jun;10(6):873-4.

15. Sasaki T, Hansford R, Zviman MM, Kolandaivelu A, Bluemke DA, Berger RD, Calkins H, Halperin HR, Nazarian S. Quantitative assessment of artifacts on cardiac magnetic resonance imaging of patients with pacemakers and implantable cardioverter-defibrillators. Circ Cardiovasc Imaging. 2011 Nov;4(6):662-70.

16. Schwitter J, Kanal E, Schmitt M, Anselme F, Albert T, Hayes DL, Bello D, Tóth A, Chang Y, van Osch D, Sommer T; Advisa MRI System Study Investigators. Impact of the Advisa MRI pacing system on the diagnostic quality of cardiac MR images and contraction patterns of cardiac muscle during scans: Advisa MRI randomized clinical multicenter study results. Heart Rhythm. 2013 Jun;10(6):864-72.

04

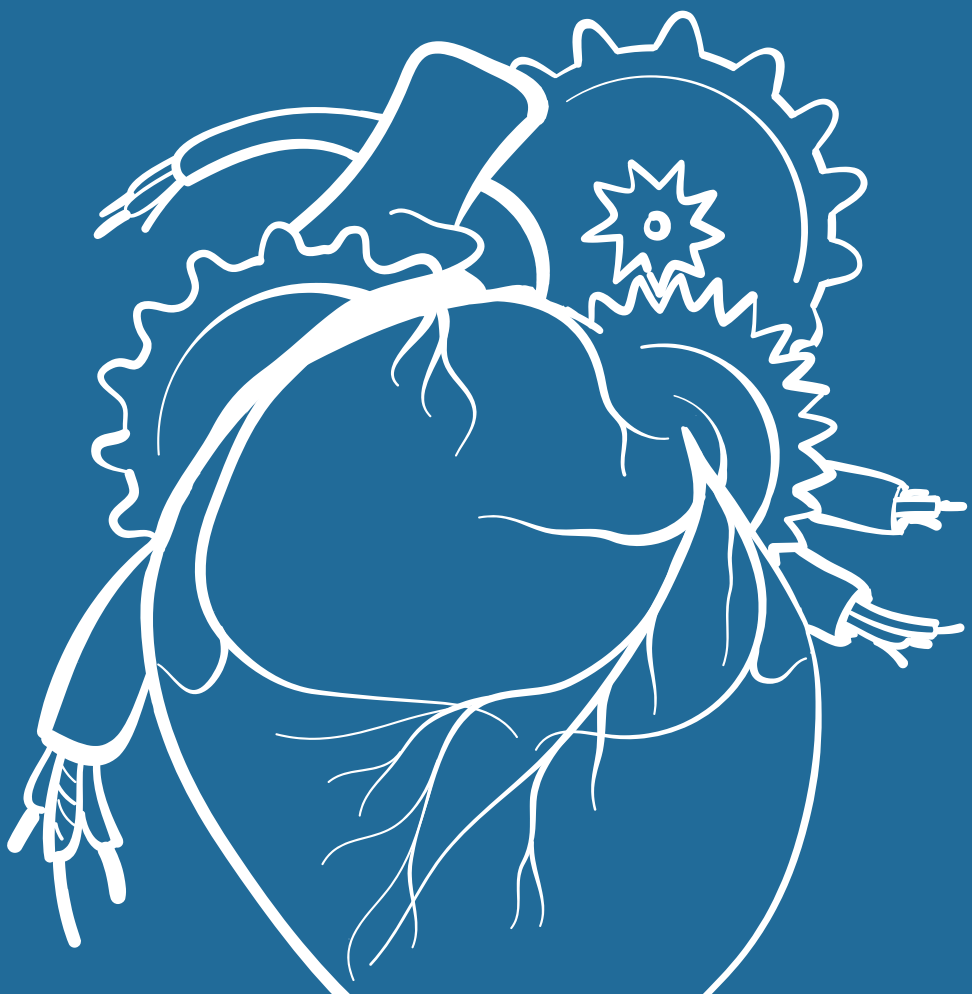

MR-FEATURE TRACKING IN PATIENTS WITH MRI-CONDITIONAL PACING SYSTEMS: THE IMPACT OF PACING

van der Graaf AW, Bhagirath P, Scheffer MG, Robles de Medina R, Götte MJ.
Journal of Magnetic Resonance Imaging. 2016;44(4):964-71.

ABSTRACT

Purpose: To perform strain analysis using use feature tracking (FT) software on conventional (non-tagged) cardiac magnetic resonance imaging (MRI) function images. With the advent of MRI-conditional pacemaker systems, effects of cardiac pacing on myocardial strain can be studied using MR. In this study the impact of pacing on left ventricular (LV) strain was investigated using MR-FT in patients with an MRI-conditional cardiac implantable electronic device (CIED).

Material and methods: FT was performed on 32 1.5T MR studies (16 patients with an MRI-conditional CIED and 16 control patients with normal scans). Short- and long-axis steady state free precession (SSFP) cines were used for the FT analysis. Strain was assessed using CVI42 software (Circle Cardiovascular Imaging, Alberta, Canada). In addition, the intra- and interobserver variability was determined using the intraclass correlation coefficient.

Results: Of the 16 patients with an MRI-conditional CIED, five patients were paced during the MRI exam. Despite the occasional presence of susceptibility artifacts induced by the CIED, radial, circumferential, and longitudinal strain parameters could be derived for all patients. Peak radial strain and peak circumferential strain were reduced during pacing when compared to the control group; for radial strain: 20.1 ± 4.7% vs. 33.1 ± 6.9%, $P < 0.001$, and for circumferential strain -7.5 ± 3.5% vs. -14.9 ± 3.2%, $P < 0.05$. Peak strain parameters were reproducible on an intra- and interobserver level.

Conclusion: MR-FT is feasible in patients with an MRI-conditional CIED and can be used to quantify regional wall motion.

INTRODUCTION

Due to the induced abnormal pattern of mechanical activation, right ventricular (RV) pacing is associated with regional remodelling and deterioration of left ventricular (LV) function [1-2]. Therefore, patients with a single-chamber pacing device are carefully followed using echocardiography in order to monitor global cardiac function. However, global function measures are insensitive to early regional dysfunction [3]. Therefore, it may be of advantage to evaluate local myocardial strain during the cardiac cycle in this patient category.

Magnetic Resonance Imaging (MRI) is the current reference standard for the accurate assessment of regional wall motion [4]. MR tissue tagging provides highly reproducible data of 3D myocardial strain [5]. However, due to the need for a dedicated pulse sequence and cumbersome post-processing procedure, tissue tagging and strain analysis have not become routine clinical tools [6].

Recently developed feature tracking (FT) software allows for retrospective detailed regional myocardial strain analysis on routine MR cine images [7]. Hence, acquisition of tagged images to derive strain parameters is not required. A study by Kuetting et al. compared the FT technique to tagged Harmonic Phase (HARP) imaging and revealed a good agreement for global strain assessment between the two techniques [8].

With the introduction of MRI-conditional cardiac implantable electronic devices (CIED), MRI has become applicable in patients with CIEDs [9-10].

The purpose of this study was to investigate the impact of pacing on LV strain using FT software applied on cardiac MR cine images of patients with MRI-conditional CIEDs.

METHODS

Patient population

This was a retrospective, single-center study. The study complies with the Declaration of Helsinki. The local medical ethical committee and the hospital scientific board approved this study.

A total of 32 MR studies were analysed; 16 studies of patient with an implanted CIED and 16 control studies.

The 16 consecutive MR investigations in CIED patients were derived from a previous study [11]. In total, 14 patients had a Medtronic Advisa MRI pacemaker system and a structurally normal heart; 2 patients without a history of coronary artery disease had a Medtronic Evera MRI Internal Cardioverter Defibrillator (ICD) system for primary prevention.

The 16 MR exams of healthy volunteers were collected from the local database. These individuals did not have any cardiovascular history or symptoms of cardiac disease. The control group was sex and age adjusted to the CIED patients. Baseline characteristics of the study population are summarised in **table 1**.

Table 1. Baseline characteristics of study population.

Parameters	**CIED patients (n=16)**	**Controls (n=16)**
Age (years)	59 ± 11	59 ± 12
Male gender, n (%)	15 (94)	15 (94)
BSA (m^2)	2.1 ± 0.2	2.1 ± 0.2
Days after device implant	271 ± 289	
Pacing indication		
- Asystole	4	
- Bradycardia	3	
- AV-block	5	
- SSS	2	
- Primary prevention (ICD)	2	
Device characteristics (impulse generator and leads)		
- Medtronic Advisa MRI & Medtronic CapSure 5086/5076	14	
- Medtronic Evera ICD MRI & Medtronic CapSure 6935	2	
Device programming during MR exam		
- VOO/DOO (asynchronous pacing)	5	
- VVI/DDI (pacing inhibited)	11	

SSS sick sinus syndrome; LVEDV left ventricular end-diastolic volume; LVESV left ventricular end-systolic volume; LVSV left ventricular stroke volume; LVEF left ventricular ejection fraction; RVEDV right ventricular end-diastolic volume; RVESV right ventricular end-systolic volume; RVSV right ventricular stroke volume; RVEF right ventricular ejection fraction

Device programming

Before entering the MRI room, pacing thresholds, P- and R-wave amplitude and lead impedance were determined and the CIED was programmed into MRI SureScan® mode [12]. During the MRI examination, the ECG signal and pulse-oximetry were used to monitor the patients and to verify continuous pacing, if applicable. After the examination, pacing thresholds, P- and R-wave amplitude and lead impedance were determined and compared to the values prior the MR investigation. Finally, original programming of the CIED was restored.

Cardiovascular magnetic resonance imaging

MR studies were performed between March 2012 and September 2014. Six examinations (four scans in the CIED group and two scans in the control group) were performed on a 1.5 Tesla Philips Intera system (Philips Healthcare, Best, The Netherlands). The remaining 26 scans were performed on a 1.5 Tesla Siemens Aera system (Siemens, Erlangen, Germany). The mean time between CIED implantation and acquisition of images was 271 days (range: 50-1109 days).

After survey scans, a retrospective triggered balanced Steady State Free Precession (SSFP) gradient echo sequence was used for cine imaging. SSFP cine images were acquired in a single breath-hold during expiration for 8-10 seconds. In all patients, a stack of short-axis (SAX) and two, three, and four-chamber long-axis (LAX) cines were obtained.

Typical image parameters were: slice thickness 6mm, slice gap 4mm, temporal resolution <50ms, repetition time 32ms, echo time 1.54ms, flip angle 57 degrees and a typical image resolution of 1.4 by 1.4mm. The number of phases within the cardiac cycle was set at 20.

The image quality and the feasibility of delineating endocardial and epicardial contours were evaluated for all scans. In the two patients with an implanted ICD system, additional Gradient Echo (GRE) LAX and SAX cines were acquired to reduce the amount of artifacts induced by the device. Typical image parameters were: slice thickness 6mm, slice gap 4mm, temporal resolution <50ms, repetition time 48ms, echo time 3.16ms and flip angle 15 degrees.

Magnetic resonance - feature-tracking

Strain analysis was performed using MR-FT software (Circle Cardiovascular Imaging, Inc, Alberta, Canada). End-diastolic and end-systolic LV contours were manually drawn on the epicardial and endocardial wall of the myocardium in LAX cine images and on basal, mid and apical levels of SAX cine images, as described previously [13].

Strain is expressed as the percentage of shortening or lengthening of a small element of myocardium in relation to its original length. Radial, circumferential and longitudinal peak strain (%), time to peak strain (ms) and degree of torsion (deg/cm) were derived. For analysis purposes, the American Heart Association (AHA) 16-segment model was used [14].

Besides strain analysis, function measures including left- and right ventricular end-diastolic volume (EDV), end-systolic volume (ESV), stroke volume (SV), ejection fraction (EF) and LV mass were determined. Two independent observers with over five years of experience in interpreting MR analysed four cases (2 SSFP and 2 GRE studies) to assess inter-observer variability (AWM & PB), while intra-observer variability was derived from the repeated analysis by the first observer (AWM).

Statistical analysis

Statistical analysis was performed using IBM SPSS Statistics for Windows, version 17.0. Data are expressed as mean ± standard deviation (SD). MR function and strain parameters were compared between the different groups using an unpaired Student *t*-test, after the data was tested for normal distribution. The intra- and inter- observer variability for strain measurements was assessed by the intraclass correlation coefficient (ICC). All statistical tests with p values < 0.05 were considered statistically significant.

RESULTS

Image quality

The mean duration of an MRI examination was 49 ± 9 min in CIED patients and 29 ± 4 min in the control group. In patients with an implanted pacemaker system, the occasional presence of artifacts, induced by the presence of the device, did not hamper endocardial and epicardial contour delineation. A typical example representing the average image quality of a SAX cine used for the drawing of contours is provided in **figure 1**.

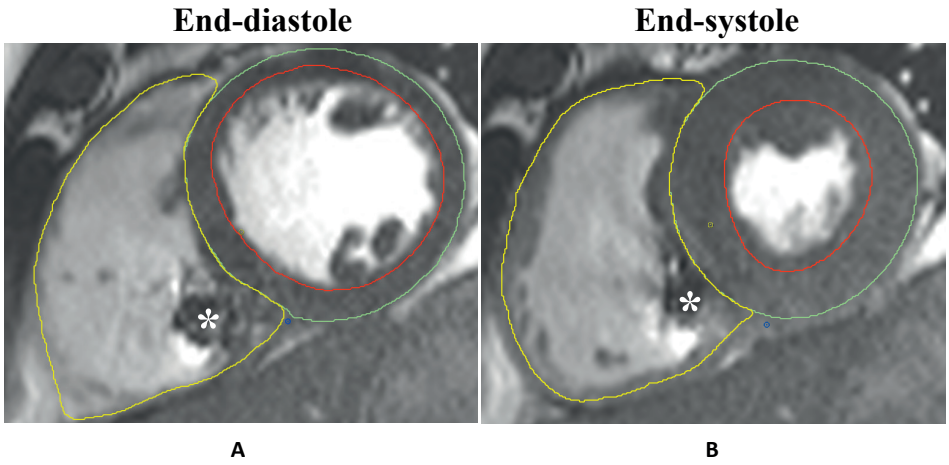

Figure 1. End-diastolic (A) and end-systolic (B) still of a short-axis cine from a patient with an implanted CIED. Despite the presence of the susceptibility artifact (indicated by the asterisks), LV and RV function could be assessed.

In the two patients with an implanted ICD system, the artifacts were more prominent due to the larger device and the presence of the RV shock-lead. In these patients, an additional GRE pulse sequence was applied. The GRE images did show fewer artifacts and allowed for a clinically relevant quantitative analysis. The difference in image quality between a standard four-chamber SSFP sequence and a GRE sequence is shown in videos 1 and 2.

Ventricular volumes and function

In all patients, LV and RV function could be assessed. MR-derived function measures are listed in **table 2**. Compared to controls, mean left and right ventricular function were reduced in patients with a CIED (LVEF 47 ± 10% vs 56 ± 6%, $p<0.05$ and RVEF 44 ± 6% vs.55 ± 6% , $p<0.001$)

Myocardial strain analysis

The mean post-processing time was 23 ± 4 min in the patients with a CIED and 18 ± 3 min in the control group. A total of 512 (16 x 32) heart segments were analysed. In **table 3**, results of the strain analysis are provided. Of the 16 patients in the CIED group, 5 patients underwent MRI during DOO pacing (4 patients with a total AV block and 1 patient with a symptomatic sick sinus syndrome), the remaining 11 patients had an intrinsic rhythm while image acquisition was performed. **Figure 2** provides an example

of a 16-segment bulls eye plot visualising the regional differences in time to peak radial strain and radial strain during pacing and during intrinsic rhythm. RV pacing results in an asynchronous activation pattern and decreased myocardial strain.

Table 2. Ventricular volumes and function.

MR parameter	CIED - pacing (n=5)	CIED - non-pacing (n=11)	Controls (n=16)
LVEDV (ml)	164 ± 24	177 ± 43	160 ± 30
LVESV (ml)	97 ± 21	93 ± 42	71 ± 20
LVSV (ml)	67 ± 13#	84 ± 14	90 ± 15
LVEF (%)	41 ± 7#	49 ± 10	56 ± 6
LV mass (g)	121 ± 17#	119 ± 18§	93 ± 24
LV mass/BSA (g/m^2)	57 ± 7#	56 ± 9§	45 ± 11
RVEDV (ml)	158 ± 17	175 ± 38	161 ± 35
RVESV (ml)	92 ± 15	96 ± 26§	74 ± 24
RVSV (ml)	66 ± 8#	79 ± 17	87 ± 15
RVEF (%)	42 ± 5#	46 ± 6§	55 ± 6

CIED-pacing vs. control, *p<0.05*; § CIED non pacing vs. control, *p<0.05*.

Table 3. Myocardial strain parameters

Strain parameters	CIED - pacing (n=5)	CIED - non-pacing (n=11)	Controls (n=16)
Peak radial strain (%)	20.1 ± 4.7#	22.3 ± 5.8§	33.1 ± 6.9
Time to peak radial strain (ms)	364.9 ± 31.3	401.5 ± 49.0§	344.0 ± 38.8
Peak circumferential strain (%)	-7.5 ± 3.5#	-8.5 ± 6.1§	-14.9 ± 3.2
Time to peak circumferential strain (ms)	358.6 ± 33.7	407.0 ± 53.7§	340.2 ± 44.7
Peak longitudinal strain (%)	-5.1 ± 1.5	-6.6 ± 2.3	-8.5 ± 1.4
Time to peak longitudinal strain (ms)	361.2 ± 32.3	403.2 ± 50.7	342.2 ± 39.4
Torsion (deg/cm)	0.5 ± 0.3	0.6 ± 0.4	0.7 ± 0.7

CIED-pacing vs. control, *p<0.05*; § CIED non pacing vs. control, *p<0.05*.

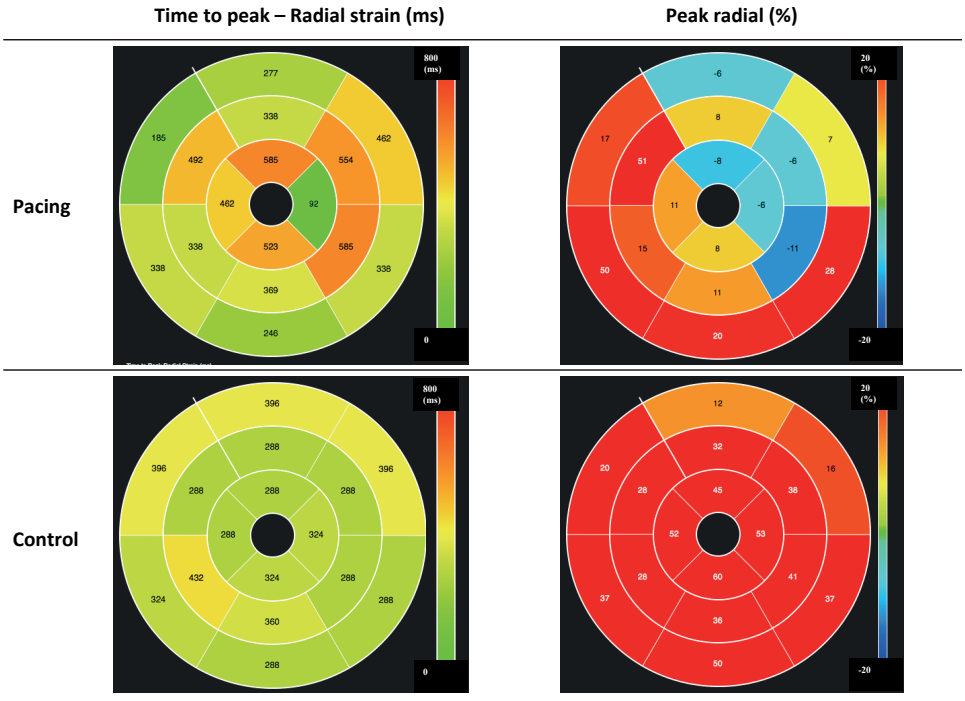

Figure 2. American Heart Association (AHA) 16-segment bulls eye plot of radial strain in a CIED patient and a healthy control. Time to peak radial strain increased and radial strain was decreased during pacing (upper panel) compared to intrinsic rhythm (lower panel). RV pacing results in delayed and decreased myocardial strain. This is most evident in the antero-lateral segments of the basal region of the heart.

Peak radial strain and peak circumferential strain were reduced during pacing (n=5) when compared to patients in the control group (radial strain: 20.1 ± 4.7% vs. 33.1 ± 6.9%; *p<0.001* and circumferential strain: -7.5 ± 3.5% vs. -14.9 ± 3.2%; *p<0.05*). A trend towards a decrease in longitudinal strain (-5.1 ± 1.5%) was observed during cardiac pacing (n=5) when compared to CIED patients (n=11) scanned during intrinsic rhythm (-6.6 ± 2.3%, *p=0.25*) and healthy controls (-8.5 ± 1.4%, *p=0.38*). **Figure 3** visualises the differences observed in myocardial strain between CIED patients with a paced rhythm during image acquisition and healthy controls. Radial, circumferential and longitudinal strain was decreased during pacing.

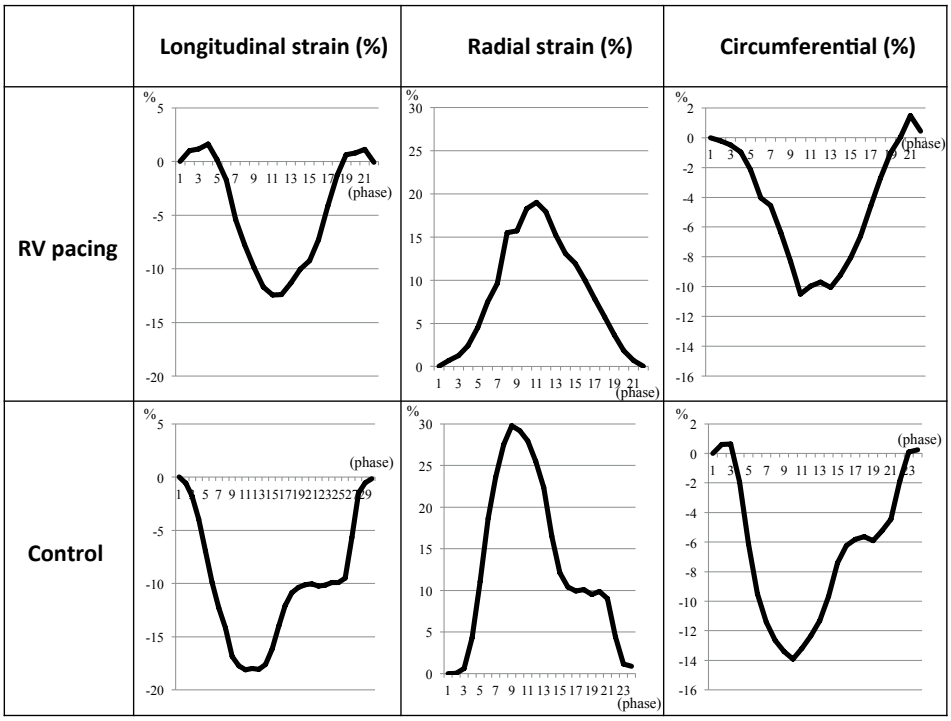

Figure 3. Whole-cycle circumferential, radial and longitudinal strain during pacing **(upper panel)** compared to strain measured in healthy volunteers **(lower panel)**. In general, the amount of myocardial strain was reduced and more delayed during RV pacing.

A trend towards a decrease in time to peak radial and circumferential strain was observed during pacing when compared to CIED patients scanned during intrinsic rhythm (time to peak radial strain: 364.9 ± 31.3ms vs. 401.5 ± 49.0ms; *p=0.12* and time to peak circumferential strain: 358.6 ± 33.7ms vs. 407.0 ± 53.7ms; *p=0.06*.

Reproducibility of MR-FT analysis

Peak strain parameters were reproducible on an intra- and inter-observer level. **Table 4** shows ICC for repeated measurements within the single and between observers. Correlations between peak strain derived from SSFP images were higher compared to the parameters derived from GRE sequences.

Table 4. Intra- and inter-observer variability for SSFP (upper panel) and GRE series (lower panel).

SSFP sequence	Intra-observer variability		Inter-observer variability	
	Mean difference ± SD	ICC (95% CI)	Mean difference ± SD	ICC (95% CI)
Peak radial strain	4.72 ± 20.16	0.70 (0.33-0.89)	-2.05 ± 12.50	0.76 (0.56-0.87)
Peak circumferential strain	0.86 ± 7.15	0.92 (0.80-0.97)	-2.41 ± 12.58	0.71 (0.49-0.85)
Peak longitudinal strain	0.65 ± 0.88	0.99 (0.98-0.99)	-0.88 ± 3.83	0.72 (0.55-0.83)
Gradient echo sequence	**Intra-observer variability**		**Inter-observer variability**	
	Mean difference ± SD	**ICC (95% CI)**	**Mean difference ± SD**	**ICC (95% CI)**
Peak radial strain	-1.23 ± 17.24	0.01 (-0.47-0.48)	1.05 ± 10.79	0.62 (0.35-0.80)
Peak circumferential strain	1.63 ± 20.77	-0.10 (-0.56-0.40)	7.78 ± 16.50	0.37 (0.02-0.63)
Peak longitudinal strain	1.71 ± 1.01	0.93 (0.85-0.97)	0.61 ± 1.56	0.88 (0.80-0.93)

DISCUSSION

This study investigated the impact of pacing on regional wall motion using MR-FT in patients with MRI-conditional pacemakers and ICDs.

For all patients in this study, strain analysis could be performed. In patients with a CIED, a delay and decrease of peak radial, peak circumferential and longitudinal strain was observed. Peak strain parameters were reproducible on an intra- and inter-observer level and comparable to results published in normal volunteers [15] and patients with ischemic cardiomyopathy [16].

In the CIED patients, adequate endocardial and epicardial delineation was possible, despite the presence of susceptibility artifacts induced by the CIED. Although additional GRE sequences in two patients with an implanted ICD system resulted in images with fewer susceptibility artifacts, the reproducibility of strain parameters was lower when compared to strain parameters derived from SSFP sequences. This may be due to the fact that the borders of the endocardium and epicardium are more difficult to discern on GRE cine images.

Assessment of regional wall motion that can be performed on routinely acquired MR images could facilitate the monitoring of myocardial strain in patients with CIEDs. This may be especially beneficial for patients receiving long-term RV pacing or in patients with poor acoustic windows for echocardiography. From literature, it is known that long-

term RV pacing is associated with deterioration of LV function [17]. Therefore, it is crucial to detect early signs of local remodelling or impaired function. For this patient category, MR-FT is a promising tool that allows follow-up and evaluation of serial changes in strain parameters. In addition, MR-FT may facilitate the incorporation of routine strain assessment in clinical practice.

Feature tracking and tissue tagging are currently available for the evaluation of myocardial strain.

In MR tissue tagging, non-invasive myocardial markers are applied by saturation planes. Subsequently, the movement of these markers is quantified during the cardiac cycle.

Cardiac MR tissue tagging provides highly reproducible data of myocardial deformation in three directions and is the current reference standard [18]. Besides the need for an advanced pulse sequence and cumbersome post-processing, tagging may be limited by the rapid fading of tags. Tag fading may hamper evaluation of the entire cardiac cycle. Scanning on a 3.0 Tesla scanner can reduce this problem [19]. However, this is not possible with current available MRI-conditional CIEDs, since these devices are only approved for 1.5T.

Feature-tracking imaging was originally designed for echocardiographic image analysis [20] and was later introduced in the field of MR. MR-FT does not require the acquisition of additional MRI images. After contour delineation of the ventricular myocardium on cine images, MR-FT calculates the motion of a tissue voxel. In contrast to speckle-tracking echocardiography or MR tissue tagging, only the border between myocardium and blood is available for tracking. Therefore, sufficient contrast between these structures is required.

Previous studies [7,8,21] have indicated that 3D myocardial deformation may be difficult to analyse using MR-FT, since the tracking of the border between myocardium and the blood pool merely represents wall thickening and epicardial-endocardial motion. This may explain the limited amount of torsion observed in this study.

MR-FT has been applied in several groups of patients e.g. dilated cardiomyopathy [22], ischemic cardiomyopathy [16], during dobutamine stress [23] and in patients with repaired tetralogy of Fallot [24]. In a more recent study by Taylor et al. [25] 100 healthy individuals underwent MR-FT assessment in order to define a normal range for the most commonly used strain parameters. In addition, this study demonstrated an excellent intra- and inter-observer variability for all circumferential and longitudinal based variables.

A limited number of studies have compared the two techniques [26-27]. A study by Hor et al. [28] reported a strong correlation between the global strain assessed with the two methods. A recent study by Wu et al. [29] confirmed this finding, but concluded that the intra- and inter-observer agreement of MR-FT was lower compared with MR tissue tagging. Based on the available literature, the value of MR-FT needs to be proven with respect to regional strain.

In this study, the feasibility of performing MR-FT is demonstrated in a limited number of patients with an MRI-conditional pacing device. In order to assess the long-term impact of pacing using MR-FT, however, a larger number of patients and a prospective study design are required. Preferably, the MR-FT results would be compared to strain measurements obtained using MR-tagging or echocardiography.

The cine images used in this study (SSFP and GRE) were acquired with a temporal resolution < 50ms. To evaluate the effect of cardiac pacing on the timing of mechanical activation in more detail, the temporal resolution used for the acquisition of the cine images is of importance [30]. Further research is needed in order to determine whether MR-FT in patients with an implanted CIED may benefit from images obtained user a higher temporal resolution. Since the border between myocardium and blood is used for tracking purposes in MR-FT, through-plane motion may affect the measurements, especially in the basal segments. Assessment of RV myocardial strain is currently not possible with the available software. Future studies are required to demonstrate the feasibility of integrating this analysis in the daily clinical practice.

CONCLUSION

Magnetic Resonance Feature Tracking is feasible in patients with an MRI-conditional pacing device. In this study, cardiac pacing was associated with a decrease in peak radial and circumferential strain. This technique may be used to monitor regional wall motion and myocardial strain in this group of patients. Further research is needed to evaluate the potential benefits of this technique in daily clinical practice.

REFERENCES

1. De Sisti A, Márquez MF, Tonet J, Bonny A, Frank R, Hidden-Lucet F. Adverse effects of long-term right ventricular apical pacing and identification of patients at risk of atrial fibrillation and heart failure. Pacing Clin Electrophysiol. 2012;35(8):1035-43.
2. Akerström F, Pachón M, Puchol A, Jimínez-López J, Segovia D, Rodríguez-Padial L, et al. Chronic right ventricular apical pacing: adverse effects and current therapeutic strategies to minimize them. Int J Cardiol. 2014;15;173(3):351-60.
3. Ibrahim el SH. Myocardial tagging by cardiovascular magnetic resonance: evolution of techniques--pulse sequences, analysis algorithms, and applications. J Cardiovasc Magn Reson. 2011;28;13:36.
4. Abbasi SA, Ertel A, Shah RV, Dandekar V, Chung J, Bhat G, et al. Impact of cardiovascular magnetic resonance on management and clinical decision-making in heart failure patients. J Cardiovasc Magn Reson. 2013;1;15:89.
5. Götte MJ, Germans T, Rüssel IK, Zwanenburg JJ, Marcus JT, van Rossem AC, et al. Myocardial strain and torsion quantified by cardiovascular magnetic resonance tissue tagging: studies in normal and impaired left ventricular function. J Am Coll Cardiol. 2006;21;48(10):2002-11.
6. Jiang K, Yu X. Quantification of regional myocardial wall motion by cardiovascular magnetic resonance. Quant Imaging Med Surg. 2014;4(5):345-57.
7. Kowallick JT, Lamata P, Hussain ST, Kutty S, Steinmetz M, Sohns JM, et al. Quantification of left ventricular torsion and diastolic recoil using cardiovascular magnetic resonance myocardial feature tracking. PLoS One 2014;6;9(10):e109164.
8. Kuetting D, Sprinkart AM, Doerner J, Schild H, Thomas D. Comparison of magnetic resonance feature tracking with harmonic phase imaging analysis (CSPAMM) for assessment of global and regional diastolic function. Eur J Radiol. 2015;84(1):100-7.
9. Kaasalainen T, Pakarinen S, Kivistö S, Holmström M, Hänninen H, Peltonen J, et al. MRI with cardiac pacing devices - safety in clinical practice. Eur J Radiol. 2014;83(8):1387-95.
10. Wollmann CG, Thudt K, Kaiser B, Salomonowitz E, Mayr H, Globits S. Safe performance of magnetic resonance of the heart in patients with magnetic resonance conditional pacemaker systems: the safety issue of the ESTIMATE study. J Cardiovasc Magn Reson. 2014;6;16;30:1-8.
11. van der Graaf AW, Bhagirath P, de Hooge J, Ramanna H, van Driel VJ, de Groot NM, Götte MJ. Non-invasive focus localisation, right ventricular epicardial potential mapping in patients with an MRI-conditional pacemaker system - a pilot study. J Interv Card Electrophysiol. 2015 Dec;44(3):227-34.
12. Wilkoff BL, Bello D, Taborsky M, Vymazal J, Kanal E, Heuer H, et al. Magnetic resonance imaging in patients with a pacemaker system designed for the magnetic resonance environment. Heart Rhythm 2011;8(1):65-73.
13. Hor KN, Baumann R, Pedrizzetti G, Tonti G, Gottliebson WM, Taylor M, et al. Magnetic resonance derived myocardial strain assessment using feature tracking. J Vis Exp. 2011;12;48:2356-61.

14. Cerqueira MD, Weissman NJ, Dilsizian V, Jacobs AK, Kaul S, Laskey WK, et al. Standardized myocardial segmentation and nomenclature for tomographic imaging of the heart. A statement for healthcare professionals from the Cardiac Imaging Committee of the Council on Clinical Cardiology of the American Heart Association. Circulation 2002;29;105(4):539-42.
15. Andre F, Steen H, Matheis P, Westkott M, Breuninger K, Sander Y, et al. Age- and gender-related normal left ventricular deformation assessed by cardiovascular magnetic resonance feature tracking. J Cardiovasc Magn Reson. 2015 10;17:25.
16. Schuster A, Paul M, Bettencourt N, Morton G, Chiribiri A, Ishida M, et al. Cardiovascular magnetic resonance myocardial feature tracking for quantitative viability assessment in ischemic cardiomyopathy. Int J Cardiol. 2013;20;166(2):413-20.
17. Ukkonen H, Tops L, Saraste A, Naum A, Koistinen J, Bax J, et al. The effect of right ventricular pacing on myocardial oxidative metabolism and efficiency: relation with left ventricular dyssynchrony. Eur J Nucl Med Mol Imaging. 2009;36(12):2042-8.
18. Edvardsen T, Gerber BL, Garot J, Bluemke DA, Lima JA, Smiseth OA. Quantitative assessment of intrinsic regional myocardial deformation by Doppler strain rate echocardiography in humans: validation against three-dimensional tagged magnetic resonance imaging. Circulation. 2002 Jul 2;106(1):50-6.
19. Singh A, Steadman CD, Khan JN, Horsfield MA, Bekele S, Nazir SA, et al. Intertechnique agreement and interstudy reproducibility of strain and diastolic strain rate at 1.5 and 3 tesla: A comparison of feature-tracking and tagging in patients with aortic stenosis. J Magn Reson Imaging. 2015;41(4):1129-37.
20. Onishi T, Saha SK, Delgado-Montero A, Ludwig DR, Onishi T, Schelbert EB, et al. Global Longitudinal Strain and Global Circumferential Strain by Speckle-Tracking Echocardiography and Feature-Tracking Cardiac Magnetic Resonance Imaging: Comparison with Left Ventricular Ejection Fraction. J Am Soc Echocardiogr. 2015;28(5):587-96.
21. Schneeweis C, Lapinskas T, Schnackenburg B, Berger A, Hucko T, Kelle S, et al. Comparison of myocardial tagging and feature tracking in patients with severe aortic stenosis. J Heart Valve Dis. 2014;23(4):432-40.
22. Buss SJ, Breuninger K, Lehrke S, Voss A, Galuschky C, Lossnitzer D, et al. Assessment of myocardial deformation with cardiac magnetic resonance strain imaging improves risk stratification in patients with dilated cardiomyopathy. Eur Heart J Cardiovasc Imaging. 2015;16(3):307-15.
23. Schneeweis C, Qiu J, Schnackenburg B, Berger A, Kelle S, Fleck E, et al. Value of additional strain analysis with feature tracking in dobutamine stress cardiovascular magnetic resonance for detecting coronary artery disease. J Cardiovasc Magn Reson. 2014;1;16(1):72.
24. Latus H, Hachmann P, Gummel K, Khalil M, Yerebakan C, Bauer J, et al. Impact of residual right ventricular outflow tract obstruction on biventricular strain and synchrony in patients after repair of tetralogy of Fallot: a cardiac magnetic resonance feature tracking study. Eur J Cardiothorac Surg. 2015;48(1):83-90.

25. Taylor RJ, Moody WE, Umar F, Edwards NC, Taylor TJ, Stegemann B, et al. Myocardial strain measurement with feature-tracking cardiovascular magnetic resonance: normal values. Eur Heart J Cardiovasc Imaging. 2015;16(8):871-81.

26. Harrild DM, Han Y, Geva T, Zhou J, Marcus E, Powell AJ. Comparison of cardiac MRI tissue tracking and myocardial tagging for assessment of regional ventricular strain. Int J Cardiovasc Imaging. 2012; 28:2009–18.

27. Lorca MC, Haraldsson H, Ordovas KG. Ventricular Mechanics: Techniques and Applications. Magn Reson Imaging Clin N Am. 2015;23(1):7-13.

28. Hor KN, Gottliebson WM, Carson C, Wash E, Cnota J, Fleck R, et al. Comparison of magnetic resonance feature tracking for strain calculation with harmonic phase imaging analysis. JACC Cardiovasc Imaging. 2010;3(2):144-51.

29. Wu L, Germans T, Güçlü A, Heymans MW, Allaart CP, van Rossum AC. Feature tracking compared with tissue tagging measurements of segmental strain by cardiovascular magnetic resonance. J Cardiovasc Magn Reson. 2014;22;16:10.

30. Padiyath A, Gribben P, Abraham JR, Li L, Rangamani S, Schuster A, et al. Echocardiography and cardiac magnetic resonance-based feature tracking in the assessment of myocardial mechanics in tetralogy of Fallot: an intermodality comparison. Echocardiography 2013;30(2):203-10.

PART 2
DEVELOPING A NOVEL NON-INVASIVE MAPPING METHODOLOGY

05

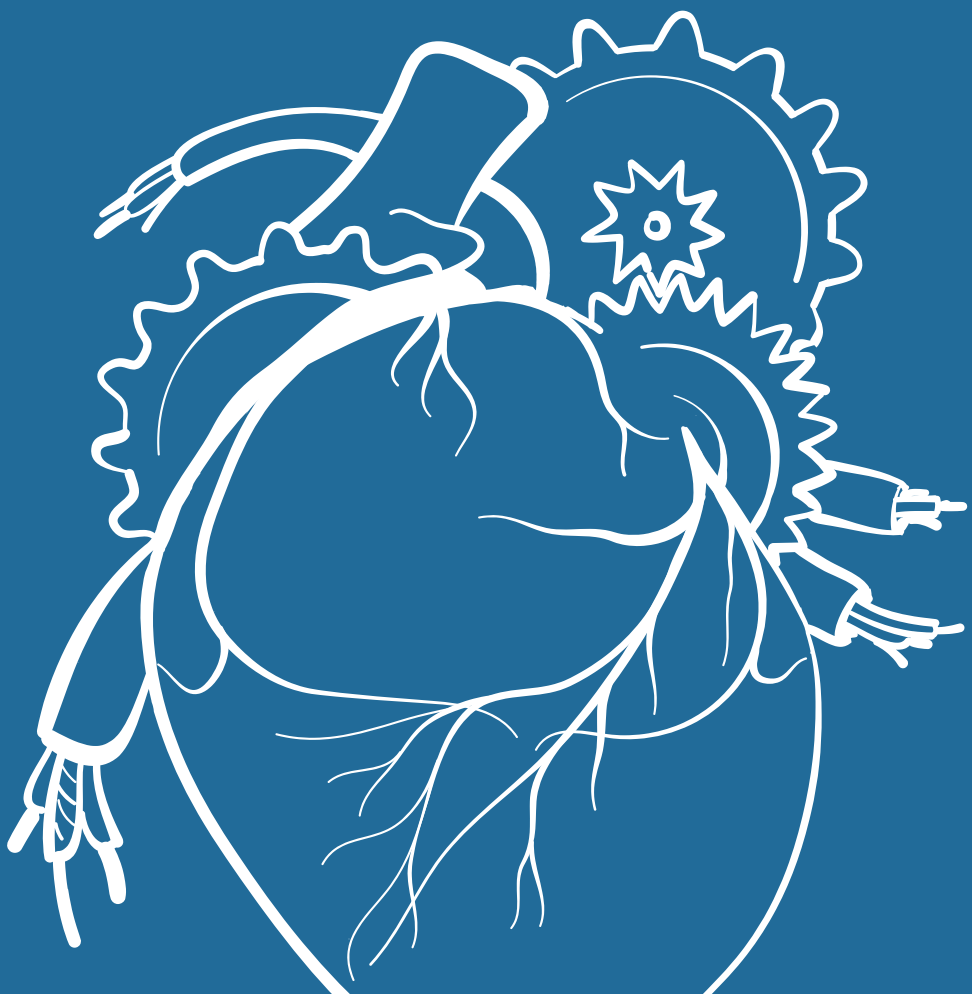

NON-INVASIVE IMAGING OF CARDIAC EXCITATION; INVERSE POTENTIAL MAPPING

van der Graaf AW, Bhagirath P, Ramanna H, van Driel VJ, de Hooge J, de Groot NM, Götte MJ.
Annals of Noninvasive Electrocardiology. 2014;19(2):105-113.

ABSTRACT

Non-invasive imaging of cardiac excitation using body surface potential mapping (BSPM) data and inverse procedures is an emerging technique that enables estimation of myocardial depolarisation and repolarisation. Despite numerous reports on the possible advantages of this imaging technique, it has not yet advanced into daily clinical practice. This is mainly due to the time consuming nature of data acquisition and the complexity of the mathematics underlying the used inverse procedures. However, the popularity of this field of research has increased and non-invasive imaging of cardiac electrophysiology is considered a promising tool to complement conventional invasive electrophysiological studies. Furthermore, the use of appropriately designed electrode vests and more advanced computers has greatly reduced the procedural time. This review provides descriptive overview of the research performed thus far and the possible future directions. The general challenges in routine application of BSPM and inverse procedures are discussed. In addition, individual properties of the biophysical models underlying the inverse procedures are illustrated.

INTRODUCTION

Through the years, various non-invasive electrocardiographic imaging techniques have emerged that estimate epicardial potentials or myocardial activation times from potentials recorded on the thorax [1-8]. The recording of potentials from a large number (32-256) of torso electrodes is referred to as Body Surface Potential Mapping (BSPM) [9]. The BSPM data can later be used in mathematical inverse procedures to calculate local epicardial potentials or myocardial activation times [10].

Although a vast amount of research illustrates the possible clinical advantages of this non-invasive imaging method, the time consuming nature of BSPM and the complexity of the mathematics underlying the inverse procedures have thus far hampered these techniques to advance into daily clinical practice.

Nevertheless, non-invasive imaging of cardiac excitation is still gaining popularity as a field of research and is considered a promising tool to complement conventional invasive electrophysiological studies [11]. The use of appropriately designed electrode vests and more advanced computers has greatly reduced the procedural time. Recently, a non-invasive imaging technique based on Electrocardiographic Imaging (ECGI) has been commercialised and has become available for clinical use in Europe [12]. Although ECGI estimates the time course of unipolar epicardial electrograms only, several studies have demonstrated that the epicardial potentials and electrograms provide substantial information about intra-myocardial activity [13-14].

This review discusses the general challenges in routine application of BSPM and inverse procedures. Descriptive overview is given to the research performed thus far and the future direction of non-invasive imaging of cardiac excitation. In addition, individual properties of the biophysical models underlying the inverse procedures are illustrated.

BODY SURFACE POTENTIAL MAPPING

Waller was the first to report on the recording of human body surface potentials in 1887 [15]. He used a capillary electrometer to systematically investigate the potential distribution associated with the beating heart. Einthoven published the first surface electrocardiogram (ECG) constructed with the string galvanometer in 1903 and later described the method for clinical 12-lead electrocardiography [16]. The use of the 12-lead ECG made it possible to study potential fields over designated areas and to investigate their variations over time.

Although the efficacy of the 12-lead ECG had been widely recognised, several researchers felt that information was lost when the recording of potentials was limited to only nine sites [17-18]. In the following years, alternative configurations using 16 to 256 torso electrodes were proposed [19-24]. Nevertheless, BSPM has never been incorporated into daily clinical practice because of uncertainty about the clinical utility. In the meantime, much experience had already been gained with the interpretation of the 12-lead ECG and this configuration continues to be the standard of routine clinical practice today.

INVERSE PROCEDURE

The *forward* problem of electrocardiography refers to estimation of body surface potentials from potentials measured on the surface of the heart. Therefore, the effect that different types of body tissue have on the cardiac potentials is simulated [25]. In contrast, the *inverse* problem of electrocardiography describes the opposite (**figure 1A**). Through an inverse procedure, the potentials on the heart surface or activation times of the myocardium are estimated using the recorded body surface potentials as source data.

In order to calculate cardiac activation times from potentials recorded on the body surface, potentials that are generated by the cardiac electrical activity in the torso volume need to be modelled. Unlike the forward problem that can be solved uniquely, the inverse problem in terms of sources is not unique [26]. Many different source configurations in the heart can correspond to the same potentials on the body surface, even for noise-free and error-free data. These different sources are termed equivalent sources because they generate the same potentials on the body surface. Therefore, the inverse problem is said to be "ill-conditioned" [27].

In order to cope with this ill-conditioned nature, most inverse procedures employ a combination of two types of models: a biophysical source model and a volume conductor model (VCM). In a biophysical source model, the heart is represented as a generator of electrical currents (**figure 2**).

The VCM reproduces the influence of different types of tissues in the thorax on the potential waveforms.

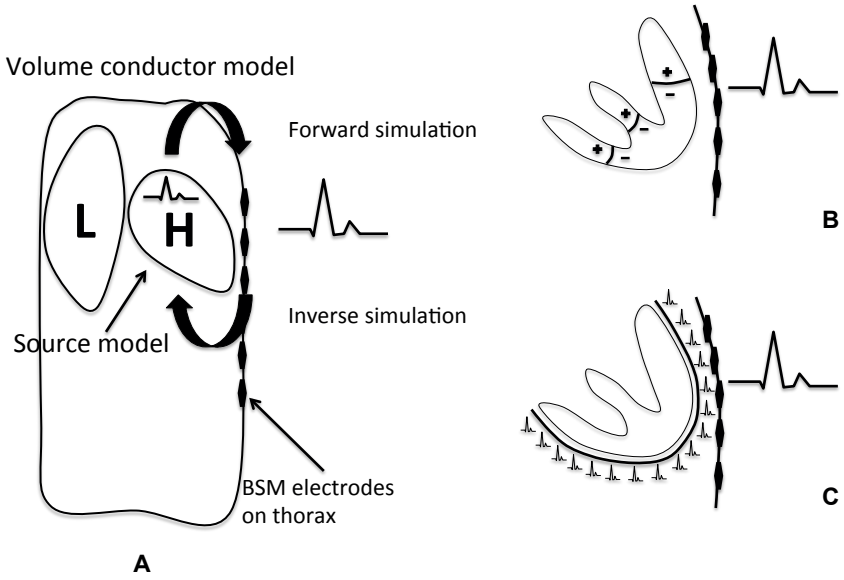

Figure 1. Forward and inverse computation. **A:** The principle of forward and inverse computation is illustrated in a VCM from a lateral view (H: heart, L: lung). In the EDL source model **(B)**, the wavefront separating resting heart cells in the myocardium from those that have undergone depolarisation, is regarded as an activation layer that moves through the heart during the cardiac cycle. In the PPS model **(C)**, a unique relationship exists between the potentials on the body surface and the potentials on the epicardium.

In order to reproduce this influence, a detailed anatomical model of the patients' thorax, incorporating the conductivity properties of the main thoracic structures, is a prerequisite. Anatomy is usually provided by a Computed Tomography (CT) or Magnetic Resonance Imaging (MRI) scan. The conductivity values used for the thorax, ventricular muscle, lungs and blood cavities can be found in literature, e.g. 0.2 S/m, 0.2 S/m, 0.04 S/m, and 0.6 S/m respectively [28-29]. The resulting simulated body surface potentials are then compared to the actual potentials recorded by the torso electrodes. Finally, the activation times and the resulting potential curves are tuned in order to obtain an optimal match between the measured and simulated ECG. Eventually, the most favourable match between simulated and measured thorax potentials is considered to be a true reflection of local cardiac activation.

The inverse problem in terms of potentials is unique; that is, in the absence of noise and errors only one epicardial potential distribution corresponds to a given body surface potential distribution. This inverse problem does not employ a model representation of the source; instead, it uses the actual epicardial potentials as a source [30].

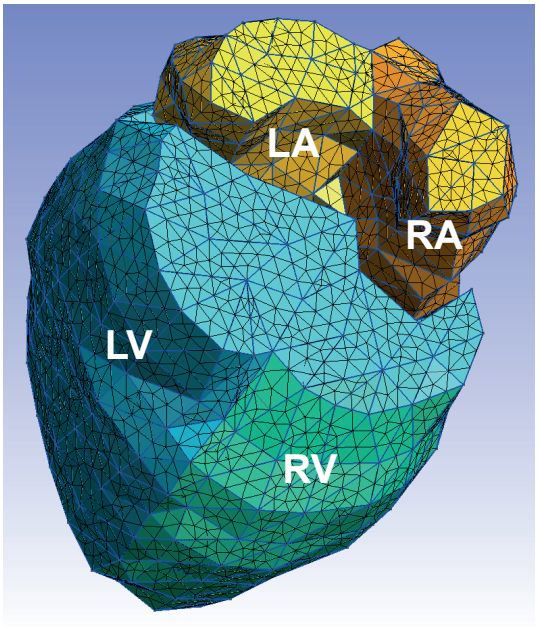

Figure 2. Triangulated mesh of a patient's heart. A triangulated heart model developed and used at our institution. This model can be used for simulations of cardiac activation. After segmentation of the different cardiac compartments on CT or MRI anatomic images, specialised software divides the volumes in triangles of equal size. The nodes and interconnecting spines of the mesh can subsequently be used to calculate probable excitation pathways.

Inverse problems are regarded to have an ill-posed nature, i.e. the desired solution is unstable and can vary significantly with the slightest noise or perturbation in the BSPM data. In order to circumvent this issue, investigators have developed several regularisation methods that impose constraints to the outcome [31]. The chosen constraints can have a tremendous influence on the outcome and are therefore a subject of constant debate. Nevertheless, regularisation is a key issue in contemporary used inverse procedures [32].

BIOPHYSICAL SOURCE MODELS

A biophysical source model represents the heart as a generator of electrical currents. The first source model to be introduced was the current dipole (CD).

Current dipole

The electrical field generated by the heart was considered equivalent to a single rotating dipole, visualised as a vector of varying strength during the cardiac cycle [33]. Hence, usage of this model is known as vectorcardiography. The effect of an approaching or receding excitation wave can be described using this model. However, multiple excitation wavefronts, spreading simultaneously through the myocardium, and regional electrical activity cannot be discriminated due to the total lack of spatial resolution of this model. Following the introduction of the current dipole, Wilson et al. introduced another source model in 1933; the equivalent double layer (EDL) [34].

Equivalent double layer model

The wavefront separating resting heart cells in the myocardium from those that have undergone depolarisation, can be regarded as a surface double layer. This activation layer moves through the heart during the cardiac cycle, reflecting cardiac electrical activity (**figure 1B**). Observed from some distance, this double layer is electrically equivalent to the net effect of the currents generated at the cellular membrane during depolarisation with a strength proportional to the local transmembrane potential [35]. However, the validity of the EDL model is disputed; in particular the assumption that ventricular cells constitute a homogeneous syncytium. In addition, an equal anisotropy (directional dependence) ratio is assumed, while fiber architecture inside the myocardium is heterogeneous with major regional variations in fiber arrangement [36].

Pericardial potential source model

Among the biophysical source models, the Pericardial Potential Source (PPS) model has been investigated most extensively [37-38]. In order to inversely compute the pericardial potential distribution from recorded potentials, the PPS model exploits a common physical fact (**figure 1C**). A unique relationship exists between the potentials on the body surface and the potentials on the epicardium, as long as the model descriptions of both surfaces are closed and no other electrical sources are present in between [39]. The entire time course of unipolar epicardial electrograms is estimated. This enables mapping depolarisation, repolarisation and other electrophysiological processes that are reflected in the S-T segment. Moreover, it has been demonstrated that the epicardial potentials and electrograms provide substantial information about intra-myocardial activity [40].

Cellular automaton (CA)

In a Cellular Automaton (CA) model, the myocardial tissue is considered to be a set of discrete elements (in either active or inactive state) connected to each other. States vary as a function of the preceding state and the state of the neighbouring elements. CA are relatively easy to program and allow fast simulations, but have serious limitations when seeking to reproduce the effects of curvature on an activation front [41]. This in turn may results in less accurate estimations on cardiac activation times to be made.

VOLUME CONDUCTOR MODELS

A VCM reproduces the influence of the different types of tissues in the thorax on the potential waveforms. The models most often used are discussed here.

Spherical element model

The spherical element model considers the volume-conducting medium to be a symmetrical homogeneous sphere. Therefore, it is not suited for accurate localisation of electrical foci, but has proven to be an efficient and fast model in vectorcardiography [42]. The attractiveness of this model relies in the fact that in such a simplistic configuration, the differential equations involved can be solved analytically, rather than by a computer.

Boundary element method

The Boundary Element Method (BEM) is a frequently used model that approximates the volume conductor properties of realistic shaped compartments. When using this approach for forward or inverse computation, it is essential to accurately obtain a patient's heart and thorax geometry. The boundaries of the organs involved are of particular interest. The properties of the enclosed tissue (e.g. anisotropy) are purposefully neglected. Hence, the influence of various types of tissues on the distribution of potentials through a volume cannot be determined. The BEM allows relatively fast calculations as long as only a limited number of boundaries are present [43].

Finite element method

On the contrary, the Finite Element Method (FEM) fully appreciates the volume and architecture of the tissue rather than just its boundaries. Although historically hampered by limited computational resources, this model is used more frequently nowadays. The ability to incorporate the effects of inhomogeneity on the transmission of electrical

impulses through the thorax is an important incentive to investigate the FEM. Although its efficiency in localizing epileptic foci in neurological patients has been demonstrated previously [44], little research has thus far been performed in cardiac patients.

NON-INVASIVE ELECTROCARDIOGRAPHIC IMAGING TECHNIQUES

Through the years, various methods using different combinations of BSPM and inverse procedures (source and volume conductor model) have been proposed. Numerous experiments were performed to determine a technique's localisation accuracy. Validation studies in humans with various pathologies are an on-going effort that should continue. The mean resolution of currently used non-invasive electrocardiographic imaging techniques is approximately 1-2 cm, though some have obtained better results [45-50].

Electrocardiographic imaging

Electrocardiographic Imaging (ECGI) uses 250 torso electrodes and combines the PPS and BEM [51]. Recently, this technique has been commercialis by CardioInsight™ (CardioInsight Technologies Inc., Ohio, USA). The clinical applicability of ECGI is currently being investigated in a multi-center trial and the first reports have been published. ECGI effectively predicted which patients would respond to Cardiac Resynchronisation Therapy (CRT), based on differences between estimated left ventricular (LV) and right ventricular (RV) mean activation times. A greater difference was associated with clinical CRT response and appeared to be a more powerful predictor than 12-lead ECG parameters [52]. The feasibility of CRT optimisation by using ECGI had been reported earlier [53].

Another study demonstrated the clinical utility in mapping simple and complex atrial tachycardia's (AT) [54]. The overall diagnostic accuracy of the non-invasive system compared to invasive EP diagnosis, as the gold standard, was 92% (100% in patients with de novo ablations and 83% in patients with previous AF ablations).

The ability of ECGI to map atrial fibrillation (AF) was investigated in several studies [55-56]. Body surface signals generated by AF are typically of low amplitude and the volume conductor smoothens the potential distribution. Because ventricular signals are typically of much greater magnitude than the atrial signals, it might be necessary in some patients with normal atrioventricular (AV) conduction to remove the ventricular signals. This can be achieved by using QRS(T) subtraction algorithms or by the administration of AV blocking agents. Hence, it can be challenging to acquire long continuous recordings of atrial signals of adequate quality.

In 2011, Wang el al. reported on the application of ECGI in a series of 25 patients undergoing catheter ablation procedures for various types of VT (**figure 3**) [57]. BSPM were recorded during episodes of sustained VT in nine patients. The remaining patients were imaged during premature ventricular contractions (PVC). The sites of origin as determined by ECGI were in agreement with the invasive electrophysiological study (EPS) in 10 of 11 RV sites (91%) and in 11 of 12 LV sites (92%). ECGI correctly categorised both focal and re-entrant mechanisms of VT, but was not able to differentiate between focal activity and micro re-entry.

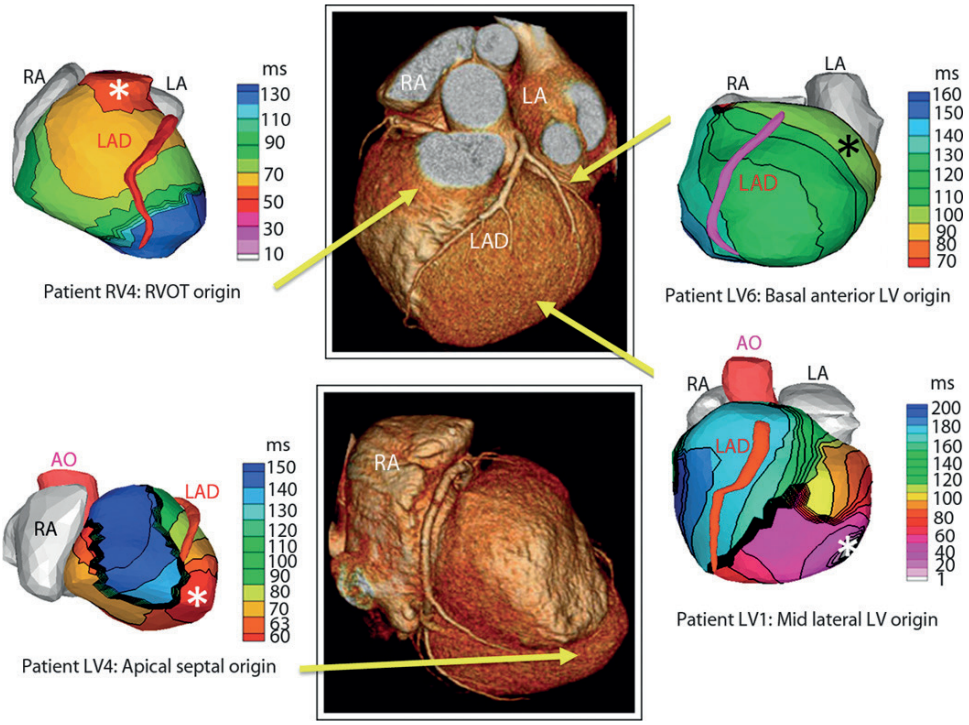

Figure 3. Non-invasive ECGI isochrone maps for localisation of VT site of origin. Epicardial isochrone maps are shown for four patients, with earliest epicardial activation marked with an asterisk. EP-study-determined sites of origin are indicated under the ECGI maps. Yellow arrows point to VT origin on a representative CT scan. RA: right atrium; LA: left atrium; AO: aorta; LAD: left anterior descending coronary artery; LV: left ventricle; RVOT: right ventricular outflow tract. From Wang Y et al. Non-invasive electroanatomic mapping of human ventricular arrhythmias with electrocardiographic imaging. Sci Transl Med. 2011;31;3(98):98ra84. With permission. Copyright AAAS / Science 2011

Electrical remodelling due to right ventricular pacing was investigated in 9 patients with an implanted dual-chamber pacemaker system [58]. This remodelling resulted in action potential prolongation near the site of abnormal activation and a marked dispersion of repolarisation. This dispersion of repolarisation is potentially arrhythmogenic and was less evident during continuous RV pacing.

When recording the atria, the ventricular signal is a problem when the ventricular rate is rapid. Analysis requires that a few cycles do not conduct to the ventricles. AT with 2:1 conduction to the ventricles pose an analytic challenge in the absence of reliable QRST subtraction software program. It can be difficult to estimate signals around the mitral annulus, which can be problematic for peri-mitral atrial flutter. In most studies, a CT scan was performed that includes the abdomen in order to register the location of all BSPM electrodes on the image. The inclusion of the abdominal region is associated with substantially higher patient radiation doses [59].

Non-invasive imaging of cardiac electrophysiology

Non-invasive Imaging of Cardiac Electrophysiology (NICE) employs 64 electrodes, the EDL and BEM [60]. NICE has been performed in 7 patients with WPW syndrome undergoing catheter ablation of the accessory pathway [61]. All ventricular accessory pathway insertion sites were identified with an accuracy of 18.7 ± 5.8 mm. In CRT and control patients, endocardial and epicardial ventricular activation were visualised non-invasively [62].

However, the atria cannot be analysed using the NICE technique and the model does not account for ventricular repolarisation. The small number of study subjects in which NICE was applied makes it difficult to fully appreciate the quality of this system. Studies on functional electrocardiographic imaging are generally limited by the small number of study subjects owing to the complexity of data acquisition and image segmentation procedures for reconstruction of patient-specific anatomical models.

AMYCARD

AMYCARD uses 83 electrodes, PPS and BEM [63]. It has been commercialised by AMYCARD LLC (AMYCARD LLC, Moscow, Russia). Since AMYCARD has only recently been installed in several Russian research centers, no data on the accuracy of this technique is yet available.

Current density reconstruction (CDR)

Another method developed by He and co-workers uses Current Density Reconstruction (CDR) to estimate the current density distribution on the endocardial surface of the LV from measured body surface potentials [64]. The dipole source model and BEM are employed in combination with 90 torso electrodes. The first report on in-vivo validation has recently been published by Lai et al. [65]. BSPM was performed in six patients with monomorphic PVC. Compared with the successful ablation site, the mean localisation error of the CDR approach was 13.8 ± 1.3 mm.

FUTURE PERSPECTIVE

Non-invasive imaging of cardiac excitation has been the focus of several investigators, but it has not yet evolved into a clinical technology that is usable in daily clinical practice. This is mainly due to technical challenges in the recording, processing and interpretation of the data. To enter the clinical arena, the physical validity of the simulations and robustness of the method must be undisputed. As far as validation is a key issue, there is a need for continued validation in humans. In addition, practical aspects of handling a great number of electrodes must be considered. Until now several multi-electrode vests have been developed, but it remains unclear to what extent these vests allow routine clinical application of BSPM.

More reliable simulations of greater physical validity are aspired in the near future. In order to achieve this, high-resolution imaging techniques and improved inverse algorithms need to be developed and integrated. For example, the integration of patient specific MRI data on cardiac fiber orientation into biophysical models (FEM) poses new challenges [66]. The selection of an appropriate source and volume conductor model may prove to be of utmost importance to construct highly accurate, patient-specific 3D simulation models for clinical use. Therefore substantial knowledge on the general challenges regarding the use of inverse procedures seems imperative.

Despite these challenges, non-invasive imaging of cardiac electrophysiology is considered a promising tool to complement conventional EPS. For example, in patients suffering from arrhythmias, ectopic foci may be localised non-invasively prior to entering the catheterisation suite. Reducing the duration of an invasive procedure and to decrease the associated exposure to radiation could be an important advantage of this application.

With regard to optimisation of pacing therapy, detailed simulation studies may be performed using patient-specific 3D computer models prior to implantation of a cardiac pacing device. By incorporating knowledge on anatomy, location of scar tissue and the site of latest mechanical activation, optimal sites for lead placement may be determined non-invasively.

In case of atrial fibrillation (AF), these techniques may offer new insights in the extent of structural and functional remodelling of the atria. Especially, when incorporating information on the extent and location of atrial fibrosis in patients undergoing Pulmonary Vein Antrum Isolation (PVAI). Through follow-up investigations, therapeutic effects or progression of substrate remodelling can be assessed and monitored carefully.

CONCLUSION

The development of robust inverse procedures has kindled renewed interest in BSPM. The combined use of inverse procedures and BSPM, referred to as non-invasive imaging of cardiac electrophysiology, is considered a promising tool to complement conventional EP studies. To enter the clinical arena, the physical validity of the simulations and robustness of individual methods must be undisputed. The selection of appropriate biophysical models may prove to be of utmost importance to construct highly accurate, patient-specific 3D simulation models for clinical use.

REFERENCES

1. Liu C, He B. Noninvasive estimation of the cardiac activation sequence using the extended Kalman Filter. IEEE Trans Biomed Eng. 2011;58:541-549.
2. Berger T, Hintringer F, Fischer G. Noninvasive imaging of cardiac electrophysiology. Indian Pacing Electrophysiol J. 2007;1;7(3):160-5.
3. Huiskamp G, Greensite F. A new method for myocardial activation imaging. IEEE Trans Biomed Eng. 1997;44(6):433-46.
4. Varma N. Variegated left ventricular electrical activation in response to a novel quadripolar electrode: Visualisation by non-invasive electrocardiographic imaging. J Electrocardiol. 2014;47(1):66-74.
5. Bokeriia LA, Revishvili ASh, Kalinin AV, et al. Hardware-software system for noninvasive electrocardiographic examination of heart based on inverse problem of electrocardiography. Med Tekh. 2008;6:1-7.
6. SippensGroenewegen A, Hauer RN, van Hemel NM, et al. Atlas of paced body surface QRS integral maps for localisation of the site of origin of postinfarction ventricular tachycardia. J Electrocardiol. l994;27(Suppl1):IO5-1I2.
7. Cakulev I, Sahadevan J, Arruda M, et al. Confirmation of Novel Noninvasive High Density Electrocardiographic Mapping with Electrophysiology Study: Implications for Therapy. Circ Arrhythm Electrophysiol. 2013;6(1):68-75.
8. Van Dam PM, Oosterdorp TF, Linnenbank AC, et al. Non-Invasive Imaging of Cardiac Activation and Recovery. Ann Biomed Eng. 2009;37(9):1739–1756.
9. Taccardi B, Punske BB, Lux RL, et al. Useful lessons from body surface mapping. J Cardiovasc Electrophysiol. 1998;9(7):773-86.
10. Hoekema R, Uijen GJ, van Oosterom A. On selecting a body surface mapping procedure. J Electrocardiol. 1999;32(2):93-101.
11. Sapp JL, Dawoud F, Clements JC, et al. Inverse solution mapping of epicardial potentials: quantitative comparison with epicardial contact mapping. Circ Arrhythm Electrophysiol. 2012;5(5):1001-9.
12. Rudy Y. Noninvasive electrocardiographic imaging of arrhythmogenic substrates in humans. Circ Res. 2013;112(5):863-74.
13. Oster HS, Taccardi B, Lux RL, et al. Electrocardiographic imaging: Noninvasive characterisation of intramural myocardial activation from inverse-reconstructed epicardial potentials and electrograms. Circulation 1998;21;97(15):1496-507.
14. Hutchinson MD, Gerstenfeld EP, Desjardins B, et al. Endocardial unipolar voltage mapping to detect epicardial ventricular tachycardia substrate in patients with nonischemic left ventricular cardiomyopathy. Circ Arrhythm Electrophysiol. 2011;4(1):49-55.

15. Waller AD. A demonstration on man of electromotive changes accompanying the heart's beat. J Physiol. (Lond) 1887;8:227-34.
16. Einthoven W. Die galvanometrische Registerung des menschlichen Elektrokardiogram: Zugleich eine Beurtheilung der Anwendung des Capillar-Elektrometers in der Physiologie. Pflügers Arch ges Physiol. 1903;99:472-480.
17. Horan LG, Hand RC, Flowers NC, et al. The influence of electrode placement in the reconstruction and analysis of body surface potential maps from limited thoracic arrays. J Electrocardiol. 1980;13(4):311-21.
18. Evans JW, Erb BD, Brody DA. Comparative proximity and remoteness characteristics of conventional electrocardiographic leads. Am Heart J. 1961;61:615-21.
19. Donnelly MP, Finlay DD, Nugent CD, et al. Lead selection: old and new methods for locating the most electrocardiogram information. J Electrocardiol. 2008;41(3):257-63.
20. Barr RC, Spach MS, Herman-Giddens S. Selection of the number and position of measuring locations for electrocardiography. IEEE Trans Biomed Eng. 1971;18(2);125-38.
21. Lux RL, Burgess MJ, Wyatt RF, et al. Clinically practical lead systems for improved electrocardiography: comparison with precordial grids and conventional lead systems. Circulation 1979;59(2):256-63.
22. Kornreich F, Montague TJ, Rautaharju PM, et al. Identification of best electrocardiographic leads for diagnosing anterior and inferior myocardial infarction by statistical analysis of body surface potential maps. Am J Cardiol. 1986;58(10):863-71.
23. Van Oosterom A. The Equivalent Surface Source Model in its Application to the T Wave. J Electrocardiol. 2002;527-535.
24. Lux RL, Smith CR, Wyatt RF, et al. Limited lead selection for estimation of body surface potential maps in electrocardiography. IEEE Trans Biomed Eng. 1978;25(3):270-6.
25. Gulrajani RM. The forward and inverse problems of electrocardiography. IEEE Eng Med Biol Mag. 1998;17(5):84-101.
26. Van Oosterom A. Source Models in Inverse Electrocardiography. Int J Bioelectromag. 2003;5;1:211-4.
27. Van Oosterom A. The inverse problem of bioelectricity: an evaluation. Med Biol Eng Comput. 2012;50(9):891-902.
28. Roth BJ. Electrical conductivity values used with the bidomain model of cardiac tissue. IEEE Trans Biomed Eng. 1997;44(4):326-8.
29. Geddes LA, Baker LE. The specific resistance of biological material: a compendium of data for the biomedical engineer and physiologist. IEEE Trans. Biomed. Eng. 1967;5:271–293.
30. Martin RO, Pilkington TC. Unconstrained inverse electrocardiography: epicardial potentials. IEEE Trans Biomed Eng. 1972;19(4):276-85.
31. Shou G, Jiang M, Xia L, et al. A comparison of different choices for the regularisation parameter in inverse electrocardiography models. Conf Proc IEEE Eng Med Biol Soc. 2006;1:3903-6.

32. Cluitmans MJ, Karel JM, Bonizzi P, et al. Wavelet-sparsity based regularisation over time in the inverse problem of electrocardiography. Conf Proc IEEE Eng Med Biol Soc. 2013;3781-4.

33. Burger HC, van Milaan JB. Heart Vector and Leads. Br Heart J. 1946;8:157-161.

34. Wilson FN, Macleod AG, Barker PS. The Distribution of Action Currents produced by the Heart Muscle and Other Excitable Tissues immersed in Conducting Media. J Gen Physiol. 1933;16:423-456.

35. van Dam PM, Tung R, Shivkumar K, et al. Quantitative localisation of premature ventricular contractions using myocardial activation ECGI from the standard 12-lead electrocardiogram. J Electrocardiol. 2013;46(6):574-9.

36. Streeter DD, Ramon C. Muscle pathway geometry in the heart wall. J Biomech Eng. 1983;105(4):367-73.

37. Spach MS, Barr RC, Lanning CF, et al. Origin of body surface QRS and T wave potentials from epicardial potential distributions in the intact chimpanzee. Circulation 1977;55(2):268-8.

38. Franzone PC, Taccardi B, Viganotti C. An approach to inverse calculation of epicardial potentials from body surface maps. Adv Cardiol. 1978;21:50-4.

39. Ramanathan C, Jia P, Ghanem R, et al. Noninvasive electrocardiographic imaging (ECGI): application of the generalized minimal residual (GMRes) method. Ann Biomed Eng. 2003;31(8):981-94.

40. Burnes JE, Taccardi B, Ershler PR, et al. Noninvasive electrocardiogram imaging of substrate and intramural ventricular tachycardia in infarcted hearts. J Am Coll Cardiol. 2001;38(7):2071-8.

41. Dossel O, Bauer W, Farina D, et al. Imaging of bioelectric sources in the heart using a cellular automaton model. Conf Proc IEEE Eng Med Biol Soc. 2005;2:1067-70.

42. Holmes JR, Alps BJ. Studies into equine electrocardiography and vectorcardiography: I. Cardiac electric forces and the dipole vector theory. Can J Comp Med Vet Sci. 1967;31(4):92-102.

43. Jamison C, Navarro C, Turner C, et al. The inverse problem utilizing the boundary element method for a nonstandard female torso. IEEE Trans Biomed Eng. 2011;58(4):876-83.

44. Fuchs M, Wagner M, Kastner J. Development of volume conductor and source models to localize epileptic foci. J Clin Neurophysiol. 2007;24(2):101-19.

45. Lee K, Lv W, Ter-Ovanesyan E, et al. Cardiac ablation catheter guidance by means of a single equivalent moving dipole inverse algorithm. Pacing Clin Electrophysiol. 2013;36(7):811-22.

46. Lai D, Sun J, Li Y, et al. Usefulness of ventricular endocardial electric reconstruction from body surface potential maps to noninvasively localize ventricular ectopic activity in patients. Phys Med Biol. 2013;7;58(11):3897-909.

47. Ghosh S, Rudy Y. Accuracy of quadratic versus linear interpolation in noninvasive Electrocardiographic Imaging (ECGI). Ann Biomed Eng. 2005;33(9):1187-201.

48. Shannon HJ, Navarro CO, Smith BA, et al. Activation patterns during selective pacing of the left ventricle can be characterized using noninvasive electrocardiographic imaging. J Electrocardiol. 2007;40(6 Suppl):S111-7.

49. Han C, Pogwizd SM, Killingsworth CR, et al. Noninvasive cardiac activation imaging of ventricular arrhythmias during drug-induced QT prolongation in the rabbit heart. Heart Rhythm 2013;10(10):1509-15.

50. Barr RC, Spach MS. Inverse calculation of QRS-T epicardial potentials from body surface potential distributions for normal and ectopic beats in the intact dog. Circ Res. 1978;42(5):661-75.

51. Ramanathan C, Ghanem RN, Jia P, et al. Noninvasive electrocardiographic imaging for cardiac electrophysiology and arrhythmia. Nat Med. 2004;10(4):422-8.

52. Ploux S, Lumens J, Whinnett Z, et al. Noninvasive electrocardiographic mapping to improve patient selection for cardiac resynchronisation therapy: Beyond QRS duration and left bundle-branch block morphology. J Am Coll Cardiol. 2013;18;61(24):2435-43.

53. Varma N, Jia P, Rudy Y. Electrocardiographic imaging of patients with heart failure with left bundle branch block and response to cardiac resynchronisation therapy. J Electrocardiol. 2007;40(6 Suppl):S174-8.

54. Shah AJ, Hocini M, Xhaet O, et al. Validation of novel 3-dimensional electrocardiographic mapping of atrial tachycardias by invasive mapping and ablation: a multicenter study. J Am Coll Cardiol. 2013;3;62(10):889-97.

55. Cuculich PS, Wang Y, Lindsay BD, et al. Noninvasive characterisation of epicardial activation in humans with diverse atrial fibrillation patterns. Circulation 2010;122:1364–1372.

56. Haissaguerre M, Hocini M, Shah AJ, et al. Noninvasive panoramic mapping of human atrial fibrillation mechanisms: a feasibility report. J Cardiovasc Electrophysiol. 2013;24(6):711-7.

57. Wang Y, Cuculich PS, Zhang J, et al. Noninvasive electroanatomic mapping of human ventricular arrhythmias with electrocardiographic imaging. Sci Transl Med. 2011;31;3(98):98ra84.

58. Marrus SB, Andrews CM, Cooper DH, et al. Repolarisation changes underlying long-term cardiac memory due to right ventricular pacing: noninvasive mapping with electrocardiographic imaging. Circ Arrhythm Electrophysiol. 2012;5(4):773-81.

59. Mettler FA Jr, Huda W, Yoshizumi TT, et al. Effective doses in radiology and diagnostic nuclear medicine: a catalog. Radiology. 2008 Jul;248(1):254-63.

60. Pfeifer B, Hanser F, Seger M, et al. Patient-specific volume conductor modeling for non-invasive imaging of cardiac electrophysiology. Open Med Inform J. 2008;2:32-41.

61. Berger T, Fischer G, Pfeifer B, et al. Single-beat noninvasive imaging of cardiac electrophysiology of ventricular pre-excitation. J Am Coll Cardiol. 2006;48:2045-2052.

62. Berger T, Pfeifer B, Hanser FF, et al. Single-beat noninvasive imaging of ventricular endocardial and epicardial activation in patients undergoing CRT. PLoS One 2011;27;6(1):e16255.

63. Denisov AM, Zakharov EV, Kalinin AV, et al. Numerical Methods for Some Inverse Problems of Heart Electrophysiology. Differential Equations 2009;45;7:1034–1043.

64. Lai D, Liu C, Eggen MD, et al. Localisation of endocardial ectopic activity by means of noninvasive endocardial surface current density reconstruction. Phys Med Biol. 2011;7;56(13):4161-76.

65. Lai D, Sun J, Li Y, et al. Usefulness of ventricular endocardial electric reconstruction from body surface potential maps to noninvasively localize ventricular ectopic activity in patients. Phys Med Biol. 2013;7;58(11):3897-909.

66. Toussaint N, Stoeck CT, Schaeffter T, et al. In vivo human cardiac fiber architecture estimation using shape-based diffusion tensor processing. Med Image Anal. 2013;17(8):1243-55.

06

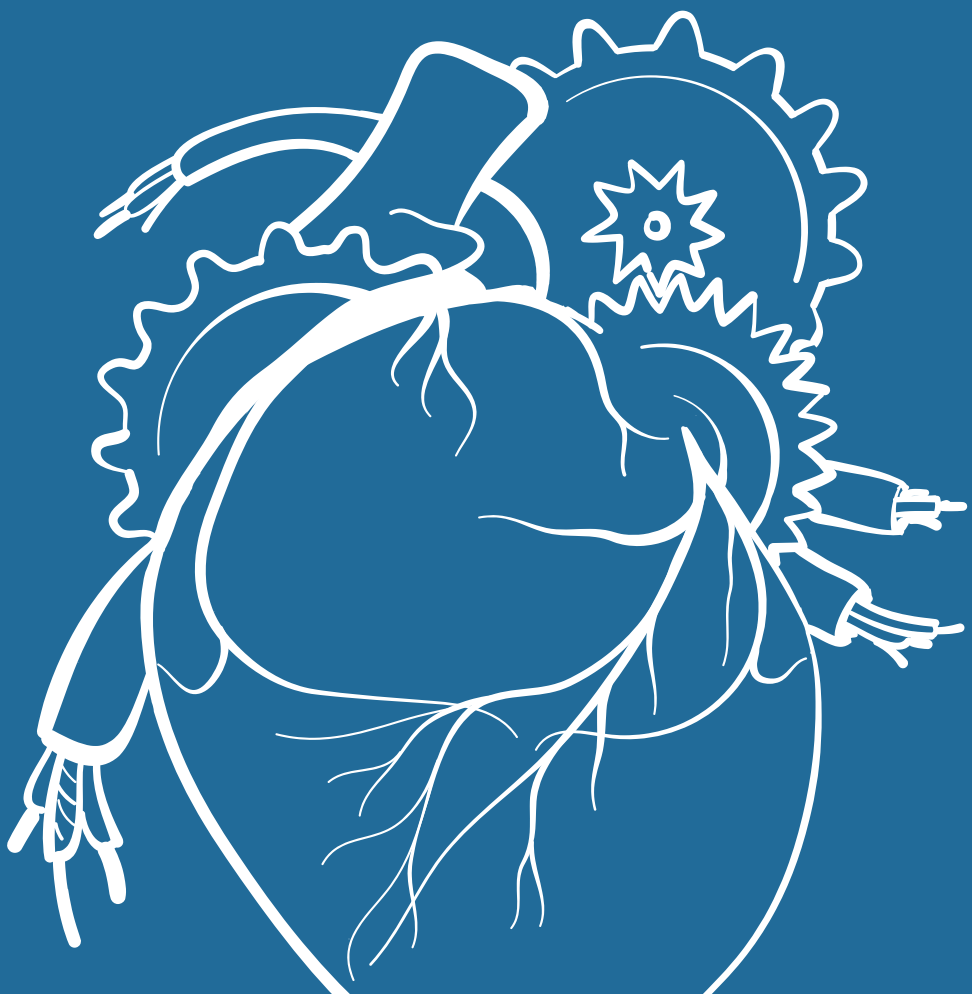

COMPUTING BODY VOLUME POTENTIALS FOR INVERSE POTENTIAL MAPPING

van der Graaf AW, Bhagirath P, van Driel VJ,
Ramanna H, de Hooge J, de Groot NM, Götte MJ.
Annals of Noninvasive Electrocardiology. 2015;20(2):132-139.

ABSTRACT

Background: In non-invasive imaging of cardiac excitation, the use of body surface potentials (BSP) rather than body volume potentials (BVP) has been favoured due to enhanced computational efficiency and reduced modelling effort. Nowadays, increased computational power and the availability of open source software enable the calculation of BVP for clinical purposes. In order to illustrate the possible advantages of this approach, the explanatory power of BVP is investigated using a rectangular tank filled with an electrolytic conductor and a patient specific three-dimensional model.

Methods: MRI images of the tank and of a patient were obtained in three orthogonal directions using a turbo spin echo MRI sequence. MRI images were segmented in three-dimensional using custom written software. Gmsh software was used for mesh generation. BVP were computed using a transfer matrix and FEniCS software.

Results: The solution for 240,000 nodes, corresponding to a resolution of 5 mm throughout the thorax volume, was computed in 3 minutes. The tank experiment revealed that an increased electrode surface renders the position of the 4 V equipotential plane insensitive to mesh cell size and reduces simulated deviations. In the patient-specific model, the impact of assigning a different conductivity to lung tissue on the distribution of volume potentials could be visualised.

Conclusion: Generation of high quality volume meshes and computation of BVP with a resolution of 5 mm is feasible using generally available software and hardware. Estimation of BVP may lead to an improved understanding of the genesis of BSP and sources of local inaccuracies.

INTRODUCTION

Non-invasive imaging of cardiac excitation using recorded body surface potentials (BSP) and mathematical inverse procedures is an active field of research that has yielded some clinical applications [1-4]. In an inverse procedure, local epicardial potentials or myocardial activation times are computed from recorded BSP. In contrast, a forward procedure estimates BSP from potentials measured on the surface of the heart [5-6].

The Boundary Element Method (BEM) has been favoured for electrocardiographic forward procedures due to enhanced computational efficiency and reduced modelling effort [7-9]. In contrast to the BEM, which yields potential information on predefined surfaces, the Finite Element Method (FEM) provides body volume potentials (BVP) (**figure 1**) [10].

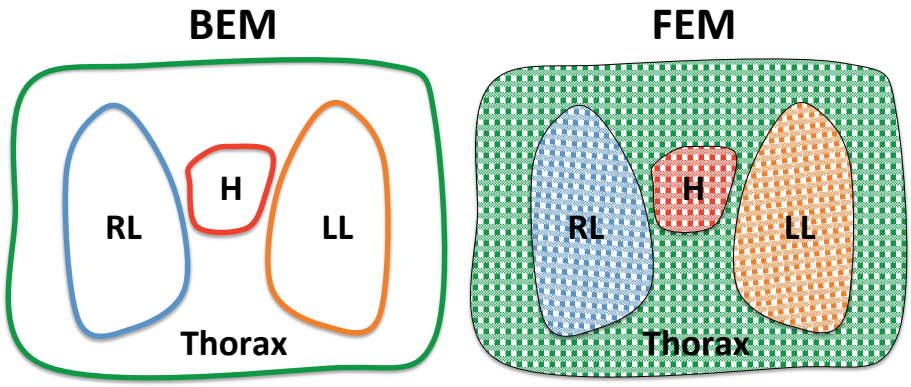

Figure 1. The Boundary Element Method (BEM) yields potential information on predefined *surfaces* only. Hence, no information on the areas between the compartments can be derived when using the BEM. The Finite Element Method (FEM) on the contrary, provides body *volume* potentials (BVP). Volume potentials can be computed as well using the BEM, by increasing the number of model compartments. However, the FEM is typically more efficient, especially when the number of model compartments is high or when anisotropic conductivity is modelled. (RL right lung; LL left lung; H heart; L liver)

Utilizing knowledge on the spatial potential field may lead to improved insight in the potential distribution throughout the thorax. Although potentials can be computed everywhere in a volume as well using the BEM by creating multiple surfaces inside the

volume, the FEM is typically more efficient for this purpose. Especially when the number of model compartments is high or when anisotropic conductivity is modelled, the FEM is recommended [11].

Although the application of BVP has been studied previously [12-13], it has never advanced into clinical practice due to its time consuming and elaborative nature. Increased computational power and the introduction of open source software enable the calculation of BVP for clinical purposes. In this study the explanatory power of BVP is illustrated by experiments performed in a simple rectangular tank. In addition, simulations in a 3D patient specific model demonstrate the possible advantage of using BVP.

METHODS

Rectangular tank

A rectangular tank of 33 x 25 x 25 cm filled with an electrolytic conductor was used. Electrodes with a surface of 2 x 2 cm were positioned in the middle of opposing sides. To block interference from nearby power sources, a 1000 Hz 8 V peak-to-peak sinusoidal power source was used. Measurements were performed using a dual beam oscilloscope, enabling monitoring the source voltage while measuring the resulting potential in the tank. The accuracy of the measurements approximated 2%, which was considered sufficient for validation purposes.

MRI images

MRI images of the rectangular tank and the patient were acquired using a Turbo Spin Echo (Black Blood) sequence in three orthogonal directions (slice thickness 8mm). Electrode positions in the tank and on the body surface were marked using liquid-filled vitamin D capsules, appearing hyper intense on MRI. The MRI scan was performed on a Siemens Aera 1.5 Tesla MRI scanner (Siemens Healthcare, Erlangen, Germany).

The study complied with the declaration of Helsinki and received approval from the local ethical committee and the institutional scientific board. Written informed consent was obtained from the patient.

Meshing

In order to achieve topological propriety, MRI images were segmented in 3D using bounding planes. No spatial smoothing was applied. The Gmsh tool [14], freely available on the Internet for non-commercial use, was used for mesh generation.

Computing BVP

Given the source potential distribution on the epicardial surface, the resulting volume potential distribution is governed by the equations below.

The current density J as a function of conductivity s and field strength E is given by ohms law:
$J = s\,E = s\,\mathrm{grad}(P)$, where P is the potential [1]

Apart from the heart there are no current sources in the thorax so:
$\mathrm{div}(J) == 0$ [2]

From [1] and [2] follows Laplace's equation:
$\mathrm{div}(s\,\mathrm{grad}(P)) == 0$ [3]

Multiplying by a test function T leads to the following variational form:
$\int \mathrm{div}(s\,\mathrm{grad}(P))\,T\,dV == \int 0 * T\,dV == 0$ [4]

Partial integration yields (n is the unit surface normal):
$\int \mathrm{div}\,(s\,\mathrm{grad}(P)\,T\,dV == \int s\,\mathrm{grad}(P).\mathrm{grad}(T)dV - \int s\,\mathrm{grad}(P).n\,T\,dS$ [5]

From [4] and [5] follows:
$\int s\,\mathrm{grad}(P).\mathrm{grad}(T)\,dV == \int s\,\mathrm{grad}(P).n\,T\,dS$ [6]

With J.n = 0 and [1] at the skin this becomes:
$\int s\,\mathrm{grad}(P).\mathrm{grad}(T)\,dV = 0$ [7]

To yield a non-trivial solution, the source potentials at the heart surface are applied as boundary conditions. There are many general-purpose FEM tools available to solve these equations. FEniCS [15], freely available for research purposes, was selected.

This software package allowed the aforementioned equation to be specified in a very natural form. All work is done by the following lines of code:

```
RHS=sigma*inner(grad(trialFunction),grad (testFunction)) * dx [1]

LHS = Constant (0)* testFunction * dx [2]

A,b = assemble_system(LHS,RHS,boundaryCond,keep_diagonal = True) [3]

solve(A,potential.vector(),b,'gmres','default') [4]
```

Note the close correspondence between lines [1] and [2] of the code and equation [6] by substituting them in equation LHS = RHS.

Computing platform

All analyses were performed on a 2.4 GHz quadcore laptop running Windows 8 OS. Solving the potential equations was delegated to a an Ubuntu 12.10 virtual machine running on this laptop, communicating with the activation modelling software by the use of synchronised message file sharing. Reference times were computed using a single core.

RESULTS

Rectangular tank

Figure 2 shows the 3D mesh of the tank. A potential of 4V peak to peak was observed in the middle of the tank. The computations using a tetrahedral mesh with 1.5 cm edge length, demonstrated a deviation of the 4V plane from the middle by about one grid cell. By refining the mesh to an edge length of 0.5 cm, this deviation was expected to diminish. Paradoxically, the deviation from the middle actually increased by about 2.5 cm, to a total deviation about 10 times larger than the mesh size (**figure 2a**).

Figure 2b and c reveal the potential gradients to increase near to the electrode. This is caused by the small contact area between the fluid and the electrodes introducing a high resistivity: R = 1 / (area x sigma) [Ohm/m]. Because R is large, the potential drop U is large according to Ohms law. Moreover, a relative misrepresentation of the electrode area by 5% leads to a relative error in this potential drop in the same order of magnitude.

Figure 2d illustrates that minor errors in the potential drop near the electrodes yield large deviations in the 4V equipotential plane. In the middle of the tank the x coordinate varies rapidly with small potential changes. By using volume information, the counterintuitive effect shown in **figure 2a** can be understood. For large electrodes, misrepresentations of their area by the mesh are relatively small. This should render the position of the 4V equipotential plane insensitive to the mesh cell size (**figure 2e**).

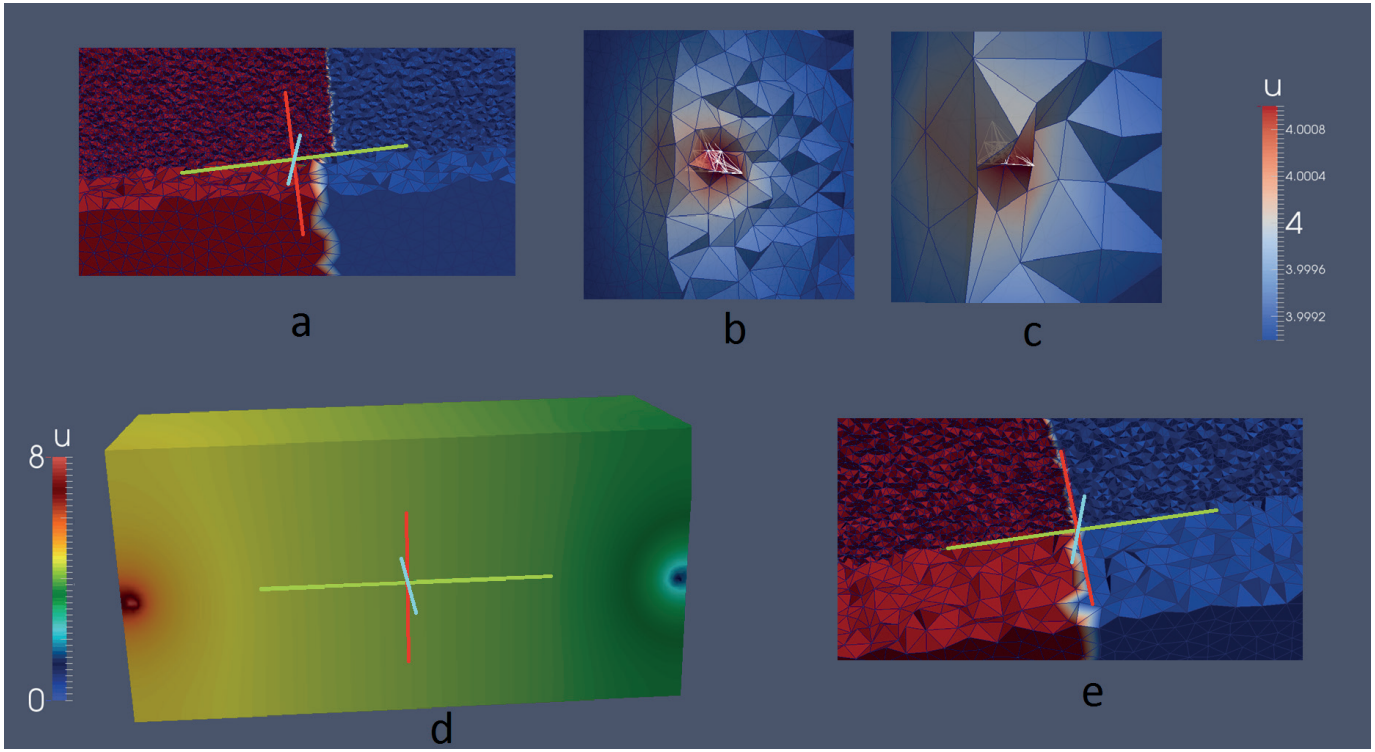

Figure 2. (a) Using a tetrahedral mesh with an edge length of 1.5 cm computed position of the 4V equipotential plane (white) deviates from the measured position that was in the middle of the tank. Refining the mesh to an edge length of 0.5 cm increases the deviation. A large potential drop was observed in the vicinity of positive electrode, which is indicated by the white wireframe, both for the fine **(b)** and the crude **(c)** grid. Artifacts depend on the exact location of the grid cells with respect to the electrodes, which may be coincidentally more asymmetric with the fine grid. **(d).** In the middle of the tank, the x coordinate (green axis) varies rapidly as a function of the potential. **(e).** Large electrodes render the position of the 4V equipotential plane insensitive to the mesh cell size at the same time decreasing the deviation from the middle.

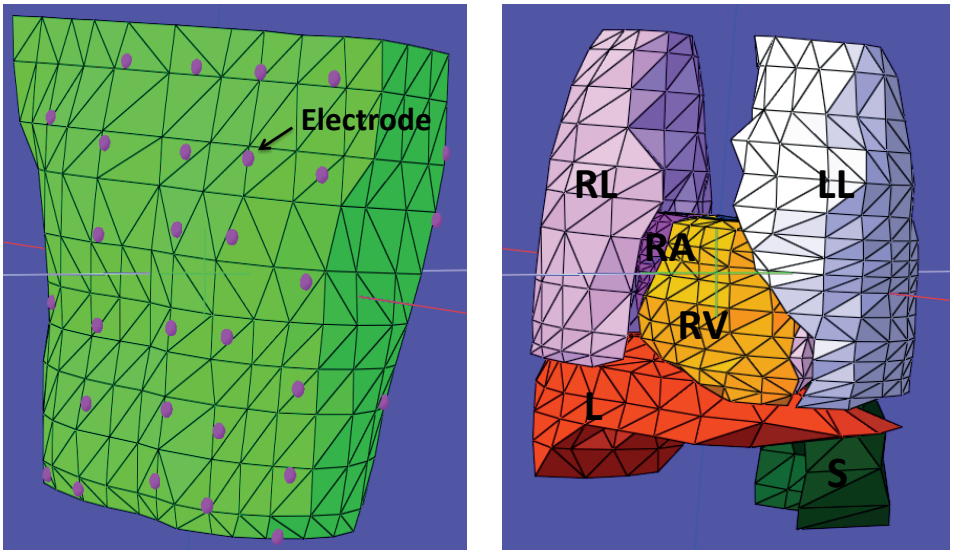

Figure 3. A 3D computer model of the human thorax with the positions of the body surface electrodes **(A)**. The electrode positions were derived from the positions of the liquid-filled vitamin D capsules, appearing hyper intense on MRI. The thorax model contains multiple compartments **(B).** (RA right atrium; RV right ventricle; S spleen)

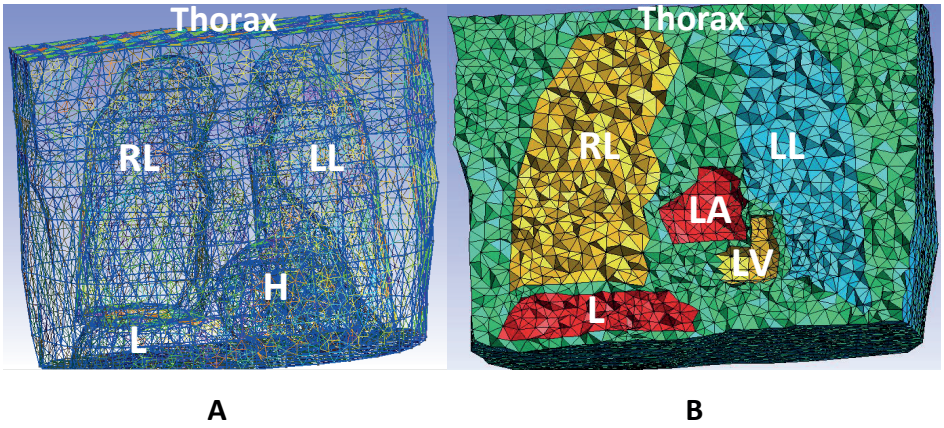

Figure 4. Locally refined multi compartment thorax 3D mesh **(A)** and volume mesh **(B)**. The mesh is error free and was generated in 25 seconds using freely available software on a 2.4 GHz single core on a laptop. No spatial smoothing was applied. (LA left atrium; LV left ventricle)

Patient torso

Figure 3 shows a multi compartment 3D computer model of a human thorax. The positions of the electrodes on the body surface were derived from the anatomic markers on MRI. **Figure 4** demonstrates the resulting 3D mesh. As can be observed the mesh is highly regular and is locally refined in the vicinity of details.

Shortest Paths of Activation

The computation of all possible shortest paths of the activation wavefront through the cardiac wall resulted in a set of epicardial isochrones yielding a time dependent epicardial potential as shown in **figure 5**.

Computing BVP

Potential equations for 13,000 mesh nodes were solved in 3 seconds utilizing a 2.4 GHz single core. Solving these equations for a mesh consisting of 240,000 nodes, corresponding to a resolution of 5 mm throughout the thorax volume, lasted 3 minutes. Two sequences of computed BVP are shown in **figure 6**, one using a mesh edge size of 0.5cm (a-j) and one using a mesh edge size of 1.5cm (k-t). The potential field permeates the lungs without visual deformation, even if their sigma is only half that of their environment.

Impact of lung tissue on BVP

The impact of variable organ conductivity on BVP was investigated using forward simulations in the human torso model. **Figure 7** illustrates the impact on the electric field when a smaller sigma (conductivity) is assigned to lung tissue **(A)**. The BVP field is compared to simulations in a homogeneous torso model **(B)**. A smaller sigma of the lung tissue leads to an increased breakthrough of the potential field.

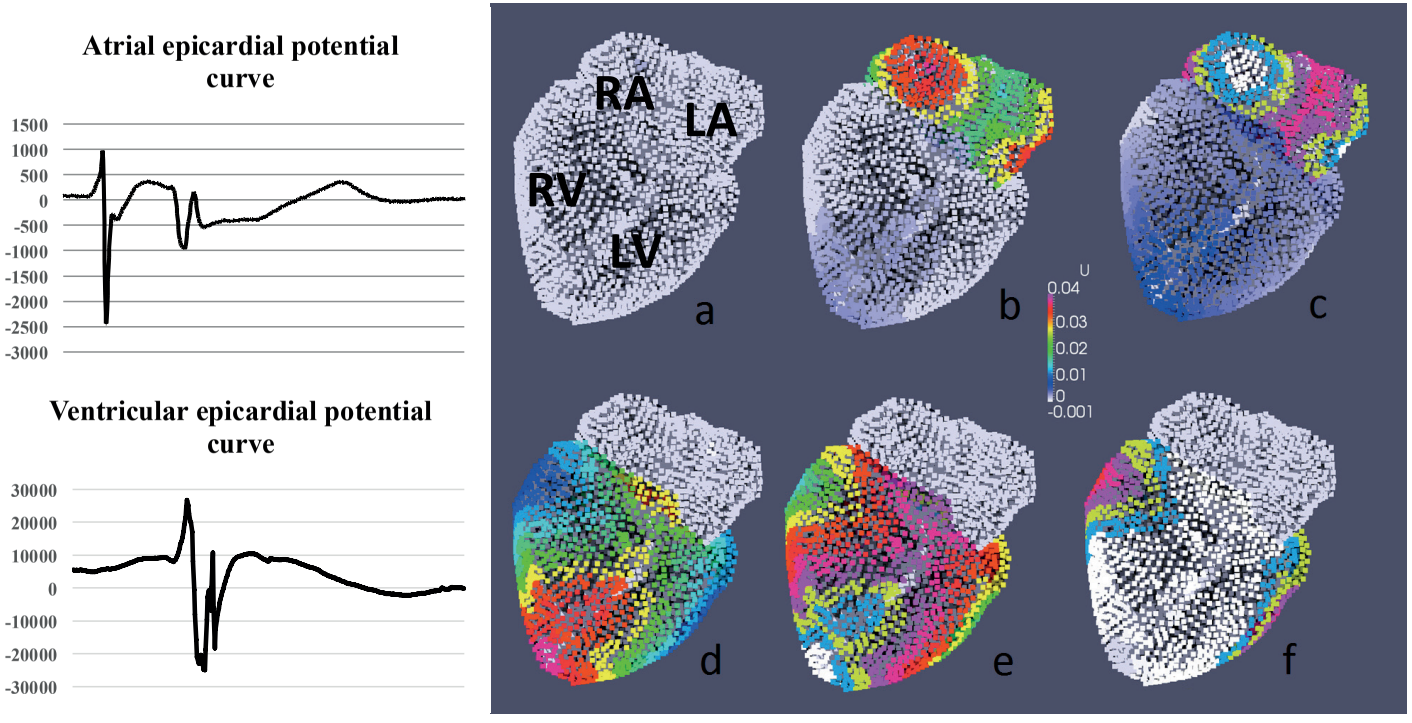

Figure 5a-f. Snapshots of the time dependent epicardial potential, taken from a sequence of 50 time steps. On the left, an example of atrial (top) and ventricular (bottom) epicardial potentials is displayed.

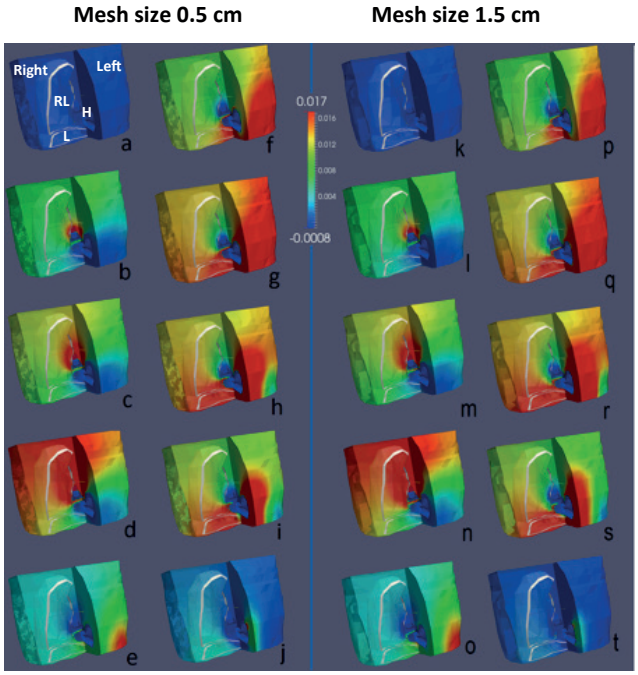

Figure 6. Anterior view of the thorax. Shown are the computed BVP during one heartbeat. **(a-j)** Mesh edge size is 0.5 cm. **(k-t)** Mesh edge size is 1.5 cm. The crude edges are artifacts from segmentation, performed in 3D. Since topology had to be preserved, no spatial smoothing was applied.

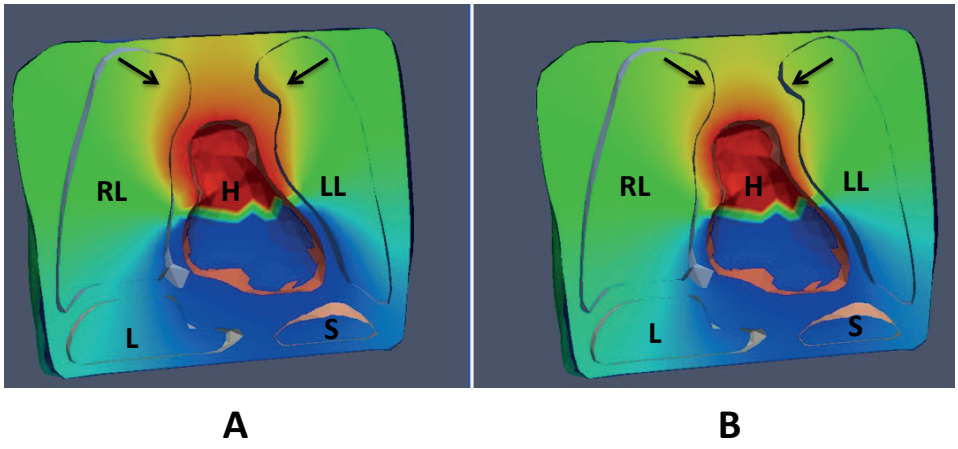

Figure 7. The impact of variable organ conductivity on BVP. A smaller sigma of the lung tissue leads to an increased breakthrough of the potential field **(A),** compared to simulations in a homogeneous torso model **(B)**.

DISCUSSION

In this study the feasibility of computing BVP for non-invasive imaging of cardiac excitation is illustrated. So far, volume potentials have been considered to be of limited value. However, computing BVP using the FEM is efficient if the number of bounding surfaces between organs taken into account is high. In addition, using the FEM rather than the BEM enables the incorporation of different anisotropies, local tissue characteristics and sigma gradients over different regions. BVP may be used to gain a better insight in the genesis of BSP and sources of local inaccuracies.

Figure 6 suggests that the computed BVP hardly depend on the mesh cell characteristic length for a ratio as big as 1:3. However, the tank experiment indicates that there are geometries where the mesh size does have a significant influence on the outcome. The FEM could be used to understand which aspects of the geometry caused the large misrepresentation of the 4V equipotential plane. By visualizing the large potential gradient near the electrodes and the small potential gradient in the middle of the box, the FEM contributed to understanding the inaccuracy of the computed position of the 4V equipotential plane.

Computation of BVP

From a computational standpoint, computing a potential field by means of the FEM is not a problem. The computation time of a 240,000 points potential field was approximately 3 minutes. Graphics processors with hundreds of computation units combined with quadcore main CPU's are becoming available at consumer prices. Generally available FEM packages are able to benefit from this just by setting some parameters and no custom coding. While the performance gain by computing the FEM in parallel may easily be tenfold. The FEniCS package has been selected because this tool has a lot of mindshare, a vivid user community and excellent documentation.

Meshing

Generating high quality meshes and solving differential equations have been part of engineering disciplines for decades. In many articles on biomedical computing, generation of a computational mesh is taken for granted. Early experiments revealed that generation of a surface mesh from a labelled voxel set often leads to irregular meshes with topological errors that are hard to repair. Several groups have developed their own meshing software and others have proposed to do away with meshing altogether [16-18]. However, the meshing itself does not appear to be the problem.

General-purpose mesh generation tools can generate high quality volume meshes in a matter of seconds for an arbitrarily complex segmentation result, provided that the segmentation contains no topological errors.

Fast generation of volume meshes and FEM solutions with generally available means has brought computation of BVP as part of non-invasive imaging of cardiac excitation within practical clinical reach. This route will further be explored, hoping to gain direct and visual insight in the sources of inaccuracies, including the so called "ill conditioning" of the inverse problem, in the required number of electrodes, numbers of less than 20 to more than 200 currently being advocated in literature [19-20], and in the optimal placement of these electrodes in individual patients.

CONCLUSION

This study illustrates that efficient generation of high quality volume meshes and computation of BVP with a resolution of 5 mm is feasible using generally available software and hardware. With the computational effort decreasing dramatically, estimation of BVP may be seasonable when the number of model compartments is high or when anisotropic conductivity is modelled. Observing the potential field everywhere in the thorax may lead to an improved understanding of the genesis of BSP and sources of local inaccuracies. In the near future, computation of BVP for non-invasive imaging of cardiac excitation may evolve towards clinical application.

REFERENCES

1. Desouza KA, Joseph SM, Cuculich PS, Ewald GA, Rudy Y. Non-invasive mapping of ventricular activation in patients with transplanted hearts. J Electrocardiol. 2013;46(6):698-701.
2. Sapp JL, Dawoud F, Clements JC, Horácek BM. Inverse solution mapping of epicardial potentials: quantitative comparison with epicardial contact mapping. Circ Arrhythm Electrophysiol. 2012;5(5):1001-9.
3. Galeotti L, van Dam PM, Loring Z, Chan D, Strauss DG. Evaluating strict and conventional left bundle branch block criteria using electrocardiographic simulations. Europace 2013;15(12):1816-1821.
4. Berger T, Pfeifer B, Hanser FF, Hintringer F, Fischer G, Netzer M, Trieb T, Stuehlinger M, Dichtl W, Baumgartner C, Pachinger O, Seger M. Single-beat non-invasive imaging of ventricular endocardial and epicardial activation in patients undergoing CRT. PLoS One 2011;27;6(1):e16255.
5. Gulrajani RM. The forward and inverse problems of electrocardiography. IEEE Eng Med Biol Mag. 1998;17(5):84-101.
6. van der Graaf AW, Bhagirath P, Ramanna H, van Driel VJ, de Hooge J, de Groot NM, Götte MJ. Noninvasive imaging of cardiac excitation: current status and future perspective. Ann Noninvasive Electrocardiol. 2014 Mar;19(2):105-13.
7. Stenroos M, Haueisen J. Boundary element computations in the forward and inverse problems of electrocardiography: comparison of collocation and Galerkin weightings. IEEE Trans Biomed Eng. 2008;55(9):2124-33.
8. Wang Y, Rudy Y. Application of the method of fundamental solutions to potential-based inverse electrocardiography. Ann Biomed Eng. 2006;34(8):1272-88.
9. Van Dam PM, Oostendorp TF, Linnenbank AC, Oosterom A van. Non-invasive imaging of cardiac activation and recovery. Ann Biomed Eng. 2009;37(9):1739-56.
10. Hunter P. FEM/BEM notes. CMISS Auckland Bioengineering Institute and Engineering Science, The University of Auckland, New Zealand. October 8, 2008:1-140.
11. Shahidi AV, Savard P, Nadeau R. Forward and inverse problems of electrocardiography: modeling and recovery of epicardial potentials in humans. IEEE Trans Biomed Eng. 1994;41(3):249-56.
12. Klepfer RN, Johnson CR, Macleod RS. The effects of inhomogeneities and anisotropies on electrocardiographic fields: a 3-D finite-element study. IEEE Trans Biomed Eng. 1997;44(8):706-19.
13. Wang D, Kirby RM, Macleod RS, Johnson CR. Inverse Electrocardiographic Source Localisation of Ischemia: An Optimisation Framework and Finite Element Solution. J Comput Phys. 2013;1;250:403-424.
14. Marchandise E, Geuzaine C, Remacle JF. Cardiovascular and lung mesh generation based on centerlines. Int J Numer Method Biomed Eng. 2013;29(6):665-82.

15. Mortensen M, Langtangen HP, Wells GN. A FEniCS-based programming framework for modeling turbulent flow by the Reynolds-averaged Navier-Stokes equations. Advances in Water Resources. 2011. DOI: 10.1016/j.advwatres.2011.02.013.
16. Wang Y, Rudy Y. Meshless methods in potential inverse electrocardiography. Conf Proc IEEE Eng Med Biol Soc. 2006;1:2558-9.
17. Li ZS, Zhu SA, He B. Solving the ECG forward problem by means of a meshless finite element method. Phys Med Biol. 2007;7;52(13):N287-96.
18. Chinchapatnam P, Rhode K, Ginks M, Nair PB, Razavi R, Arridge SR, Sermesant M. Voxel Based Adaptive Meshless Method for Cardiac Electrophysiology Simulation. Lecture Notes in Computer Science 2009;5528:182-190.
19. Rudy Y. Noninvasive electrocardiographic imaging of arrhythmogenic substrates in humans. Circ Res. 2013;1;112(5):863-74.
20. Van Dam PM, Tung R, Shivkumar K, Laks M. Quantitative localisation of premature ventricular contractions using myocardial activation ECGI from the standard 12-lead electrocardiogram. J Electrocardiol. 2013;46(6):574-9.

07

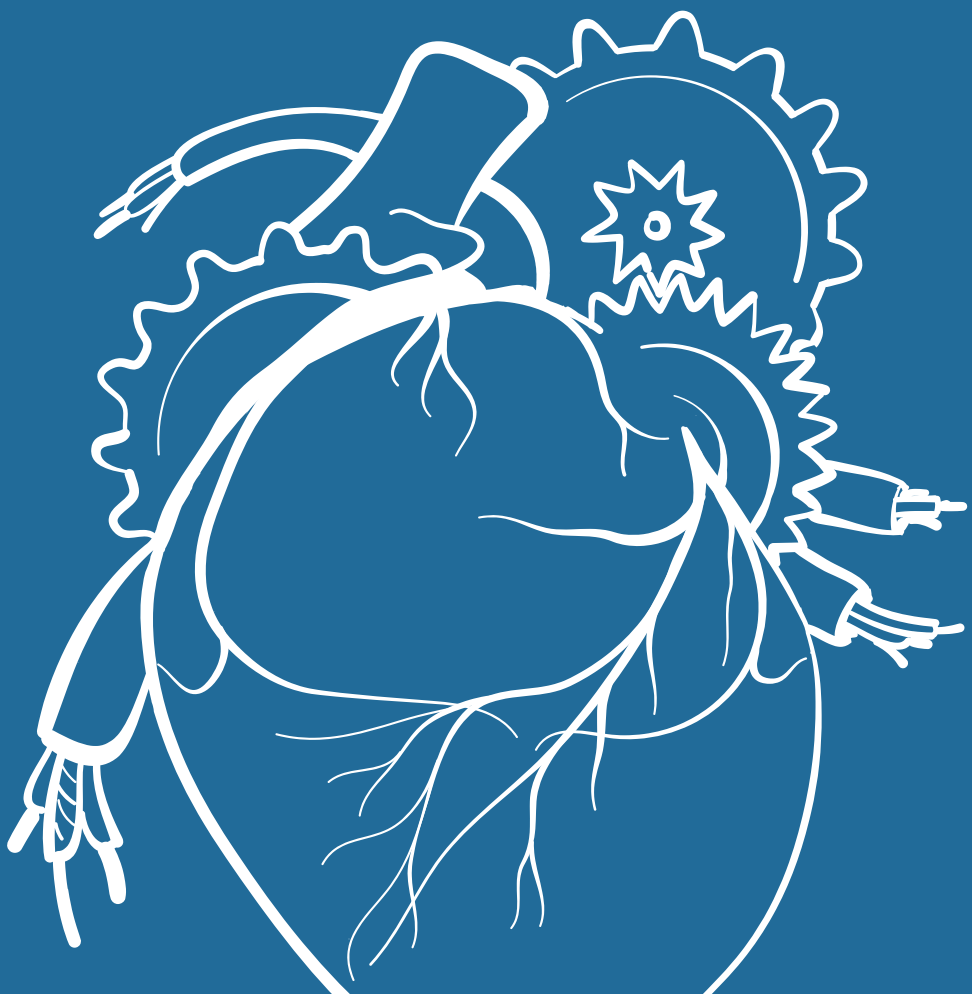

INTEGRATED WHOLE-HEART COMPUTATIONAL WORKFLOW FOR INVERSE POTENTIAL MAPPING AND PERSONALISED SIMULATIONS

Bhagirath P, van der Graaf AW, de Hooge J, de Groot NM, Götte MJ.
Journal of Translational Medicine. 2016;14;1-7.

ABSTRACT

Background: Integration of whole-heart activation simulations and inverse potential mapping (IPM) could benefit the guidance and planning of electrophysiological procedures. Routine clinical application requires a fast and adaptable workflow. These requirements limit clinical translation of existing simulation models. This study proposes a comprehensive finite element model (FEM) based whole-heart computational workflow suitable for IPM and simulations.

Methods: Three volunteers and eight patients with premature ventricular contractions underwent body surface potential (BSP) acquisition followed by a cardiac MRI scan. The cardiac volumes were segmented from the MRI images using custom written software. The feasibility to integrate tissue-characteristics was assessed by generating meshes with virtual edema and scar. Isochronal activation maps were constructed by identifying the fastest route through the cardiac volume using the Möller–Trumbore and Floyd–Warshall algorithms. IPM's were reconstructed from the BSP's.

Results: Whole-heart computational meshes were generated within seconds. The first point of atrial activation on IPM was located near the crista terminalis of the superior vena cave into the right atrium. The IPM demonstrated the ventricular epicardial breakthrough at the attachment of the moderator band with the right ventricular free wall. Simulations of sinus rhythm were successfully performed. The conduction through the virtual edema and scar meshes demonstrated delayed activation or a complete conductional block respectively.

Conclusion: The proposed FEM based whole-heart computational workflow offers an integrated platform for cardiac electrical assessment using simulations and IPM. This workflow can incorporate patient-specific electrical parameters, perform whole-heart cardiac activation simulations and accurately reconstruct cardiac activation sequences from BSP's.

BACKGROUND

Inverse potential mapping (IPM) and simulations of cardiac activation are promising computational techniques for non-invasive assessment of rhythm disorders [1-2]. Recent studies have examined the role of simulation models for personalizing catheter ablation strategies [3-4]. Furthermore, catheter ablation guidance by IPM shows a higher accuracy when compared to conventional mapping procedures [5-6].

In general, IPM requires a (computational) mesh representing the thoracic and cardiac volumes to reconstruct cardiac activation sequences from body surface potentials (BSP). Similarly, realistic simulations demand for a patient-specific mesh, incorporating functional information about tissue characteristics such as electrical conductivity, mechanical deformation and fiber orientation [3,4,7]. In contrast to meshes used solely for visualisation (shells), the computational meshes for these purposes require topologically correct segmentations.

Although the currently available models are useful, they are very time consuming [4], or too comprehensive (multiple parameters) [7], and therefore not ready for use on a routine basis in the clinical arena.

In addition, none of the currently available methods provide an integrated whole-heart (topologically correct) mesh, incorporating both the atria and ventricles. This limits a comprehensive and integrated study of whole-heart electrical interaction.

This article proposes a comprehensive finite element model based whole-heart computational workflow suitable for IPM and efficient personalised simulations. The clinical feasibility of reconstructing IPM was explored using BSP's of healthy volunteers and patients with premature ventricular contractions (PVC's).

Subsequently, the simulation features were explored by generating activation maps (isochrones) in different models of human hearts, both normal and with structural heart disease.

METHODS

The computational workflow for whole-heart electrical assessment consists of four steps (**figure 1**). These steps involve (1) acquisition of BSP, (2) acquisition of subject specific geometry using cardiac magnetic resonance imaging (MRI), (3) topologically correct segmentation and generation of the computational mesh and (4) utilizing the mesh for reconstructing cardiac surface potentials or conducting simulations.

Study population

Three healthy volunteers and eight patients with symptomatic or therapy resistant premature ventricular contractions (PVC) participated in this investigation. The study complied with the declaration of Helsinki and received approval from the local ethical committee (METC Zuidwest Holland study number NL38156.098.11) and the institutional scientific board. Written informed consent was obtained from the volunteers.

Body surface potential acquisition

An MRI scout scan was performed to approximate the position of the heart with respect to the thorax. Subsequently, 62 (+3 limbs) electrodes were applied to the subject's torso, centralised over the heart. Body surface potentials (BSP) were acquired using a 65 channel ActiveTwo system (BioSemi B.V., Amsterdam, The Netherlands). Once the acquisition was completed, the electrode locations were marked with MRI markers enabling accurate identification of the electrode positions.

Image acquisition

MRI studies were obtained on a 1.5 Tesla Aera scanner (Siemens Healthcare, Erlangen, Germany). Blackblood imaging was performed using a Half-Fourier Acquisition Single Shot Turbo Spin Echo (HASTE) pulse-sequence to acquire three perpendicular stacks (axial, coronal and sagittal). The scan provides coverage from the neck till lower abdomen. Images were acquired during free breathing using navigator gating (diaphragm) with 1 mm window. ECG gating was used to acquire views during the diastolic phase of the cardiac cycle. Typical imaging parameters were: a spatial resolution of $1.2 \times 1.2 \times 6$ mm, TR/TE 744/42 ms and flip angle = 160°.

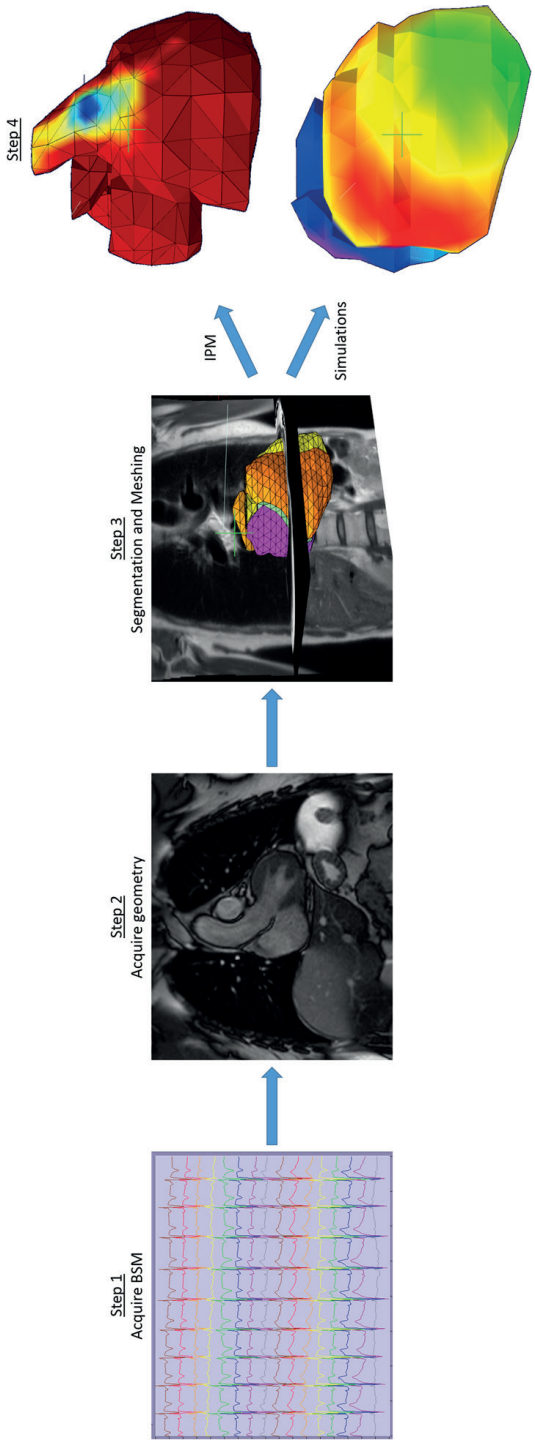

Figure 1. Workflow of the integrated whole-heart computational models. *Step 1* represents the acquisition of the multichannel body surface potentials; *step 2* acquisition of geometry in 3D (1D shown); *step 3* depicts the topologically correct whole-heart segmentation in the transversal and coronal plane of a volunteer; *step 4* the workflow can generate both inverse potential maps (*top*) and simulations (*bottom*) using the information supplied in the previous steps.

WHOLE-HEART COMPUTATIONAL MODEL

Anatomical and electrical components

A topologically correct description of the whole-heart anatomy was constructed using the different cardiac structures such as atrial and ventricular endocard and epicard, the inter-ventricular septum (IVS) and inter-atrial septum (IAS), and tricuspid and mitral valvular plane (Additional file 1: Video 1). These different structures were used to generate the cardiac volumes required to represent a whole-heart. In order to incorporate the electrical pathways and to account for the differences in conductivity, the conduction system of the heart was also modelled. The origin of activation for sinus rhythm was defined at the lateral border of the superior vena cava and right atrium junction, approximating the location of the sinus node. The right and left bundle branches were also defined.

Topology

A formal description was composed to define the topological properties of the segmentation result. This description contained a definition of all tissue volumes involved in terms of topological elements, i.e. patches, shells and hulls.

Patch

A patch is a set of facets denoting an elementary surface part. Example: patches.heart_LA_outer = Patch (index) denotes the outer surface of the left atrium. A unique colour index describes the relation between the topological description and the coloured planes that make up the segmentation.

Shell

A shell is a set of patches denoting a closed surface. Example: shells.heart_outer = Shell patches.heart_LA_outer,_patches.heart_RA_outer,_patches.heart_LV_outer,_patches.heart_RV_outer) denote the whole outer surface of the heart.

Hull

A hull is a three dimensional piece of tissue having uniform properties which may be irregularly shaped. A hull is bound by one or more shells where the first-mentioned shell is the outer surface of the hull and remaining shells are the inner surfaces of holes in the hull. Example: hulls.heart = Hull (shells.heart_outer, shells.heart_LA_inner, shells.heart_RA_inner, shells.heart_LV_inner, shells.heart_RV_inner) denote the hart walls. In this example the heart is simplistically pictured as a closed volume with four holes, two for the atria and two for the ventricles.

Image segmentation and mesh generation

The three perpendicular stacks of MRI images were loaded in a custom developed software tool. Subsequently, the pre-defined anatomical and electrical components were segmented. The extra-cardiac thoracic volumes (lungs and thorax) were assigned conductivity values (Σ) described in the literature; lungs (0.04 S/m) and thorax (0.2 S/m) [8]. To investigate the feasibility of incorporating tissue properties, two segmentations were created containing pre-defined regions of edema (speed 0.2 m/s and Σ 0.0325 S/m) and scar tissue (speed 0 m/s and Σ 0 S/m) respectively.

The software tool was used to generate a script containing the geometrical description of the topologically correct segmentation result. From this script input a high quality 2D/3D mesh can be instantly generated. This mesh is compound, i.e. it is divided in labelled sub-meshes conforming organ boundaries, and suitable for computational use e.g. sub-volume properties and boundary conditions. The script generated by the segmentation tool was used as input to the GMSH mesh generator to construct the computational mesh [9].

Inverse potential mapping and simulation of cardiac activation

The IPM's were reconstructed by multiplication of the BSP's with $\mathbf{(T^TT+\lambda^2I)^{-1}T^T}$ where T is the transfer matrix and $\lambda = 0.01$. As described previously, this provided the cardiac surface potentials from which the IPM was derived [10]. Simulations were performed using a fixed conduction velocity model. In concordance with the literature, an effective conduction velocity of 0.6 m/s was defined for both atrial and ventricular myocardium [11]. Based on the same literature the bundle branches were assigned a speed (2 m/s) and delay (0 m/s).

The simulations were performed (1) computing direct connections between all mesh nodes using the Möller–Trumbore algorithm [12] followed by (2) solving the shortest path problem amongst the computed paths using the Floyd–Warshall algorithm [13]. The mesh nodes were assigned a potential versus time activation curve. A standard potential curve was chosen for this purpose. For each individual node, this curve was offset by the local activation time which was computed by the first come first serve principle. Based upon the results of the simulations an isochronal activation map was generated.

RESULTS

Baseline characteristics of the three volunteers and eight patients (N = 11) are provided in **table 1**. All volunteers had normal electrocardiograms. In both volunteers and patients the MRI examination was performed in 12 ± 2 min; there were no complications. Clinical characteristics are provided in **table 1**.

Table 1. Clinical characteristics of study patients.

	Volunteers	Patients
n	3	8
Age (years)	28 ± 3	46 ± 13
BMI	22.1 ± 1.4	25.2 ± 6.7
Female (%)	1 (33 %)	7 (88 %)
LVEF (%)	55 ± 2	50 ± 3

Whole-heart computational model

For each individual, five different volumes were defined at the atrial level consisting of the left and right atrium, IAS and the mitral and tricuspid valvular planes. The ventricular volumes were defined as the left and right ventricle and IVS (Additional file 1: Video 1). Limited interaction (<5 min) was required to create the meshes with (virtual) structural heart disease.

Mesh generation was typically completed in seconds and required no further post-processing.

IPM in sinus rhythm

During sinus rhythm, the first point of activation on the potential map of all study patients was located near the crista terminalis of the superior vena cave into the right atrium (**figure 2**a). The first point of ventricular epicardial breakthrough was located at the right ventricular free wall. This corresponds to the location where the moderator band was attached to the ventricular myocardium (**figure 2**b). During this time, a high potential distribution is observed at the right atrial wall, indicating the atrial repolarisation (**figure 2**a).

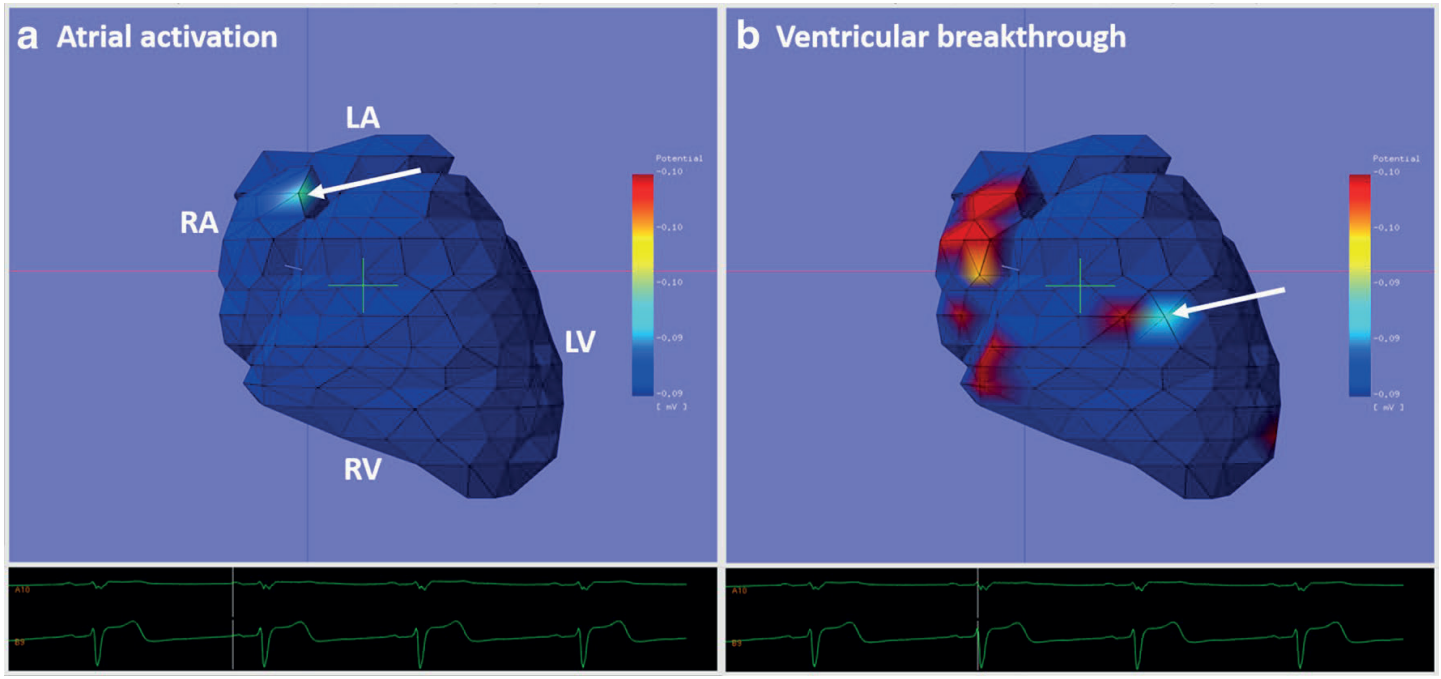

Figure 2. IPM in a healthy volunteer during sinus rhythm. The left panel **a** depicts the IPM at the start of the atrial depolarisation (P wave) and the right panel **b** depicts the IPM at the start of the ventricular depolarisation (QRS). The first point of atrial activation is observed near the entrance of the Superior Vena Cave (*white arrow*) into the Right Atrium. The first point of ventricular epicardial breakthrough is observed at the RV free wall (*white arrow*) at the site of the moderator band.

Simulations

The cardiac activation cycle (sinus rhythm) was successfully simulated on all healthy computational meshes. The generated virtual isochrones maps depicted cardiac activation patterns in accordance with the literature (**Figure 3**; Additional file 2: Video 2) [14]. The simulations for computational meshes with structural abnormalities (edema and scar), were also completed successfully. The mesh with a pre-defined virtual edema region demonstrated a delayed activation pattern (**figure 4**), whereas, a complete conductional block was observed for the computational mesh containing virtual transmural scar (**figure 4**).

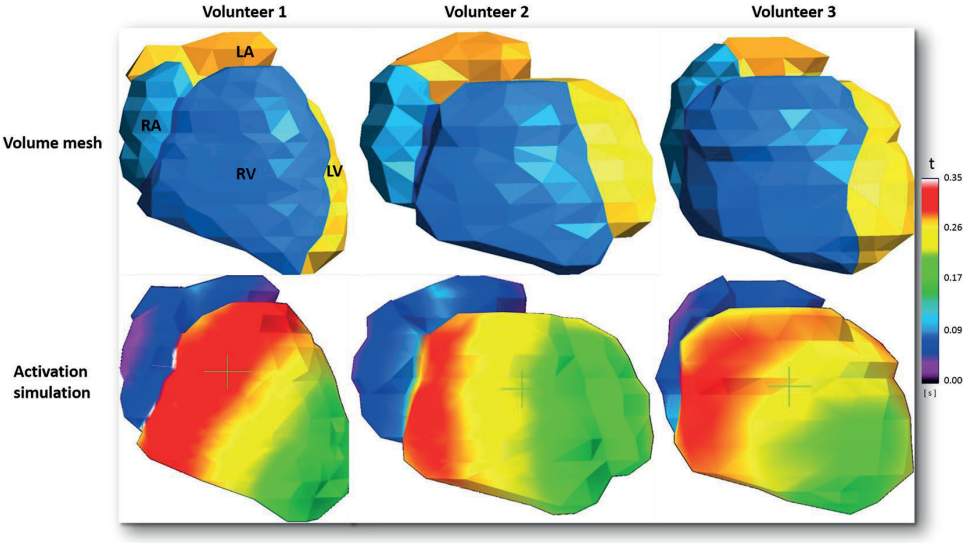

Figure 3. Simulation of normal cardiac activation on whole-heart computational meshes. *Top row* depicts computational volume meshes generated from the three different segmentations. *Bottom row* depicts isochrone maps generated after performing a cardiac activation simulation on the computational mesh.

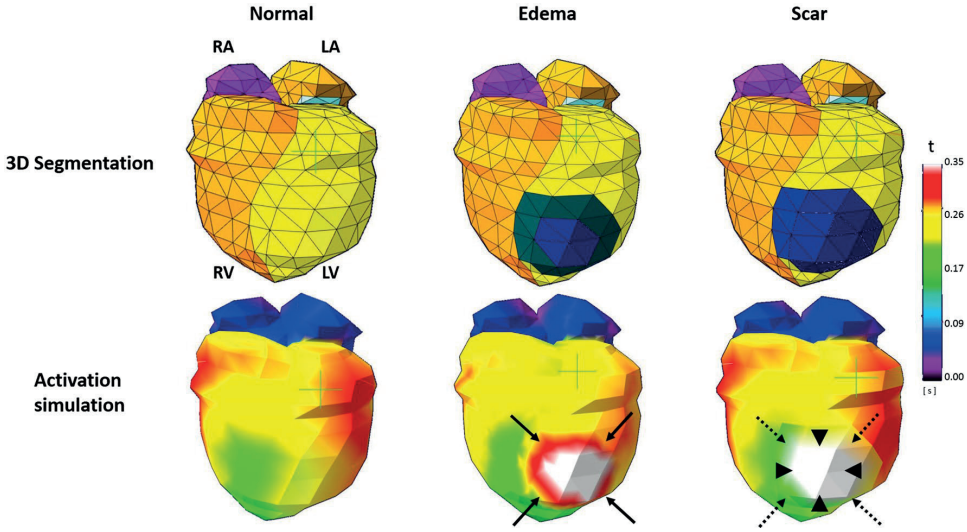

Figure 4. Feasibility of cardiac activation simulation on customised meshes with pre-defined structural abnormalities. *Top row* depicts the segmentations created using the custom made tool. The *middle* and *right column* segmentations have a pre-defined structural abnormality. The impact of these abnormalities is visible on the corresponding simulations. A delayed activation can be observed in the isochrone map for regions with edema (*solid black arrows*). The computational mesh containing a transmural scar (*black arrowheads* and *dotted black arrows*), demonstrates a total conduction block.

DISCUSSION

To our knowledge, this is the first study to integrate and evaluate IPM and cardiac activation simulations within a clinically applicable whole-heart workflow. The proposed computational workflow provided accurate IPM reconstructions and enabled patient-specific simulations to be performed.

The use of MRI enables visualisation and incorporation of tissue-characteristics in computational meshes. In addition, an integrated IPM and simulation based approach facilitates a comprehensive assessment of arrhythmias and underlying substrate. These two factors significantly contribute towards the clinical applicability of this workflow and offer a unique environment for the development and evaluation of patient tailored therapeutic strategies.

Inverse potential mapping

The IPM localised the origin of atrial activity to the anatomically known location of the sinus node [15], suggesting the correctness of the model. These results imply that sinus node function and also dysfunction may be non-invasively characterised and assessed using IPM.

Simulations

The simulations of sinus rhythm performed on the computational meshes generated reliable results when compared to measurements reported in the literature [14]. Simulations performed on the personalised meshes incorporating virtual edema and scar resulted in a different activation pattern with delayed conduction and conduction block respectively.

These observations illustrate the wide range of simulations which can be obtained utilizing this simulation model. This can be clinically relevant for patients presenting with arrhythmias with a history of a disease associated with fibrosis such as myocardial infarction and myocarditis.

The ability to reconstruct atrial depolarisation and repolarisation can also contribute to novel clinical insights in the electrical substrate of complex supra-ventricular tachycardias such as left atrial flutter and atrial fibrillation.

Whole-heart computational model

Although only a few pathologies involve the atria and ventricles simultaneously, a combined assessment remains relevant for a comprehensive study of atrio-ventricular electro-mechanical coupling and electrical interaction.

The atrial contraction presents such an example. It has been reported that pressure modulation due to atrial contractions can remotely alter the electrical behaviour and activation pattern of the ventricular myocytes [16-17]. A whole-heart model is required to incorporate such complex relations and to provide physiologically accurate simulations.

Limitations

The simulations performed in this study used a standardised set of epicardial potentials recorded in a structurally normal human heart. Furthermore, the currently used simulation algorithm applied fixed conduction velocities for the cardiac volumes. However, the aim of the current study was to develop a clinically applicable and

reliable method for isochrones generation. The evaluation of this algorithm could be successfully performed using one set (atrial and ventricular) of epicardial potentials. The generated simulation results were accurate for all subjects when compared to previous descriptions in the literature [14]. Therefore, the absence of patient specific epicardial potentials and usage of a fixed conduction model was not considered as a limitation.

The customised meshes were constructed to test the feasibility of incorporating tissue properties. The conductivity and speed values for edema and scar tissue were based on estimates. Although, this can be considered as a substantial limitation, the simulations with patient-specific geometries (incorporating scar and edema) demonstrated realistic results, and underline the feasibility of the simulation algorithm.

A next step would be combining simulations with reconstructed IPM in order to non-invasively characterise tissue.

Future directions

Future research will focus on evaluating the IPM algorithm for patients undergoing catheter ablation for ectopic ventricular beats. The simulation algorithm will be further evaluated and optimised in patients with structural heart disease and arrhythmias. Furthermore, future work will perform comparison between simulations, reconstructed IPM and invasively acquired epicardial potentials to evaluate potential reconstruction errors related to patient specific differences in epicardial potentials.

CONCLUSION

The proposed finite element model based whole-heart computational workflow offers an integrated platform for cardiac electrical assessment using IPM and simulations. The IPM algorithm can accurately reconstruct reliable cardiac activation sequences from BSP's. The simulation model was able to incorporate patient-specific electrical parameters and rapidly perform whole-heart cardiac activation simulations. The use of MRI substantially contributes towards the clinical applicability.

This workflow offers the prospect to improve patient selection and personalise therapeutic strategies for interventional electrophysiological procedures. Future studies should investigate the role of this innovative approach for analysis of complex atrial and ventricular arrhythmias.

REFERENCES

1. Ramanathan C, Ghanem RN, Jia P, Ryu K, Rudy Y. Noninvasive electrocardiographic imaging for cardiac electrophysiology and arrhythmia. Nat Med. 2004;10:422–428.
2. Keldermann RH, ten Tusscher KHWJ, Nash MP, Bradley CP, Hren R, Taggart P, et al. A computational study of mother rotor VF in the human ventricles. Am J Physiol Heart Circ Physiol. 2009;296:H370–H379.
3. Krueger MW, Seemann G, Rhode K, Keller DUJ, Schilling C, Arujuna A, et al. Personalisation of atrial anatomy and electrophysiology as a basis for clinical modeling of radio-frequency ablation of atrial fibrillation. IEEE Trans Med Imaging. 2013;32:73–84.
4. Ashikaga H, Arevalo H, Vadakkumpadan F, Blake RC, Bayer JD, Nazarian S, et al. Feasibility of image-based simulation to estimate ablation target in human ventricular arrhythmia. Heart Rhythm. 2013;10:1109–1116.
5. Erkapic D, Greiss H, Pajitnev D, Zaltsberg S, Deubner N, Berkowitsch A et al. Clinical impact of a novel three-dimensional electrocardiographic imaging for non-invasive mapping of ventricular arrhythmias—a prospective randomized trial. Europace. 2015;17(4):591–7.
6. Jamil-Copley S, Bokan R, Kojodjojo P, Qureshi N, Koa-Wing M, Hayat S, et al. Noninvasive electrocardiographic mapping to guide ablation of outflow tract ventricular arrhythmias. Heart Rhythm. 2014;11:587–594.
7. Sermesant M, Chabiniok R, Chinchapatnam P, Mansi T, Billet F, Moireau P, et al. Patient-specific electromechanical models of the heart for the prediction of pacing acute effects in CRT: a preliminary clinical validation. Med Image Anal. 2012;16:201–215.
8. Oostendorp T, Nenonen J, Korhonen P. Noninvasive determination of the activation sequence of the heart: application to patients with previous myocardial infarctions. J Electrocardiol. 2002;35(Suppl):75–80.
9. Geuzaine C, Remacle JF. Gmsh: a three-dimensional finite element mesh generator with built-in pre- and post-processing facilities. Int J Numer Meth Eng. 2009;79(11):1309–1331.
10. Bhagirath P, van der Graaf M, van Dongen E, de Hooge J, van Driel V, Ramanna H, et al. Feasibility and accuracy of cardiac magnetic resonance imaging-based whole-heart inverse potential mapping of sinus rhythm and idiopathic ventricular foci. J Am Heart Assoc. 2015;4:e002222.
11. Kleber AG, Janse MJ, Fast VG. Fast, normal and abnormal conduction in the heart. In: Handbook of physiology. Section 2 The cardiovascular system, vol. 1 The heart. Oxford: Oxford University Press; 2001. p. 455–530.
12. Möller T, Trumbore B. Fast, minimum storage ray-triangle intersection. J Graph. Tools. 1997;2(1):21–8.
13. Floyd RW. Algorithm 97: shortest path. Commun ACM. 1962;5(6):345.
14. Durrer D, van Dam RT, Freud GE, Janse MJ, Meijler FL, Arzbaecher RC. Total excitation of the isolated human heart. Circulation. 1970;41:899–912.

15. Sanchez-Quintana D, Cabrera JA, Farre J, Climent V, Anderson RH, Ho SY. Sinus node revisited in the era of electroanatomical mapping and catheter ablation. Heart. 2005;91:189–194.

16. ter Keurs HE, Rijnsburger WH, van Heuningen R, Nagelsmit MJ. Tension development and sarcomere length in rat cardiac trabeculae. Evidence of length-dependent activation. Circ Res. 1980;46:703–714.

17. Zwanenburg JJM, Gotte MJW, Kuijer JPA, Hofman MBM, Knaapen P, Heethaar RM, et al. Regional timing of myocardial shortening is related to prestretch from atrial contraction: assessment by high temporal resolution MRI tagging in humans. Am J Physiol Heart Circ Physiol. 2005;288:H787–H794.

PART 3
APPLICATION OF NON-INVASIVE MAPPING IN VOLUNTEERS & PATIENTS

08

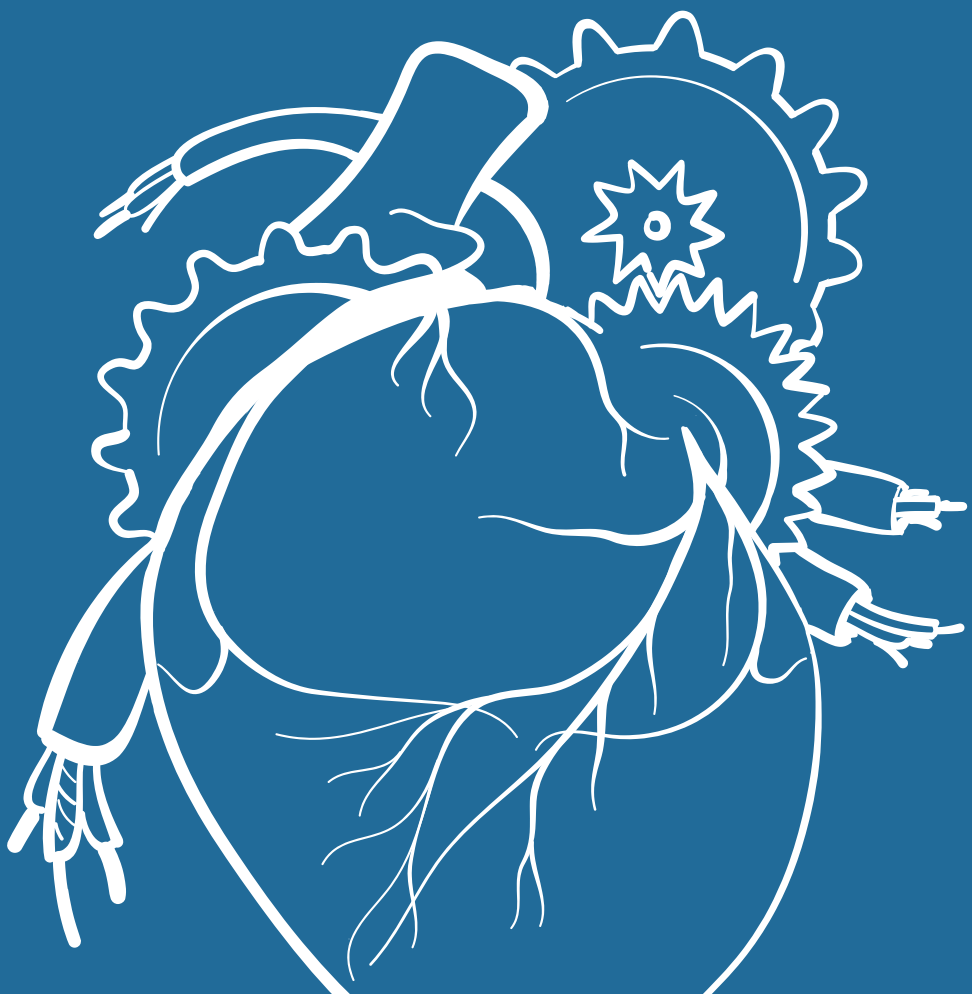

NON-INVASIVE INVERSE POTENTIAL MAPPING; THE IMPACT OF ELECTRODE POSITIONING

van der Graaf AW, Bhagirath P, de Hooge J, de Groot NM, Götte MJ.
Clinical Research in Cardiology. 2016;105(1):79-88.

ABSTRACT

Introduction: In inverse potential mapping, local epicardial potentials are computed from recorded body surface potentials (BSP). When BSP are recorded with only a limited number of electrodes, in general biophysical a priori models are applied to facilitate the inverse computation. This study investigated the possibility of deriving epicardial potential information using only 62 torso electrodes in the absence of an a priori model.

Methods: Computer simulations were used to determine the optimal in vivo positioning of 62 torso electrodes. Subsequently, three different electrode configurations, i.e., surrounding the thorax, concentrated precordial (30 mm inter-electrode distance) and super-concentrated precordial (20 mm inter-electrode distance) were used to record BSP from three healthy volunteers. Magnetic resonance imaging (MRI) was performed to register the electrode positions with respect to the anatomy of the patient. Epicardial potentials were inversely computed from the recorded BSP. In order to determine the reconstruction quality, the super-concentrated electrode configuration was applied in four patients with an implanted MRI-conditional pacemaker system. The distance between the position of the ventricular lead tip on MRI and the inversely reconstructed pacing site was determined.

Results: The epicardial potential distribution reconstructed using the super-concentrated electrode configuration demonstrated the highest correlation ($R = 0.98$; $p < 0.01$) with the original epicardial source model. A mean localisation error of 5.3 mm was found in the pacemaker patients.

Conclusion: This study demonstrated the feasibility of deriving detailed anterior epicardial potential information using only 62 torso electrodes without the use of an a priori model.

INTRODUCTION

Inverse potential mapping (IPM) is a promising technique that may complement conventional invasive electrophysiological (EP) studies [1-2]. In IPM, local epicardial potentials are inversely computed from recorded body surface potentials (BSP) [3]. Typically, 252 electrodes surrounding the thorax are used to record BSP [4-5].

When a smaller number of recording electrodes is used, optimal electrode positioning is important. In the past, several studies have addressed this topic. Early studies focused on the detection and elimination of redundant information in the recorded BSP [6–10]. Later, biophysical a priori models, i.e., computer models that enable the in silico mimicking of in vivo conditions by using pre-programmed settings relating to physical properties, e.g., conduction velocity, fiber orientation, anisotropy, activation pathways, were introduced to compensate for the limited BSP data actually recorded [11]. In general, inverse procedures involving 64 or fewer electrodes always apply an a priori activation model.

The purpose of this study was to investigate the feasibility of IPM using only 62 torso electrodes in the absence of an a priori model. A simulation using 252 electrodes served as a reference for desired image quality. Simulations were performed using various electrode configurations. Three different electrode positions using 62 electrodes were subsequently applied on healthy volunteers to record BSP. From the recorded BSP, epicardial potentials were reconstructed. The amount of detail and the correlation with the original source model were assessed. To evaluate the localisation error and size of the smallest visible detail, this mapping technique was applied in four patients with an implanted MRI-conditional DDD pacemaker system.

METHODS

Computer simulations

3D model

Simulations were performed using a 3D thorax model. This model was constructed after manual segmentation of different structures and organs on anatomic magnetic resonance imaging (MRI) images using custom written software. The model incorporated the whole-heart (including atria, ventricles, septum), liver, lungs, spleen, and torso surface. To each of these tissue elements conductivities were assigned as reported in

literature (thorax: 0.2 S/m, lungs: 0.04 S/m, liver: 0.03 S/m and spleen: 0.04 S/m) [12]. Gmsh software [13] was used for the generation of a volume mesh, required for the simulations (**figure 1**).

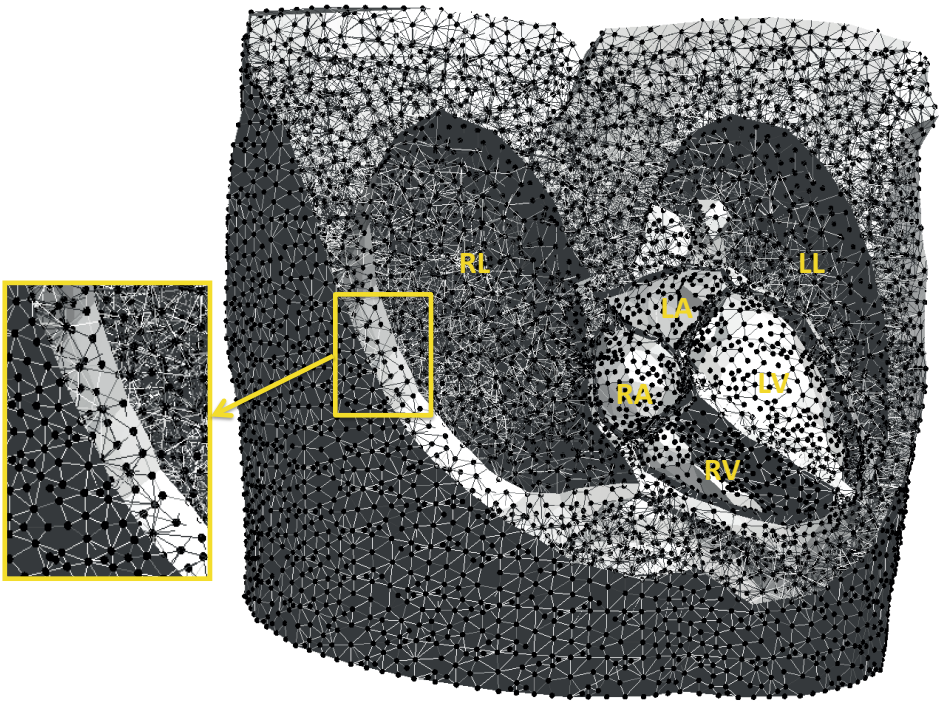

Figure 1. Example of a 3D volume mesh used for the simulations. This volume mesh was generated after segmentation of the thoracic organs on the MRI images. RL right lung, LL left lung, RA right atrium, LA left atrium, RV, right ventricle, LV left ventricle.

Forward simulation

Figure 2 provides a complete overview of the forward and inverse procedures used in this research, as described previously [14].

Propagation of electrical activity through the tissue elements of the whole-heart model was simulated using Moller-Trumbore [15] and Floyd-Warshall algorithms [16], yielding isochrones. From these isochrones, time dependent epicardial source potentials were computed by applying location specific activation curves. From the source potentials and in conjunction with the different tissue conductivities, BSP were computed by

multiplication with the transfer matrix *T*. From these BSP, ECG potentials were computed by spatial sampling. In order to approximate real-life conditions, noise was added to the simulated ECG potentials with a signal-to-noise ratio (SNR) of 21 dB.

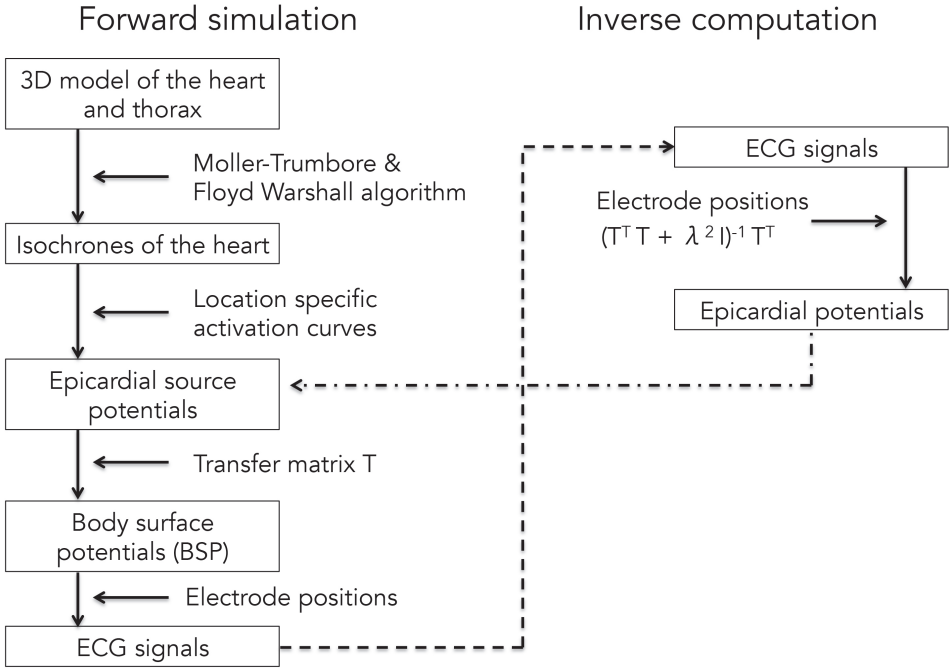

Figure 2. Flowchart visualizing the processes associated with forward simulations and inverse computations.

Inverse reconstruction of epicardial potentials from simulated ECG potentials

Epicardial potentials (*P*epi) were calculated from the ECG potentials (*P*bs) using $Pepi = (TTT + \lambda 2I) - 1TTPbs$ where *T* is the forward transfer matrix and λ is the regularisation strength, initially determined by simulation with patient-specific geometries. For all electrode configurations, the correlation between the initial source epicardial potentials (used for the simulation of ECG potentials) and the reconstructed epicardial potentials was computed. In addition, for all electrode configurations, correlation was calculated for 16 identical points on the anterior epicardium. These values were plotted in a graph to visualise correlation trends. To exclude systematic errors due to grid artifacts, all computations were performed on different grids. Four different electrode configurations were used in the simulations (**figure 3**).

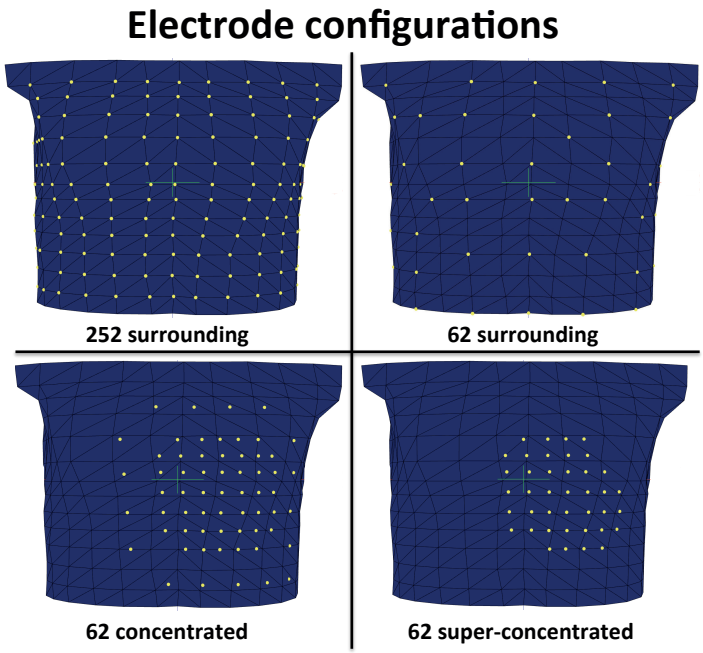

Figure 3. Anterior view of the thorax. Four different electrode configurations were used for the simulation part of the study: 252 electrodes surrounding the thorax, 62 surrounding the thorax, 62 concentrated (inter-electrode distance 30mm) and super-concentrated (inter-electrode distance 20mm). The yellow markers on the 3D thorax model represent the electrodes.

Reference configuration 252 electrodes surrounding the thorax. This configuration served as a reference, since this number of electrodes is the current standard in body surface potential mapping (BSPM).

- *Configuration I* 62 electrodes surrounding the thorax.
- *Configuration II* 62 concentrated (30 mm inter-electrode distance) electrodes directly overlaying the heart.
- *Configuration III* 62 super-concentrated (20 mm inter-electrode distance) electrodes directly overlaying the heart.

Inverse reconstruction of recorded human data

Study population

Three different electrode layouts were subsequently used to record data in three healthy volunteers (mean age 28 ± 1 year).

To evaluate the localisation error and size of the smallest visible detail, four male patients (mean age 58 ± 12 years old) with an implanted MRI-conditional DDD pacemaker system (Advisa MRI™ Surescan®, Medtronic Inc., Minneapolis, MN, USA) and a structurally normal heart were enrolled. Patient characteristics are provided in **table 1**. The RV lead tip was positioned either in the RV apex (2 patients), or in the right ventricular outflow tract (RVOT) (2 patients).

Table 1. Patient characteristics.

Patient	Age (yrs)	Sex	RV lead tip location	Pacing indication	Relevant comorbidity
1	66	M	Apex	Asystole	Hypertension
2	42	M	Apex	Asystole	Hemochromatosis
3	69	M	RVOT	AV-block	-
4	54	M	RVOT	Chronotropic Incompetence	-

Written informed consent was obtained from all participants. This study complied with the declaration of Helsinki and received approval from the local ethical committee and the institutional scientific board.

Body Surface Potential Mapping

Three different electrode layouts were used to record data in the healthy volunteers.

- *Configuration I* 62 electrodes surrounding the thorax.
- *Configuration II* 62 concentrated (30 mm inter-electrode distance) electrodes directly overlaying the heart.
- *Configuration III* 62 super-concentrated (20 mm inter-electrode distance) electrodes directly overlaying the heart.

BSP were recorded using a 65-channel (62 thorax electrodes) ActiveTwo BSPM system with passive electrodes and shielded cables (BioSemi BV, Amsterdam, The Netherlands). A sampling rate of 2048 Hz was selected and every data acquisition was performed for 60 s.

In the pacemaker patients, BSP were recorded using the 62 super-concentrated electrode configuration (configuration III). Potentials were recording during right ventricular (RV) pacing at a rate exceeding the intrinsic rate with at least 15 beats/min (paced AV-delay 70 ms).

Every BSP recording was immediately followed by an MRI scan in order to register the electrode positions to the anatomy of the volunteer.

Magnetic Resonance Imaging

After each BSPM recording, MRI markers were applied to replace all torso electrodes. These markers were used to locate the electrode positions on the MRI images, thereby minimizing the systematic error in the inverse procedure.

Axial, coronal and sagittal anatomical images were obtained using a Turbo Spin Echo (black blood) sequence during breath hold (slice thickness 6 mm, no gap between slices).

MRI was performed on a Siemens Aera 1.5 Tesla MRI scanner (Siemens Healthcare, Erlangen, Germany).

For patients with an implanted pacemaker, pacing thresholds, P- and R-wave amplitude and lead impedance were determined before entering the MRI room and the pacemaker system was programmed into MRI SureScan® mode [17]. These parameters were again determined after the examination and compared to the initial values. Finally, original programming of the pacemaker was restored.

Inverse reconstruction of recorded ECG data

From the MRI images, a 3D thorax model was constructed comprising the epicardial surface and the thorax volume conductor, accounting for lungs, liver and spleen. Epicardial potentials were calculated from the recorded BSP (P_{bs}) using $P_{epi} = (T^T T + \lambda^2 I)^{-1} T^T P_{bs}$, where T is the forward transfer matrix and λ is the regularisation strength. Following each BSP recording, epicardial activation sequences were inversely reconstructed and visualised

Evaluation of the quality of the inverse results

To evaluate the quality of the results, ECGs were reconstructed from the inverse by forward transformation. The correlation between the recorded ECG potentials and the computed ECG potentials was subsequently determined.

Note that while an a priori activation model was used for simulations to optimise the electrode positioning, no such model was used to perform the inverse reconstruction from recorded human BSP.

Patients with an implanted pacemaker system

Localisation error

An investigator blinded to the actual ventricular lead tip position, identified the site of earliest depolarisation on the colour-coded epicardial potential map. Subsequently, the distance between this site and the position of the ventricular lead tip on the MRI images was determined. Hence, the localisation error was quantified as the distance between the true pacing location and the pacing location projected from the inverse.

Amount of true detail

The amount of detail was evaluated by performing a threshold-test on the epicardial potential peak induced by a pacing stimulus at a well-known electrode location. When the threshold was set too high, the potential peak would split, suggesting false detail.

The minimum size of the inversely mapped potential peak induced by pacing is determined by the highest threshold value that does not cause the peak to split. The detail shown in this case is true, rather than false (**figure 4**).

The smallest visible detail was quantified as the maximum point spread cross-section in mm of the potential peak due to pacing.

Computing platform

All analyses were performed on a 2.4 GHz quadcore laptop running the Windows 8 OS. Solving the potential equations was delegated to an Ubuntu 12.10 virtual machine running on this laptop. Correlation coefficients were determined using Pearson's product moment correlation coefficients as computed by the NumPy library.

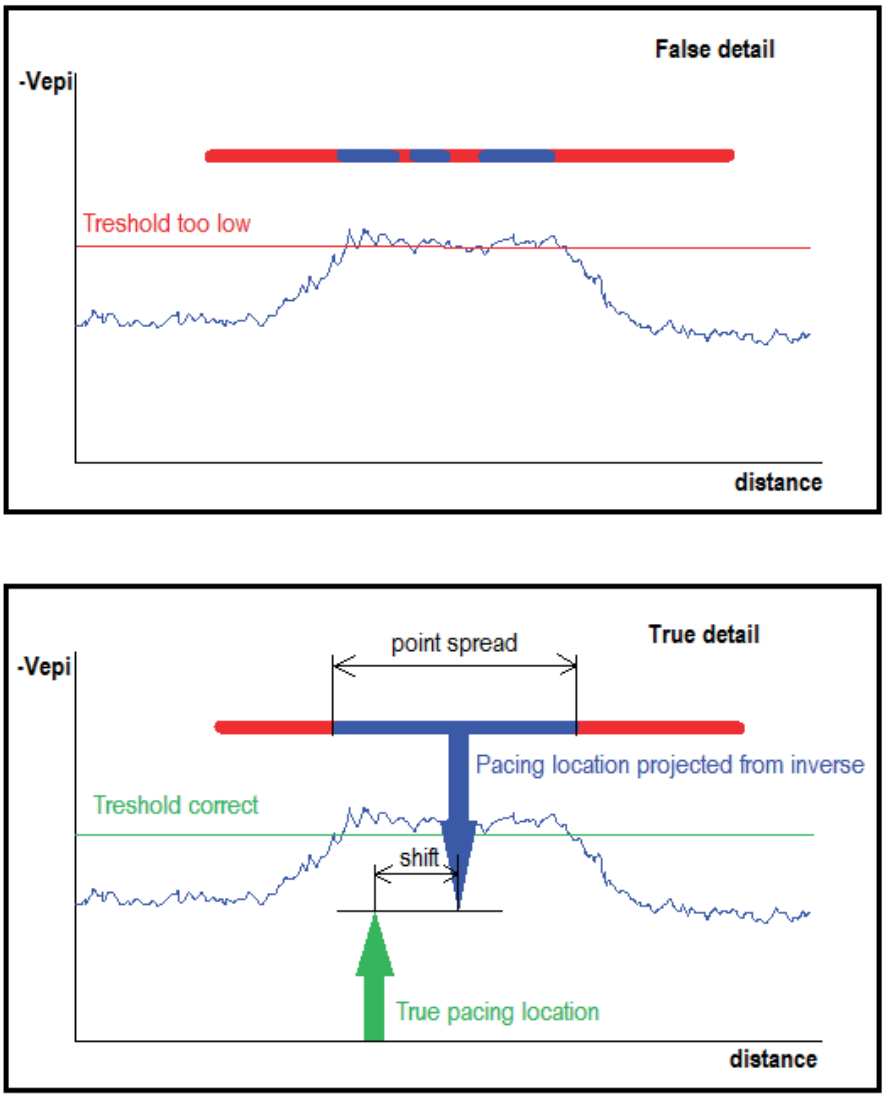

Figure 4. The amount of detail was evaluated by performing a threshold-test on an epicardial potential peak induced by a pacing stimulus. When the threshold is set too high, the potential peak will split, suggesting false detail (upper panel). The highest threshold value that does not cause the potential peak to split, reflects the minimum amount of true detail in the inversely reconstructed potential (lower panel).

RESULTS

Computer simulations

252 electrodes surrounding the thorax

This electrode layout provided a high image quality (**figure 5**a, video 1). Right ventricular breakthrough could be easily discerned. An overall high correlation ($R = 0.96$; $p < 0.01$) with the source model was found. The correlation map (**figure 5**b) clearly demonstrated a reduced correlation in areas with increased electrode spacing.

62 electrodes surrounding the thorax

This electrode configuration resulted in a poor image quality (**figure 5**d, video 2). Several gaps appeared in the epicardial potential map, indicating loss of information in these areas. A reduced overall correlation compared to the source model was found ($R = 0.92$; $p < 0.01$) (**figure 5**e).

62 electrodes concentrated (30mm inter-electrode distance)

When concentrating all available electrodes on the anterior part of the thorax in the region directly overlaying the heart, a clinical relevant image of the potentials on the anterior epicardium was obtained (**figure 5**g, video 3). **Figure 5**h shows that the correlation with the source model greatly improved ($R = 0.97$; $p < 0.01$), compared to the configuration using 62 electrodes surrounding the thorax.

62 electrodes super-concentrated (20mm inter-electrode distance)

By reducing the inter-electrode distance to 20 mm, image quality improved. The depolarisation front appeared to be more homogeneous (**figure 5**j, video 4). This was confirmed by a slightly higher correlation with the source model ($R = 0.98$; $p < 0.01$), compared to that obtained using the 30 mm electrode spacing configuration. As can be observed in **figure 5**k, IPM using the super-concentrated electrode configuration provided the highest correlation with the source model.

Inverse reconstruction of recorded human data

The BSP recording and MRI examination lasted approximately 60 min. Segmentation and data processing lasted approximately 150 min. Correlation coefficients between measured and reconstructed ECGs were >0.94 for all leads used in the inversion and >0.97 for 85 % of those leads.

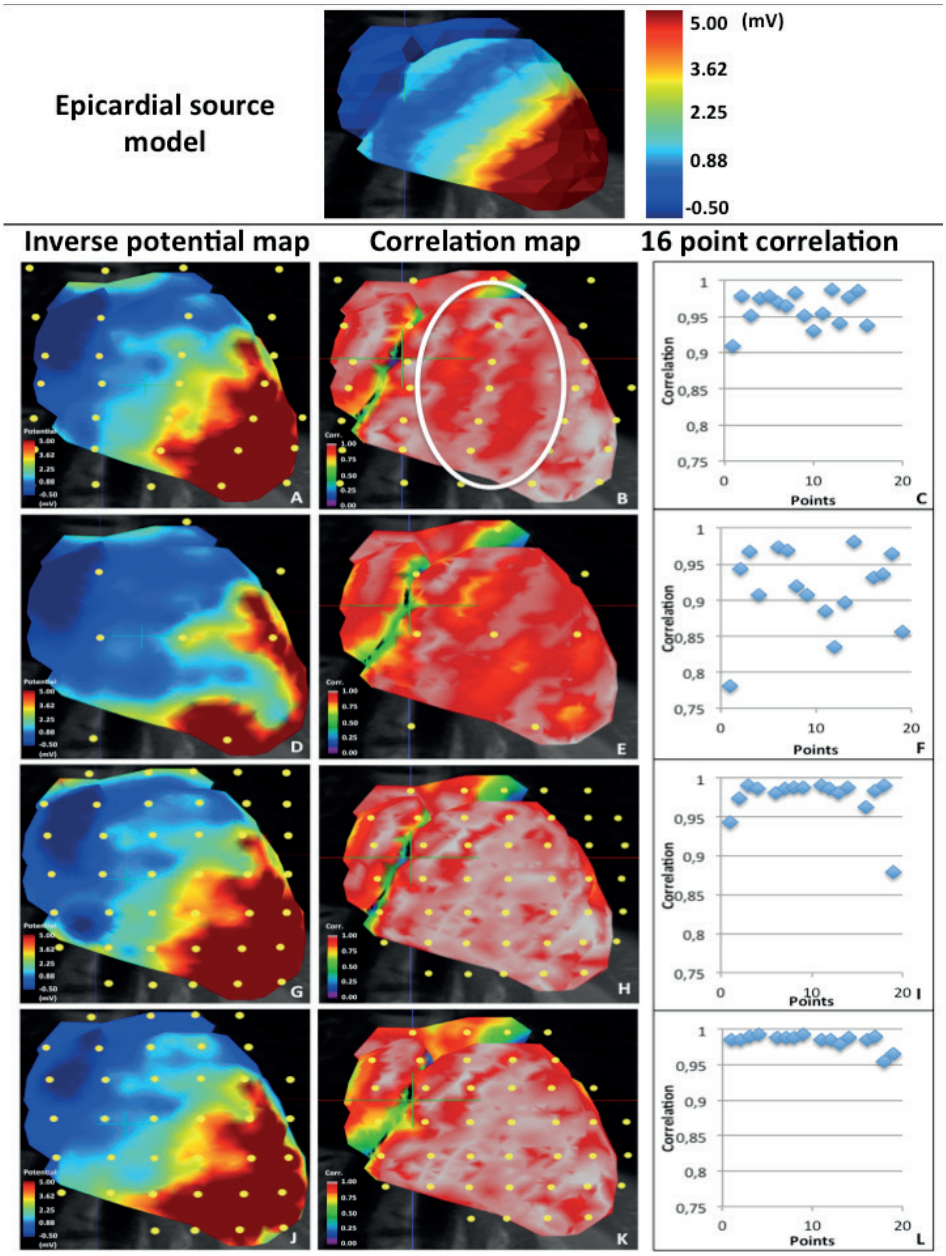

Figure 5. Epicardial source model at 30ms into the QRS (upper panel). Epicardial potential map at 30ms into the QRS, temporal correlation map and correlation plot of 16 sampling points for every simulated electrode layout (lower panel). A-C: 252 electrodes surrounding the thorax, D-F: 62 surrounding the thorax, G-I: 62 concentrated, J-L: super-concentrated. A reduced correlation was observed in areas between two electrodes (encircled in 4B). The highest correlation with the epicardial source model was obtained with the super-concentrated electrode placement.

62 electrodes surrounding the thorax

The 62 electrodes surrounding the thorax did not provide clinical sufficient information (video 5). Only ventricular epicardial activation could be reconstructed using this configuration. Regions with no or low signal variance were observed as gaps in the reconstructed epicardial potentials.

62 electrodes concentrated (30mm inter-electrode distance)

Concentrated positioning of the 62 available electrodes, directly above the heart, improved the overall resolution (video 6). Although reduced in size and number, areas of low signal were still present when using this electrode configuration.

62 electrodes super-concentrated (20mm inter-electrode distance)

Higher concentration of the electrode configuration (20 mm inter-electrode distance) resulted in a substantial increase of image resolution (video 7). Atrial and ventricular activation could be clearly distinguished and spatially localised in the reconstructed epicardial activation sequence. **Figure 6** shows epicardial potential maps for six instants of time during the QRST interval. In all three volunteers, similar results were obtained.

Reconstruction of pacing sites

None of the patients reported any complaints during or after the MRI examination. Pacing thresholds and leads impedances remained unaffected by the MRI scan in all patients.

For all patients, the site of earliest ventricular depolarisation could be identified. In two patients, depolarisation started in the superior part of the right ventricular septum. In remaining patients, the site of earliest depolarisation was located in the apical region of the right ventricle.

In vivo evaluation of localisation error and amount of detail

A mean localisation error of 5.3 mm was found. The mean size of the smallest visible detail during pacing, determined by a threshold test, was 7 mm. Individual values are listed in **table 2**.

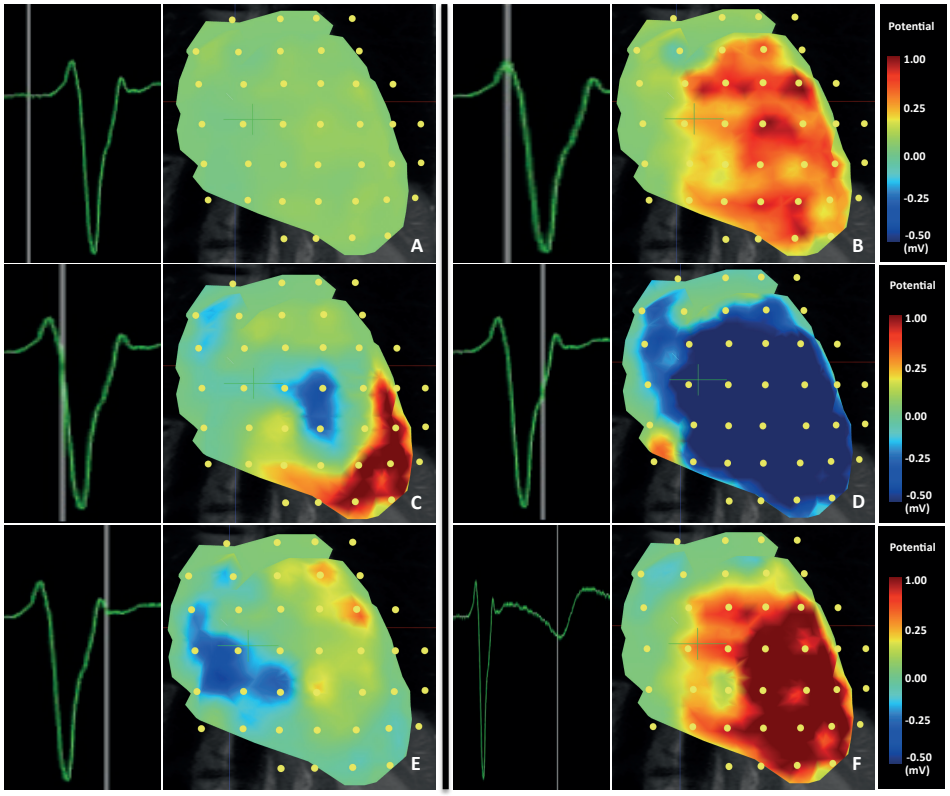

Figure 6. Epicardial potentials during a QRST interval inversely estimated from human BSP recorded using the super-concentrated (20mm inter-electrode distance) electrode configuration. Right ventricular breakthrough can be observed in panel C.

Table 2. Localisation errors and amount of detail in pacemaker patients.

	Localisation error (mm)	Max point spread (mm)
Patient 1 (RV apex)	5	7
Patient 2 (RV apex)	5	8
Patient 3 (RVOT)	5	7
Patient 4 (RVOT)	6	6

DISCUSSION

This study investigated the optimal positioning of only 62 torso electrodes for IPM in the absence of an a priori model. Computer simulations were used to improve insight and predict image quality of different electrode configurations. A configuration of 62 electrodes positioned on the anterior part of the thorax, with a 20 mm inter-electrode distance, provided the highest amount of detail in the epicardial potential maps of the anterior side of the heart.

In addition, the epicardial potential distribution reconstructed using this configuration demonstrated the highest correlation ($R = 0.98$; $p < 0.01$) with the original epicardial source model. Using this configuration, a minimum occurring at 10 ms into the QRS near V1, reflecting right ventricular breakthrough could be discerned. This finding is in accordance with previous observations reported by Taccardi in 1963 [18] and Okamoto et al. in 1990 [19].

The results of application of this method in patients with implanted pacemakers indicated a clinically relevant reconstruction quality. A mean localisation error of 5.3 mm was found in the pacemaker patients.

Clinical relevance of this study

Inverse potential mapping is a promising but also challenging modality to gain further insight into cardiac substrates and arrhythmia mechanisms in a non-invasive fashion. This study focused on simplification of the procedure by applying a reduced number of recording electrodes. The ventricular paced beats analysed in this study served as ectopic ventricular foci. The mapping approach presented in this paper may help to tailor the invasive electrophysiological procedure to the individual patient. The concentrated electrode configuration may make it an attractive clinical alternative in situations where this specific view is required.

Importance of simulations

The possibility to simulate epicardial potentials from random electrode configurations facilitated a stepwise approach towards optimal electrode positioning. In this way, the simulations guided the placement of the electrodes. In addition, the validity of the simulations could be determined by application of the selected configurations in vivo. The validity of the simulations was subsequently confirmed by the results obtained in patients with implanted pacemaker systems.

A-priori model

In literature [20–22], inverse procedures involving 64 or fewer electrodes always apply an a priori activation model. Although detailed images may be obtained using even <20 electrodes, the number of degrees of freedom in this situation fundamentally limits the number of pathology related activation patterns that can be represented. This is further elaborated upon in appendix and in **figure 7**.

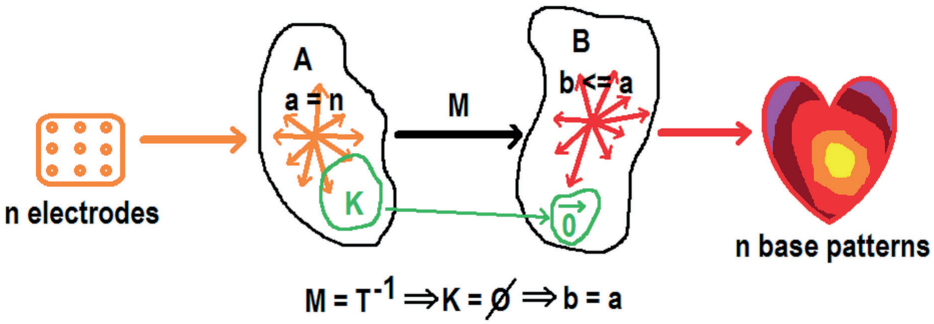

Figure 7. Linear mapping M denotes the ideal reconstruction, reflecting the unknown but exact linear quasi-stationary field equations. M maps n independent electrode signals onto at most n independent epicardial base vectors. Note that, by definition of M, no reconstruction method can do better. In practice, ill conditioning will render certain subsets of epicardial patterns indistinguishable, reducing the dimension of the solution space.

Obtaining detailed images of cardiac surface potentials using a limited number of electrodes, without excluding a wide variety of pathological activation patterns by constraining the solutions using an a priori activation model derived from healthy myocardial tissue, requires focusing all degrees of freedom on a limited region of interest on the cardiac surface.

MRI

Although computed tomography (CT) is frequently preferred due to the speed of the acquisition process, MRI allows reliable function analysis, assessment of wall motion abnormalities and highly detailed characterisation of tissue [23–26]. Unlike CT, MRI does not use radiation. Hence, MRI is the preferred imaging modality to be repeatedly used in patients. In recent years, the safe performance of MRI in patients with non-MRI-conditional pacing devices has been demonstrated [27–29]. In addition, MRI-conditional devices have been introduced, decreasing the risk of potential hardware or software interactions [30].

Limitations of this study

Application of 62 anterior electrodes with an inter-electrode distance of 20 mm enables detailed reconstruction of an anterior view of the epicardial potentials in the absence of an a priori model. Information on the posterior area of the heart could not be reconstructed from the BSP recorded using the anterior positioned super-concentrated electrode configuration. By increasing the total number of recording electrodes and by positioning electrodes on the back of the thorax this can be resolved. But since the application of a large number of electrodes is time consuming, implementation in the clinical arena may still be challenging. Hence, an optimal balance between information content and clinical utility is pursued. Parallel computation of the inverse solution will further reduce the post-processing time.

In the presence of a limited number of electrodes, electrode positioning is crucial. In order to achieve a high resolution, it is very important to position the electrodes directly overlaying the heart. Because this may be difficult to determine, a rapid exploratory MRI scan (scout anatomical images) prior to BSPM may help to optimise electrode positioning. Regarding the small number of patients in this study, further research is needed to further evaluate the clinical benefits of this non-invasive mapping strategy.

Future perspective

Although IPM is considered a promising technique to complement conventional invasive electrophysiological procedures, it has not yet advanced to routine clinical application. This is mainly due to the time consuming nature of the acquisition and post-processing of the data. The possibility to derive detailed information on cardiac excitation from a rapid and simplified BSPM procedure may facilitate clinical implementation. The ability to perform detailed simulations using patient data may provide clinicians valuable insight into the potential impact of their treatment. Non-invasive characterisation of arrhythmogenic foci or substrates, prior to invasive electrophysiological or device implant procedures, may help to increase therapeutic outcome. Further research is required to provide evidence of the effectiveness and accuracy of this approach to IPM.

CONCLUSION

The purpose of this study was to investigate the feasibility of IPM using only 62 torso electrodes without the aid of an a priori model. By concentrating the available electrodes in the area directly overlaying the heart, a high-resolution anterior view of the epicardial potentials can be obtained. Application of this mapping approach in patients with

implanted MRI-conditional pacemakers demonstrated a clinically relevant inverse reconstruction accuracy. Further research needs to be performed to further evaluate the clinical benefits of this technique.

REFERENCES

1. Jamil-Copley S, Bokan R, Kojodjojo P, Qureshi N, Koa-Wing M, Hayat S, Kyriacou A, Sandler B, Sohaib B, Wright I, Davies DW, Whinnett Z, S Peters N, Kanagaratnam P, Lim PB. Noninvasive electrocardiographic mapping to guide ablation of outflow tract ventricular arrhythmias. Heart Rhythm 2014;11(4):587-94.
2. Sapp JL, Dawoud F, Clements JC, Horácek BM. Inverse solution mapping of epicardial potentials: quantitative comparison with epicardial contact mapping. Circ Arrhythm Electrophysiol. 2012;5(5):1001-9.
3. Gulrajani RM. The forward and inverse problems of electrocardiography. IEEE Eng Med Biol Mag. 1998;17(5):84-101, 122.
4. Ramanathan C, Ghanem RN, Jia P, Ryu K, Rudy Y. Noninvasive electrocardiographic imaging for cardiac electrophysiology and arrhythmia. Nat Med. 2004;10(4):422-8.
5. Rudy Y. Noninvasive electrocardiographic imaging of arrhythmogenic substrates in humans. Circ Res. 2013;112(5):863-74.
6. Lux RL, Evans AK, Burgess MJ, Wyatt RF, Abildskov JA. Redundancy reduction for improved display and analysis of body surface potential maps. I. Spatial compression. Circ Res. 1981;49(1):186-96.
7. Hoekema R, Uijen GJ, van Oosterom A. On selecting a body surface mapping procedure. J Electrocardiol. 1999;32(2):93-101.
8. Lux RL, Smith RF, Abildskov JA. Limited lead selection for estimating body surface potentials in electrocardiography. IEEE Biomed Eng. 1978;25:270-6.
9. Finlay DD, Nugent CD, Donnelly MP, Black ND. Selection of optimal recording sites for limited lead body surface potential mapping in myocardial infarction and left ventricular hypertrophy. J Electrocardiol. 2008;41(3):264-71.
10. Messinger-Rapport BJ, Rudy Y. Noninvasive recovery of epicardial potentials in a realistic heart-torso geometry. Normal sinus rhythm. Circ Res. 1990;66(4):1023-39.
11. van Oosterom A. The dominant T wave and its significance. J Cardiovasc Electrophysiol. 2003;14(10 Suppl):S180-7.
12. Oostendorp T, Nenonen J, Korhonen P. Noninvasive determination of the activation sequence of the heart: application to patients with previous myocardial infarctions. J Electrocardiol. 2002;35 Suppl:75-80.
13. Marchandise E, Geuzaine C, Remacle JF. Cardiovascular and lung mesh generation based on centerlines. Int J Numer Method Biomed Eng. 2013;29(6):665-82.
14. van der Graaf AW, Bhagirath P, van Driel VJ, Ramanna H, de Hooge J, de Groot NM, Götte MJ. Computing Volume Potentials for Noninvasive Imaging of Cardiac Excitation. Ann Noninvasive Electrocardiol. 2014 Jul 17.

15. Möller T and Trumbore B. Fast, Minimum Storage Ray/Triangle Intersection. J Graph Tools. 1997;2;1:21-28.
16. Floyd RW. Algorithm 97: Shortest Path. Communications of the ACM 1962;5;(6):345.
17. Wollmann CG, Thudt K, Kaiser B, Salomonowitz E, Mayr H, Globits S. Safe performance of magnetic resonance of the heart in patients with magnetic resonance conditional pacemaker systems: the safety issue of the ESTIMATE study. J Cardiovasc Magn Reson. 2014;6;16;30:1-8.
18. Taccardi B. Distribution of heart potentials on the thoracic surface of normal human subjects. Circ Res. 1963;12:341-52.
19. Okamoto Y, Musha T, Harumi K. Reduction of the number of electrodes in the measurement of body surface potential distribution. Front Med Biol Eng. 1990;2(4):283-92.
20. van Dam PM, Tung R, Shivkumar K, Laks M. Quantitative localisation of premature ventricular contractions using myocardial activation ECGI from the standard 12-lead electrocardiogram. J Electrocardiol. 2013;46(6):574-9.
21. Seger M, Hanser F, Dichtl W, Stuehlinger M, Hintringer F, Trieb T, Pfeifer B, Berger T. Non-invasive imaging of cardiac electrophysiology in a cardiac resynchronisation therapy defibrillator patient with a quadripolar left ventricular lead. Europace 2014;16(5): 743-749.
22. Bokeriia LA, Revishvili ASh, Kalinin AV, Kalinin VV, Liadzhina OA, Fetisova EA. Hardware-software system for noninvasive electrocardiographic examination of heart based on inverse problem of electrocardiography. Med Tekh. 2008;(6):1-7.
23. Abbasi SA, Ertel A, Shah RV, Dandekar V, Chung J, Bhat G, Desai AA, Kwong RY, Farzaneh-Far A. Impact of cardiovascular magnetic resonance on management and clinical decision-making in heart failure patients. J Cardiovasc Magn Reson. 2013;1;15:89.
24. Petrov G, Kelle S, Fleck E, Wellnhofer E. Incremental cost-effectiveness of dobutamine stress cardiac magnetic resonance imaging in patients at intermediate risk for coronary artery disease. Clin Res Cardiol. 2015;104(5):401-9.
25. Schuster A, Ishida M, Morton G, Bigalke B, Moonim MT, Nagel E. Value of cardiovascular magnetic resonance imaging in myocardial hypertrophy. Clin Res Cardiol. 2012;101(3):237-8.
26. Schumm J, Greulich S, Sechtem U, Mahrholdt H. T1 mapping as new diagnostic technique in a case of acute onset of biopsy-proven viral myocarditis. Clin Res Cardiol. 2014;103(5):405-8.
27. Nazarian S, Hansford R, Roguin A, Goldsher D, Zviman MM, Lardo AC, Caffo BS, Frick KD, Kraut MA, Kamel IR, Calkins H, Berger RD, Bluemke DA, Halperin HR. A Prospective Evaluation of a Protocol for Magnetic Resonance Imaging of Patients With Implanted Cardiac Devices. Ann Intern Med. 2011;155:415-24.
28. Jilek C, Lennerz C, Stracke B, Badran H, Semmler V, Reents T, Ammar S, Fichtner S, Haller B, Hessling G, Deisenhofer I, Kolb C. Forces on cardiac implantable electronic devices during remote magnetic navigation. Clin Res Cardiol. 2013;102(3):185-92.

29. Boilson BA, Wokhlu A, Acker NG, Felmlee JP, Watson RE Jr, Julsrud PR, Friedman PA, Cha YM, Rea RF, Hayes DL, Shen WK. Safety of magnetic resonance imaging in patients with permanent pacemakers: a collaborative clinical approach. J Interv Card Electrophysiol. 2012;33:59–67.

30. Ferreira AM, Costa F, Tralhão A, Marques H, Cardim N, Adragão P. MRI-conditional pacemakers: current perspectives. Med Devices (Auckl). 2014;7;7:115-24.

APPENDIX I

Let n be the number of electrodes, let a be the dimension of the linear span A of the electrode potential vectors and let b be the dimension of the linear span B of the reconstructed epicardial potential vectors. Then a = n and b <= a, since the base vectors of B are, by linearity of the quasi stationary electrical field equations, obtained by a linear mapping M from the base vectors of A, that may have a kernel K of dimension k > 0. In general b = a, since M will be non-degenerate as is illustrated in **figure 7**. Note that the exact nature of the parameter estimation procedure plays no role in this fundamental relationship.

09

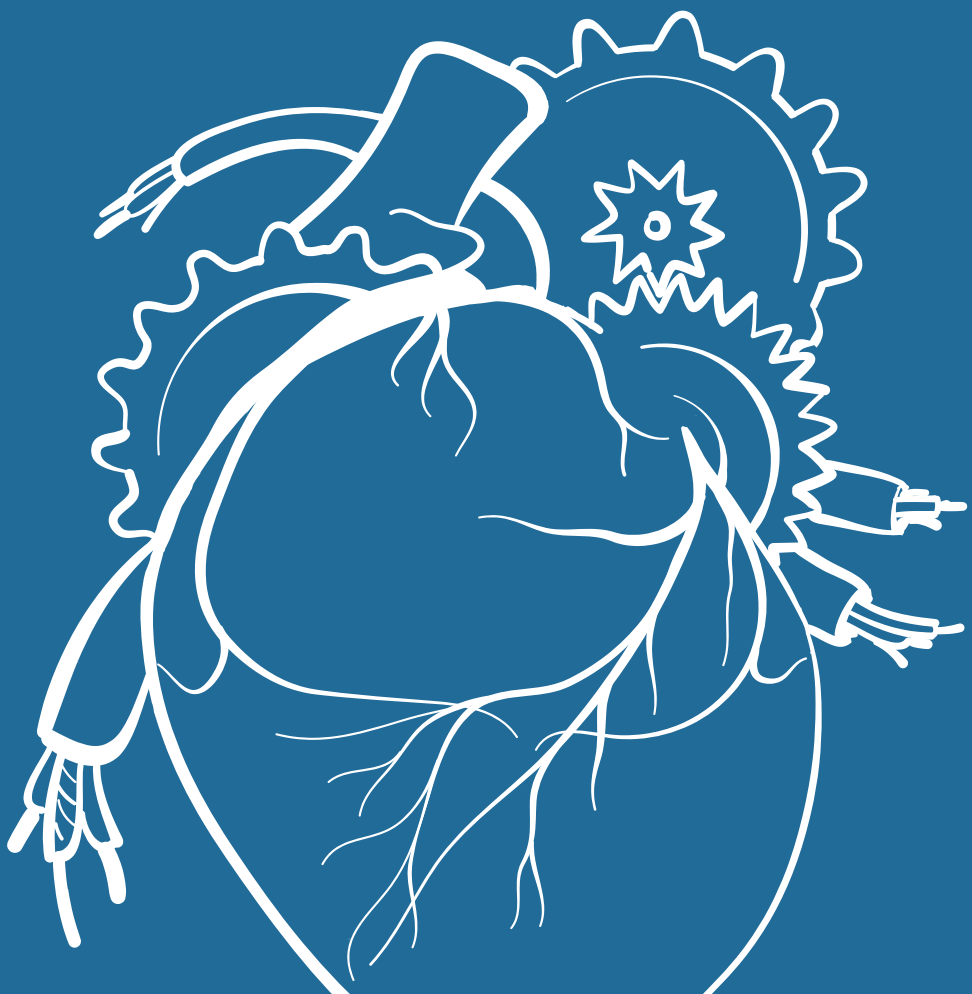

NON-INVASIVE FOCUS LOCALISATION; RIGHT VENTRICULAR EPICARDIAL POTENTIAL MAPPING IN PATIENTS WITH AN IMPLANTED MRI-CONDITIONAL PACEMAKER SYSTEM

van der Graaf AW, Bhagirath P, de Hooge J,
Rammana H, van Driel VJ, de Groot NM, Götte MJ.
Journal of Interventional Cardiac Electrophysiology. 2015;44(3):227-234.

ABSTRACT

Background: With the advent of magnetic resonance imaging (MRI) conditional pacemaker systems, the possibility of performing MRI in pacemaker patients has been introduced. Besides for the detailed evaluation of atrial and ventricular volumes and function, MRI can be used in combination with body surface potential mapping (BSPM) in a non-invasive inverse potential mapping (IPM) strategy. In non-invasive IPM, epicardial potentials are reconstructed from recorded body surface potentials (BSP). In order to investigate whether an IPM method with a limited number of electrodes could be used for the purpose of non-invasive focus localisation, it was applied in patients with implanted pacing devices. Ventricular paced beats were used to simulate ventricular ectopic foci.

Methods: Ten patients with an MRI-conditional pacemaker system and a structurally normal heart were studied. Patient-specific 3D thorax volume models were reconstructed from the MRI images. BSP were recorded during ventricular pacing. Epicardial potentials were inversely calculated from the BSP. The site of epicardial breakthrough was compared to the position of the ventricular lead tip on MRI and the distance between these points was determined.

Results: For all patients, the site of earliest epicardial depolarisation could be identified. When the tip of the pacing lead was implanted in vicinity to the epicardium, i.e. right ventricular (RV) apex or RV outflow tract, the distance between lead tip position and epicardial breakthrough was 6.0 ± 1.9 mm.

Conclusion: In conclusion, the combined MRI and IPM method is clinically applicable and can identify sites of earliest depolarisation with a clinically useful accuracy.

INTRODUCTION

Invasive electrophysiological procedures are often complicated by considerable fluoroscopic time, non-inducibility of the arrhythmia or hemodynamic instability of the patient [1]. Therefore, pre-procedural and non-invasive localisation of arrhythmogenic foci may improve the clinical outcome and reduce the duration of the invasive procedures [2].

To this intent, over the last decade various non-invasive mapping strategies, e.g. electrocardiographic imaging (ECGI) [3], non-invasive imaging of cardiac electrophysiology (NICE) [4] and AMICARD [5] have been introduced. Despite numerous reports on the possible advantages of non-invasive mapping, this approach has not yet advanced into daily clinical practice as a routine tool. This is either due to the impracticability associated with the use of up to 254 torso electrodes or to the limited data available from *in vivo* studies with respect to the accuracy and validity of the estimated epicardial potentials or intramural activation times.

With the advent of magnetic resonance imaging (MRI) conditional pacemaker systems, the possibility of performing MRI in pacemaker patients has been introduced [6]. Besides for the detailed evaluation of atrial and ventricular volumes and function, MRI can be used in combination with body surface potential mapping (BSPM) in a non-invasive inverse potential mapping (IPM) strategy.

This pilot study investigated the feasibility of non-invasive focus localisation using a limited number of 62 electrodes in patients with an implanted MRI-conditional pacemaker system. Ventricular paced beats were used to simulate ectopic foci. The estimated site of earliest epicardial breakthrough was compared to the position of the ventricular lead tip, and the distance between these sites was determined.

METHODS

Patient selection

Inverse potential mapping was performed in ten male patients (mean age 64 ± 5 years old) with an implanted MRI-conditional DDD pacemaker system (Advisa MRI™ Surescan®, Medtronic Inc., Minneapolis, MN, USA) and a structurally normal heart. Patient characteristics are provided in **table 1**.

Table 1. Patient characteristics.

Patient	Age (yrs)	Pacing indication	PR (ms)	QRS (ms)	QTc (ms)	Relevant comorbidity
1	66	Asystole	138	102	399	Hypertension
2	42	Asystole	148	96	363	Hemochromatosis
3	64	Bradycardia	180	94	384	Hypercholesterolemia
4	69	AV-block	190	180	380	-
5	70	AV-block	216	150	427	-
6	61	SSS + AV-block	314	128	411	Hypertension
7	69	AV-block	204	169	474	-
8	54	Chronotropic Incompetence	204	98	424	Paroxysmal AF
9	65	SSS†	268	100	395	-
10	79	Bradycardia	227	126	380	-

†SSS sick sinus syndrome.

The study complied with the declaration of Helsinki and received approval from the local ethical committee and the institutional scientific board. Written informed consent was obtained from all patients.

An overview of the complete workflow is provided in **figure 1**.

Body Surface Potential Mapping

Body surface potentials (BSP) were recorded using a 65-channel (62 torso + 3 limb electrodes) ActiveTwo BSPM system with passive electrodes and shielded cables (BioSemi BV, Amsterdam, The Netherlands). The BSP electrodes were positioned on the anterior thorax using a 20-mm inter-electrode distance (**figure 1**d) [7]. BSP were recorded in supine position at a sampling rate of 2048 Hz for 10 s during right ventricular (RV) pacing at a rate exceeding the intrinsic rate with at least 15 beats per minute (paced AV-delay 70 ms).

Magnetic Resonance Imaging

After BSPM, MRI markers were applied to replace all torso electrodes. These markers were used to locate the electrode positions on the MRI images, thereby minimizing the systematic error in the inverse procedure. Before entering the MRI room, pacing thresholds, P- and R-wave amplitude, and lead impedance were determined and the pacemaker system was programmed into MRI SureScan® mode [8].

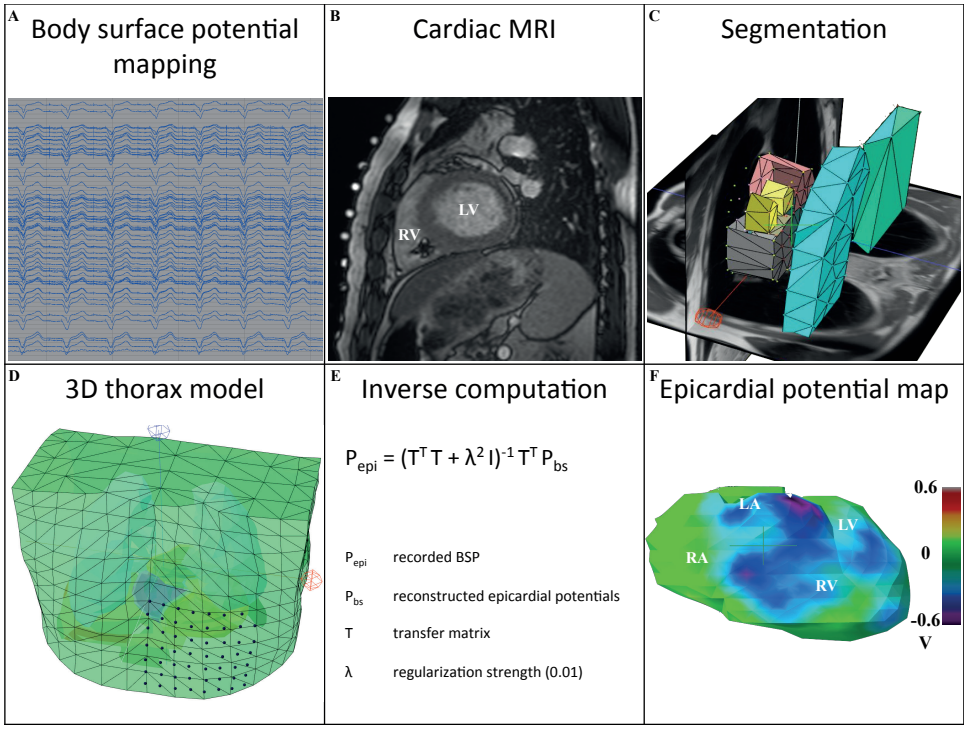

Figure 1. Complete workflow **(A-F)** for a non-invasive IPM procedure.

In order to control lung volume, breath holding was practiced with the patient prior to the examination. A stack of ECG-triggered, T2-weighted, bright blood images (slice thickness, 6 mm) was acquired to record the anatomy of the thorax and register the position of the RV lead tip and torso electrodes. Subsequently, cardiac function was assessed using steady state free precession (SSFP) short-axis, three- and four-chamber cines (slice thickness, 6 mm, temporal resolution <50 ms). All images were obtained during breath-hold on a Siemens Aera 1.5 Tesla MRI scanner (Siemens Healthcare, Erlangen, Germany). Cardiac function was analysed using CMR42® software (Circle Cardiovascular Imaging, Calgary, Alberta, Canada).

After the examination, pacing thresholds, P- and R-wave amplitude and lead impedance were determined and compared to the initial values. Finally, original programming of the pacemaker was restored.

Data processing

3D thorax model

For every patient, a detailed anatomical thorax model, including a 3D whole-heart model, was constructed from the MRI images. Thoracic structures including the heart with all four compartments, lungs, liver and spleen were manually segmented directly in 3D using custom-written software. Conductivities were assigned to each of these structures as known from literature (thorax, 0.2 S/m; lungs, 0.04 S/m; liver, 0.03 S/m and spleen, 0.04 S/m) [9]. A triangulated 3D thorax model was reconstructed using Gmsh software [10].

Inverse computation

For each patient, a single paced beat within the 10 seconds acquisition window was selected for inverse computation. The electrograms do not require any specific editing prior to processing. Epicardial potentials (P_{epi}) were calculated from the recorded body surface potentials (P_{bs}) using $P_{epi} = (T^T T + \lambda^2 I)^{-1} T^T P_{bs}$ where T is the forward transfer matrix and λ is the regularisation strength (0.01). Finally, an epicardial potential map of a single paced ventricular beat was reconstructed.

Ventricular lead tip position and the site of earliest depolarisation

An investigator (PB), blinded to the actual ventricular lead tip position, identified the site of earliest depolarisation on the colour-coded epicardial potential map. Subsequently, the distance between this site and the position of the ventricular lead tip on the MRI images was determined.

Correlation

In order to evaluate the reproducibility of the applied IPM method, two different paced beats were analysed for each patient. The epicardial potential distribution was reconstructed independently. Subsequently, the correlation between the epicardial potentials estimated from the two different beats was calculated using custom-written software.

Computing platform

Results are shown as mean ± SD and are expressed as absolute values. All analyses were performed on a 2.4-GHz quad core laptop running the Windows 8 OS. Solving the potential equations was delegated to an Ubuntu 12.10 virtual machine running on this laptop.

RESULTS

The BSP recording and MRI examination lasted approximately 60 min. None of the patients reported any complaints during or after the MRI examination. Pacing thresholds and leads impedances remained unaffected by the MRI scan in all patients.

Despite the presence of a pacemaker, image quality was good to excellent in all patients and allowed for left and right ventricular function assessment (**figure 2**, panels A, C and E). MRI-derived global function measures are listed in **table 2**.

Table 2. MRI parameters.

Patient	LVEDV (ml)	LVESV (ml)	LVSV (ml)	LVEF (%)	RVEDV (ml)	RVESV (ml)	RVSV (ml)	RVEF (%)
1	147	60	87	59	145	55	91	62
2	133	66	67	50	172	104	69	40
3	135	73	63	46	153	94	58	38
4	193	114	79	41	151	85	66	44
5	153	89	63	41	163	107	55	34
6	175	75	100	57	165	80	86	52
7	187	108	80	43	150	85	66	44
8	157	72	84	54	209	122	87	42
9	177	92	85	48	160	90	70	44
10	113	58	55	48	166	111	55	33

LVEDV left ventricular end-diastolic volume; LVESV left ventricular end-systolic volume; LVSV left ventricular stroke volume; LVEF left ventricular ejection fraction; RVEDV right ventricular end-diastolic volume; RVESV right ventricular end-systolic volume; RVSV right ventricular stroke volume; RVEF right ventricular ejection fraction.

Figure 2 (panels B, D and F) provides typical examples of MRI images used to identify the position of RV lead and the RV lead tip.

Potential maps

Epicardial potentials were inversely reconstructed and the distribution was visualised using potential maps. For all patients, the site of earliest ventricular depolarisation could be identified. **Figure 3** shows 3 typical examples of the potential distributions reconstructed from the BSP recorded during pacing from different locations.

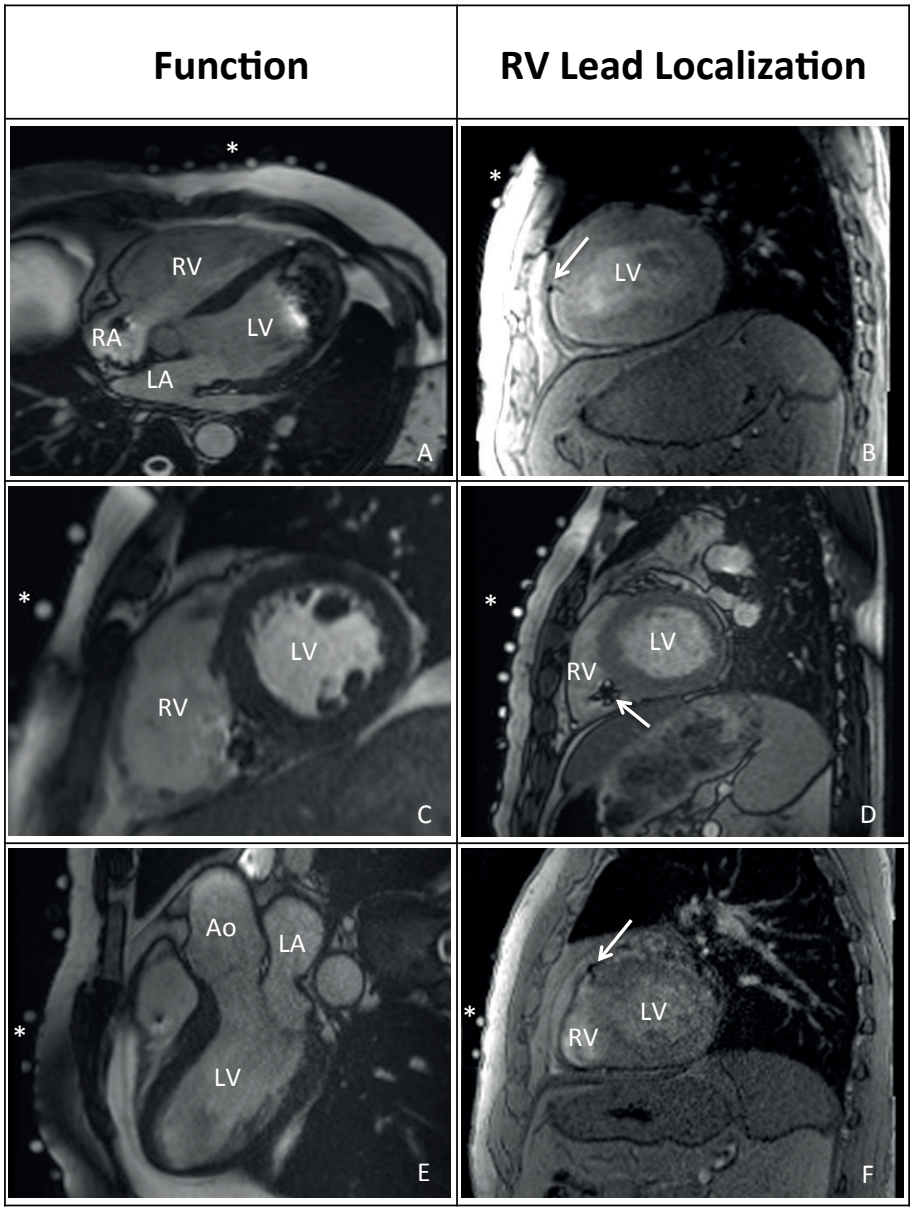

Figure 2. Left panel: End-diastolic frames from four-chamber **(A)**, short-axis **(C)** and three-chamber **(E)** Steady State Free Precession (SSFP) CINE images. Despite regional artifacts, caused by either the impulse generator or the pacing leads, the image quality allows for accurate assessment of LV and RV volumes and function. LA left atrium, LV left ventricle, RA right atrium, RV right ventricle, Ao aorta. **Right panel:** Three examples **(B, D & F)** of the T2-weighted, bright blood images used to localise the RV pacing lead (white arrows). The asterisks indicate the MRI markers that represent the location of the BSP electrodes.

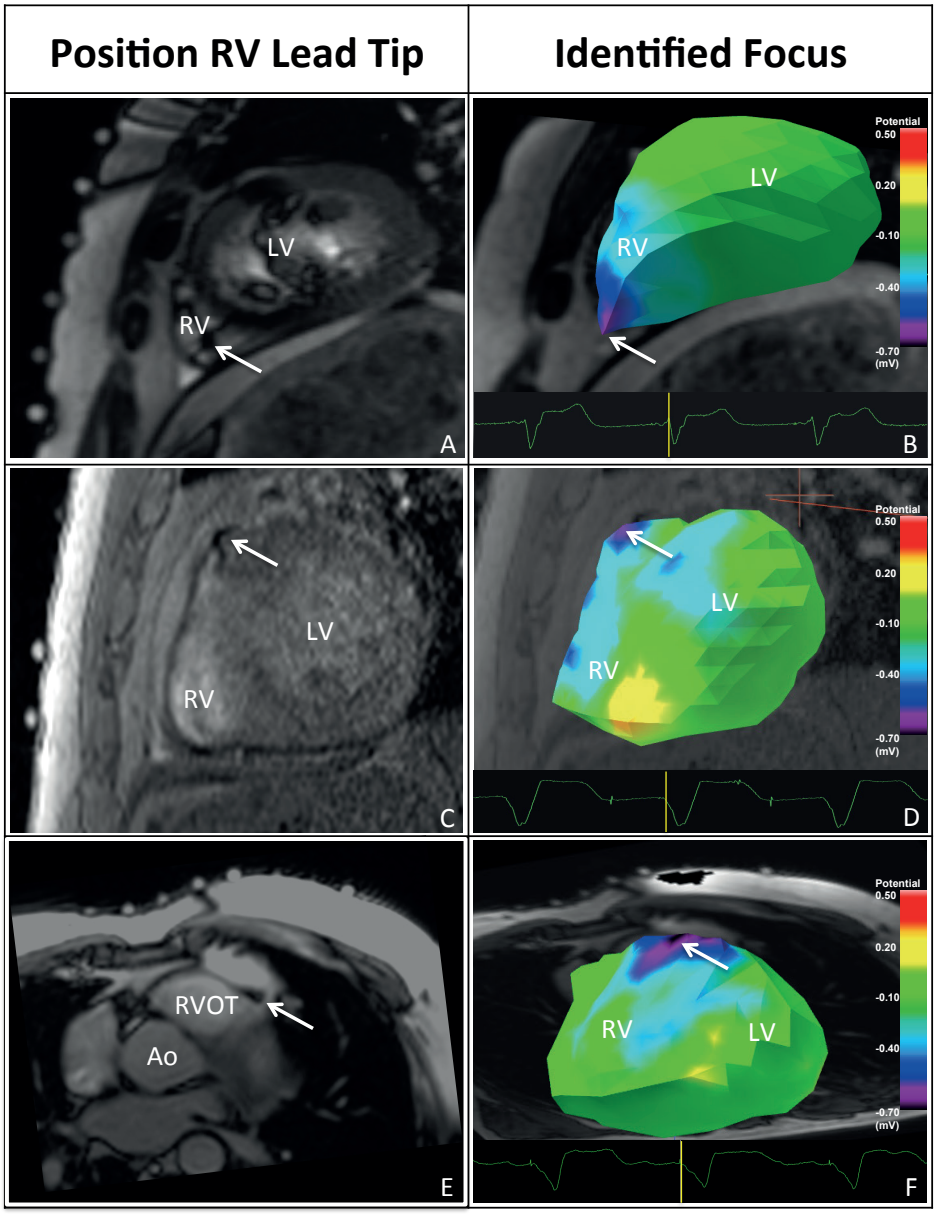

Figure 3. RV lead tip position and site of earliest depolarisation on the potential maps. Pacing from the RV apex **(A & B)**, high in the mid-ventricular septum **(C & D)** and right ventricular outflow tract **(E & F)**.

In two patients (patient 4 and 8), depolarisation started in the superior part of the right ventricular septum. A rapid subsequent depolarisation of the right ventricular free wall was observed (video 1).

In two patients (patient 1 and 2), the site of earliest depolarisation was located in the apical region of the right ventricle. From that point, depolarisation spread rapidly to the basal portion of both the RV and left ventricle (LV) (video 2).

Localisation

In patients with the tip of the pacing lead close to the epicardium (apex or right ventricular outflow tract), the distance between lead tip position and epicardial breakthrough was 6.0 ± 1.9mm.

For the patients with the tip of the pacing lead implanted in the middle of the mid-ventricular septum, the observed site of epicardial breakthrough varied substantially across the right ventricular free wall. In these patients, the intrinsic distance from the lead tip to the epicardium was relatively large (range: 5-30mm). This distance contributes significantly to the measured localisation error (range: 11-45mm).

Correlation

In all patients, a high correlation ($r = 0.97\text{-}0.99$, $p < 0.001$) between the epicardial potential distributions of two different paced beats was calculated (**table 3**). Correlation values were visualised using correlation maps (**figure 4**).

Table 3. Distance epicardial focus to lead tip and correlation between two different paced beats.

Patient	Position RV lead tip	Distance epicardial focus to lead tip (mm)	Correlation (r)
1	Apex	4	0.996
2	Apex	5	0.997
3	Mid-septum	45	0.978
4	RVOT	6	0.997
5	Mid-septum	20	0.995
6	Infero-septum	25	0.979
7	Mid-septum	11	0.999
8	RVOT	9	0.994
9	Infero-septum	13	0.999
10	Mid-septum	43	0.966

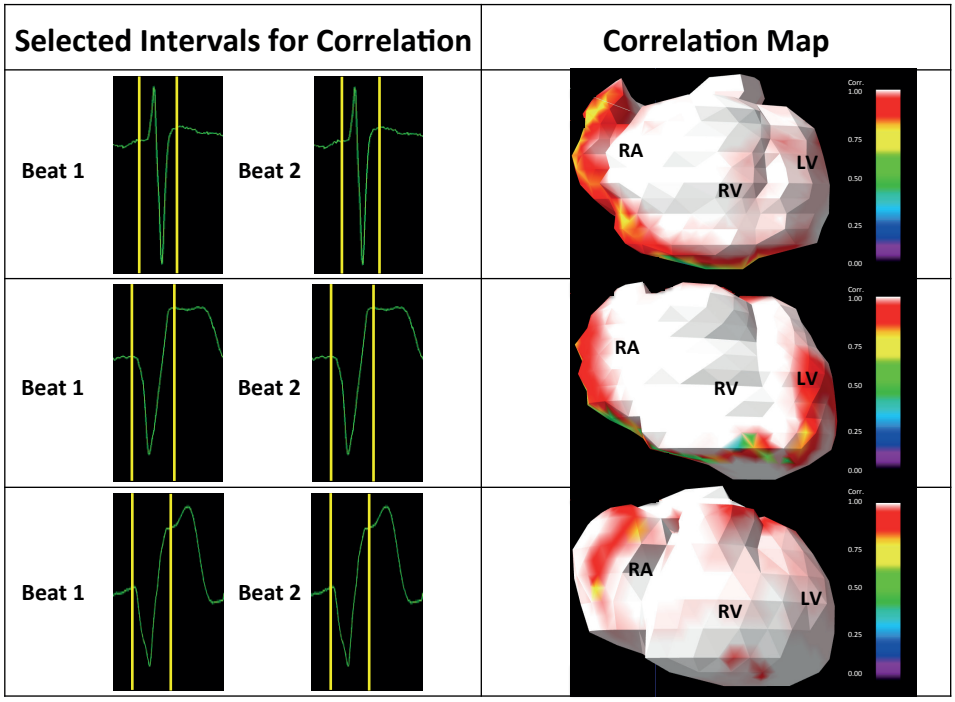

Figure 4. Three examples of intervals selected for correlation analysis **(left panel)** and the corresponding correlation maps **(right panel)**. In all patients, a high correlation ($r = 0.97$-0.99, $p < 0.001$) between the epicardial potential distribution of two different paced beats was found.

DISCUSSION

This is one of the first *in vivo* studies in patients with an MRI-conditional pacemaker system, in which a combined MRI and IPM approach was applied to non-invasively determine the origin and epicardial potential distribution during pacing. In patients with the tip of the pacing lead close to the epicardium, a localisation error of 6.0 ± 1.9 mm was found.

This clinically relevant accuracy and the less cumbersome nature of the present IPM method may facilitate non-invasive localisation of ectopic ventricular foci in patients suffering from ventricular arrhythmia prior to entering the catheterisation suite.

In addition, this offers the prospect of thoroughly investigating *in vivo* electrical and mechanical activation patterns in patients with an implanted MRI-conditional pacemaker system.

Novelty of this work

IPM in patients with MRI-conditional pacemaker systems

To our knowledge, this is one of the first reports on the application of IPM in patients with implanted MRI-conditional pacemaker systems. Most validation studies on non-invasive mapping were performed in animal hearts using computed tomography (CT) or in humans during conventional electrophysiological studies [11–14].

In the past, a limited number of patients with an implanted pacemaker have been studied for validation purposes. In these studies, ECGI uses 254 torso electrodes and CT images to calculate epicardial potentials. In only one patient with an implanted cardiac resynchronisation therapy (CRT) device, a localisation error of 7 mm for the RV pacing lead and 11 mm for the LV lead has been reported [15].

NICE uses 65 electrodes and MRI images to estimate endo- and epicardial activation times. NICE has been applied in ten patients with an implanted CRT device [16] and in one patient with a CRT device and a quadripolar LV lead [17]. No localisation errors could be determined in these studies. Due to the non-MRI compatibility of the devices used, the MRI scan was performed prior to implantation of the device, whereas BSP were recorded after implantation. Hence, co-registration of the device, the anatomy of the patients and torso electrodes was not performed.

Recently, Revishili et al. [18] demonstrated the accuracy of a novel non-invasive epi- and endocardial electrophysiology system (NEEES) in 29 patients with implanted devices (26 CRT devices in three dual-chamber pacemakers). The mean distance from the non-invasively predicted pacing site to the anatomic reference site was 10.8 ± 5.4 mm for the right atrium, 7.7 ± 5.8 mm for the right ventricle and 7.9 ± 5.7 mm for the left ventricle. However, the authors state that members processing the NEEES data were not completely blinded for the exact position of each pacing lead on the available CT images.

Anterior concentrated electrodes

In this study, all BSP electrodes were positioned in a matrix, directly overlaying the heart. By concentrating the electrodes, a localisation error of 6.0 ± 1.9 mm was found for patients with the tip of the pacing lead close to the epicardium. The rapid positioning of this electrode array may facilitate the incorporation of this technique in clinical practice.

Epicardial potentials

Currently, only epicardial potentials can be reconstructed from the recorded BSP. Reconstruction of both epicardial and endocardial activation would require the application of an a priori activation model (e.g. NICE, NEEES). Use of a priori models mandates various assumptions to be made and limits the number of pathology related activation patterns that can be represented.

As described previously by Rudy and co-workers, epicardial potentials contain information on intramural and endocardial activation even before the epicardium is activated [19]. Epicardial potentials of the complete cardiac cycle can be non-invasively reconstructed and isochrones or activation times can be derived from the reconstructed potentials [20].

In patients with implanted pacing devices, visualisation of epicardial activation may provide additional insight into the efficacy of the pacing strategy. Changes in depolarisation or repolarisation or other signs of adverse pacing effects may be detected at an early stage. Various studies have demonstrated that long-term ventricular pacing may have various unintended adverse electrophysiological and mechanical effects [21-22]. In order to better understand the underlying (patho-) physiological mechanisms, it is important to further develop clinically applicable, non-invasive techniques that facilitate an integrated electro-mechanical assessment.

MRI

Using MRI as a reference for the RV lead tip position is a novelty. The introduction of MRI-conditional pacemaker systems enables the use of MRI for IPM. Unlike CT, MRI is not associated with radiation exposure. MRI-conditional devices can be programmed in an MRI safe mode, which makes the device less susceptible to the magnetic energy of the MRI environment and decreases the risk of hard- or software interactions.

Besides visualizing the lead position, MRI may provide valuable information on the mechanical activation in patients with implanted pacemaker systems. In contrast to CT, MRI enables the safe performance of follow-up studies. In addition, MRI is the gold standard for the detailed assessment of atrial and ventricular volumes, function and wall motion abnormalities [23]. Moreover, the presence and the extent of myocardial scar tissue can be determined, which may influence cardiac electrical activation patterns and may impact the effects of pacing [24].

The presence of an implanted device generates image artifacts that may compromise image quality. By adapting the scan strategy, the amount of artifacts produced by the implanted pacemaker system can be kept at a minimum [25]. Ventricular function is usually assessed in the short-axis view. These images are mildly affected by the distortion caused by the presence of a pacemaker. Left and right ventricular function could be assessed for all patients in this study.

Limitations of the study

The site of epicardial breakthrough on the epicardial potential map was compared to the position of the ventricular lead tip on MRI and the distance between these points was determined. The position of the RV lead tip was determined using the susceptibility artifact caused by the lead tip on the MRI images (figures 2 and 3). Alternatively, CT may be used for this purpose. Nevertheless, the scattering of radiation causes the overall image quality to decline. In addition, the metallic artifact caused by the lead will hamper the localisation of the tip of lead [26].

For several patients, the reported distance from the lead tip to the site of earliest depolarisation on the epicardial potential maps includes the distance from the lead tip in the septum to the epicardium. Septal insertion of the lead tip increases the intrinsic distance from the lead tip to the site of epicardial breakthrough. This is a limitation of the reconstruction of epicardial potentials. Therefore, the localisation accuracy is probably severely underestimated in this group of patients.

The anterior concentration of BSP electrodes does not allow for accurate investigation of depolarisation on the posterior wall. This pilot study focussed on investigating the feasibility of performing IPM in patients with an implanted MRI-conditional pacemaker system. The current research did not describe the accuracy of localizing foci in the inferior wall of the RV or LV. Atrial stimuli were not analysed in the current study.

It has been shown that prematurity of ectopic foci can affect cardiac activation patterns. This was not explored in this current study by introducing different coupled extra-stimuli during RV pacing.

The accuracy of localizing epicardial breakthrough may be affected by extensive scar in patients with prior infarction or severe cardiomyopathy. For this reason and in consideration of the limited size of the study population, additional research needs to be performed to further explore the clinical benefit of IPM in combination with MRI in patients suffering from a wide range of pathologies.

CONCLUSION

In this study, an IPM method using a limited number of electrodes was applied in patients with an MRI-conditional pacemaker system. For all patients, the epicardial potential distribution could be reconstructed from BSP recorded during pacing. In patients with the tip of the pacing lead close to the epicardium, a localisation accuracy of 6.0 ± 1.9 mm was found. Application of this method in patients suffering from ventricular arrhythmia may enable accurate non-invasive localisation of ectopic ventricular foci prior to entering the catheterisation suite.

REFERENCES

1. Erkapic D, Greiss H, Pajitnev D, Zaltsberg S, Deubner N, Berkowitsch A, et al. Clinical impact of a novel three-dimensional electrocardiographic imaging for non-invasive mapping of ventricular arrhythmias-a prospective randomized trial. Europace. 2015;17(4):591-7.
2. Jamil-Copley S, Bokan R, Kojodjojo P, Qureshi N, Koa-Wing M, Hayat S, et al. Noninvasive electrocardiographic mapping to guide ablation of outflow tract ventricular arrhythmias. Heart Rhythm. 2014;11(4):587-94.
3. Vijayakumar R, Silva JN, Desouza KA, Abraham RL, Strom M, Sacher F, et al. Electrophysiologic Substrate in Congenital Long QT Syndrome: Noninvasive Mapping With Electrocardiographic Imaging (ECGI). Circulation. 2014;25;130(22):1936-43.
4. Berger T, Fischer G, Pfeifer B, Modre R, Hanser F, Trieb T, et al. Single-beat noninvasive imaging of cardiac electrophysiology of ventricular pre-excitation. J Am Coll Cardiol. 2006;21;48(10):2045-52.
5. Bokeriia LA, Revishvili ASh, Kalinin AV, Kalinin VV, Liadzhina OA, Fetisova EA. Hardware-software system for noninvasive electrocardiographic examination of heart based on inverse problem of electrocardiography. Med Tekh. 2008;6:1-7.
6. Ferreira AM, Costa F, Tralhão A, Marques H, Cardim N, Adragão P. MRI-conditional pacemakers: current perspectives. Med Devices (Auckl). 2014;7;7:115-24.
7. van der Graaf AW, Bhagirath P, de Hooge J, de Groot NM, Götte MJ. A-Priori Model Independent Inverse Potential Mapping; The Impact of Electrode Positioning. Clin Res Cardiol. 2016;105(1)79-88.
8. Wollmann CG, Thudt K, Kaiser B, Salomonowitz E, Mayr H, Globits S. Safe performance of magnetic resonance of the heart in patients with magnetic resonance conditional pacemaker systems: the safety issue of the ESTIMATE study. J Cardiovasc Magn Reson. 2014;6;16;30:1-8.
9. Oostendorp T, Nenonen J, Korhonen P. Noninvasive determination of the activation sequence of the heart: application to patients with previous myocardial infarctions. J Electrocardiol. 2002;35 Suppl:75-80.
10. Marchandise E, Geuzaine C, Remacle JF. Cardiovascular and lung mesh generation based on centerlines. Int J Numer Method Biomed Eng. 2013;29(6):665-82.
11. Oster HS, Taccardi B, Lux RL, Ershler PR, Rudy Y. Electrocardiographic imaging: Noninvasive characterisation of intramural myocardial activation from inverse-reconstructed epicardial potentials and electrograms. Circulation. 1998;21;97(15):1496-507.
12. Cakulev I, Sahadevan J, Arruda M, Goldstein RN, Hong M, Intini A, et al. Confirmation of Novel Noninvasive High Density Electrocardiographic Mapping with Electrophysiology Study: Implications for Therapy. Circ Arrhythm Electrophysiol. 2013;6(1):68-75.
13. Sapp JL, Dawoud F, Clements JC, Horacek BM. Inverse solution mapping of epicardial potentials: quantitative comparison with epicardial contact mapping. Circ Arrhythm Electrophysiol. 2012;5(5):1001-9.

14. Ghanem RN, Jia P, Ramanathan C, Ryu K, Markowitz A, Rudy Y. Noninvasive electrocardiographic imaging (ECGI): comparison to intraoperative mapping in patients. Heart Rhythm. 2005;2(4):339-54.
15. Ramanathan C, Ghanem RN, Jia P, Ryu K, Rudy Y. Electrocardiographic Imaging (ECGI): A Noninvasive Imaging Modality for Cardiac Electrophysiology and Arrhythmia. Nat Med. 2004;10:422-428.
16. Berger T, Pfeifer B, Hanser FF, Hintringer F, Fischer F, Netzer M, et al. Single-beat noninvasive imaging of ventricular endocardial and epicardial activation in patients undergoing CRT. PLoS One. 2011 27;6(1):e16255.
17. Seger M, Hanser F, Dichtl W, Stuehlinger M, Hintringer F, Trieb T, et al. Non-invasive imaging of cardiac electrophysiology in a cardiac resynchronisation therapy defibrillator patient with a quadripolar left ventricular lead. Europace. 2014;16(5):743-9.
18. Revishvili AS, Wissner E, Lebedev DS, Lemes C, Deiss S, Metzner A, et al. Validation of the mapping accuracy of a novel non-invasive epicardial and endocardial electrophysiology system. Europace. 2015;17(8):1282-8.
19. Rudy Y. Noninvasive electrocardiographic imaging of arrhythmogenic substrates in humans. Circ Res. 2013;1;112(5):863-74.
20. Oster HS, Taccardi B, Lux RL, Ershler PR, Rudy Y. Noninvasive electrocardiographic imaging: reconstruction of epicardial potentials, electrograms, and isochrones and localisation of single and multiple electrocardiac events. Circulation. 1997;5;96(3):1012-24.
21. De Sisti A, Márquez MF, Tonet J, Bonny A, Frank R, Hidden-Lucet F. Adverse effects of long-term right ventricular apical pacing and identification of patients at risk of atrial fibrillation and heart failure. Pacing Clin Electrophysiol. 2012;35(8):1035-43.
22. Akerström F, Pachón M, Puchol A, Jiménez-López J, Segovia D, Rodríguez-Padial L, et al. Chronic right ventricular apical pacing: adverse effects and current therapeutic strategies to minimize them. Int J Cardiol. 2014;15;173(3):351-60.
23. Abbasi SA, Ertel A, Shah RV, Dandekar V, Chung J, Bhat G, et al. Impact of cardiovascular magnetic resonance on management and clinical decision-making in heart failure patients. J Cardiovasc Magn Reson. 2013;1;15:89.
24. Bleeker GB, Kaandorp TA, Lamb HJ, Boersma E, Steendijk P, de Roos A, et al. Effect of posterolateral scar tissue on clinical and echocardiographic improvement after cardiac resynchronisation therapy. Circulation. 2006;21;113(7):969-76.
25. Khan JN, Singh A, Pakkal MV, McCann GP. MRI-safe pacemakers and reduction of cardiac MRI artefacts with right-sided implantation. Eur Heart J Cardiovasc Imaging. 2013;14(8):830.
26. Sasaki T, Hansford R, Zviman MM, Kolandaivelu A, Bluemke DA, Berger RD, et al. Quantitative assessment of artifacts on cardiac magnetic resonance imaging of patients with pacemakers and implantable cardioverter-defibrillators. Circ Cardiovasc Imaging. 2011;4(6):662-70.

10

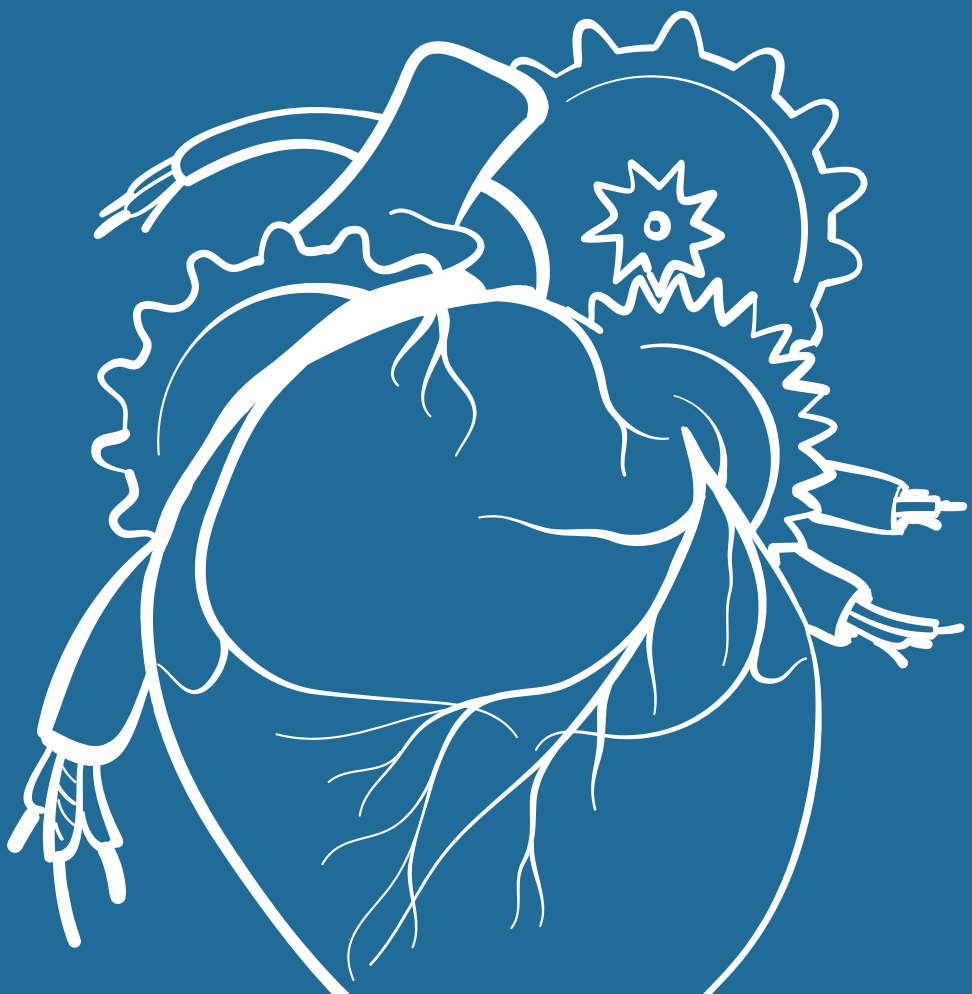

FEASIBILITY AND ACCURACY OF CARDIAC MAGNETIC RESONANCE IMAGING–BASED WHOLE-HEART INVERSE POTENTIAL MAPPING OF SINUS RHYTHM AND IDIOPATHIC VENTRICULAR FOCI

Bhagirath P, van der Graaf AW, van Dongen EA, de Hooge J, van Driel VJ, Ramanna H, de Groot NM, Götte MJ.
Journal of the American Heart Association. 2015; 4(10): e002222.

ABSTRACT

Background: Inverse potential mapping (IPM) non-invasively reconstructs cardiac surface potentials using body surface potentials. This requires a volume conductor model (VCM), usually constructed from computed tomography; however, computed tomography exposes the patient to harmful radiation and lacks information about tissue structure. Magnetic resonance imaging (MRI) is not associated with this limitation and might have advantages for mapping purposes. This feasibility study investigated a magnetic resonance imaging–based IPM approach. In addition, the impact of incorporating the lungs and their particular resistivity values was explored.

Methods and results: Three volunteers and 8 patients with premature ventricular contractions scheduled for ablation underwent 65-electrode body surface potential mapping. A VCM was created using magnetic resonance imaging. Cardiac surface potentials were estimated from body surface potentials and used to determine the origin of electrical activation. The IPM-defined origin of sinus rhythm corresponded well with the anatomic position of the sinus node, as described in the literature. In patients, the IPM-derived premature ventricular contraction focus was 3-dimensionally located within 8.3±2.7 mm of the invasively determined focus using electroanatomic mapping. The impact of lungs on the IPM was investigated using homogeneous and inhomogeneous VCMs. The inhomogeneous VCM, incorporating lung-specific conductivity, provided more accurate results compared with the homogeneous VCM (8.3±2.7 and 10.3±3.1 mm, respectively; P=0.043). The interobserver agreement was high for homogeneous (intraclass correlation coefficient 0.862, P=0.003) and inhomogeneous (intraclass correlation coefficient 0.812, P=0.004) VCMs.

Conclusion: Magnetic resonance imaging–based whole-heart IPM enables accurate spatial localisation of sinus rhythm and premature ventricular contractions comparable to electroanatomic mapping. An inhomogeneous VCM improved IPM accuracy.

INTRODUCTION

Inverse potential mapping (IPM) allows for non-invasive reconstruction of epicardial activation patterns. The most frequently used IPM method is based on a homogeneous volume conductor model (VCM) constructed from computed tomography images [1]. This technique is being applied increasingly for analysis of idiopathic ventricular foci and guidance of catheter ablation [2,3].

Although clinically useful, this computed tomography–based approach has important limitations. The most important limitation, besides the exposure to radiation and associated risk of malignancies [4], is the inability to characterise tissue in detail. Magnetic resonance imaging (MRI) does not have these limitations and is considered the gold standard for tissue characterisation, in particular for edema and fibrosis. Although most publications underscore the fact that both computed tomography and MRI can be used, MRI is less frequently used for IPM [5-7].

In addition, the use of a homogeneous VCM could also be considered a limitation because it may not appropriately incorporate the effects of specific tissue-conductivity characteristics such as those from the lungs (ie, inhomogeneous conditions) [8].

This study investigated the feasibility of whole-heart IPM using a VCM derived from MRI. The clinical applicability of this approach was evaluated in healthy volunteers and patients with idiopathic ventricular foci. In addition, the influence of tissue impedance on the results of IPM was studied using 2 different VCMs. A homogeneous thoracic VCM (model 1) was compared with an inhomogeneous VCM in which, in addition to thoracic impedance, the resistance value of the lungs was included (model 2).

METHODS

Patient population

The study population consisted of 3 healthy volunteers and 8 patients with symptomatic or therapy-resistant premature ventricular contractions (PVCs). The study complied with the Declaration of Helsinki and received approval from the local ethics committee (METC Zuidwest Holland study NL38156.098.11) and the institutional scientific board. Written informed consent was obtained from the study participants.

Body surface potential acquisition

An MRI scout scan was performed to approximate the position of the heart with respect to the thorax. Subsequently, 62 (+3 limb) electrodes were applied to each participant's torso, centralised over the heart. Body surface potentials (BSPs) were acquired using a 65-channel ActiveTwo system (BioSemi BV). Once the acquisition was completed, the electrode locations were marked with MRI markers, enabling accurate identification of the electrode positions.

Image acquisition

MRI studies were obtained using a 1.5T Aera scanner (Siemens Healthcare). Blackblood imaging was performed using a half-Fourier acquisition single-shot turbo spin-echo, or HASTE, pulse sequence to acquire 3 perpendicular stacks (axial, coronal, and sagittal) from the neck to the lower abdomen.

Images were acquired during free breathing using navigator gating (diaphragm) with a 1-mm window. ECG gating was used to acquire images during the diastolic phase of the cardiac cycle. Typical imaging parameters were spatial resolution of 1.2×1.2×6 mm, repetition time/echo time 744/42 ms, and flip angle of 160°.

VCM and computational algorithm

The MRI images were segmented using a custom-developed tool. This tool generates a script containing the geometric description (points, lines and planes, and directed line loops) of the segmentation. Subsequently, the script was meshed using GMSH [9]. Conductivity for the homogeneous VCM (model 1) was specified at 0.2 Siemens per meter (S/m) [10]. The inhomogeneous VCM (model 2) had a similar summation but also contained specific conductivity values for the lungs, specified at 0.04 S/m.10

Cardiac surface potentials were calculated from BSPs using the following equation in which CSP indicates cardiac surface potentials, T is the transfer matrix, and λ is the regularisation strength:

$$CSP = (T^T T + \lambda^2 I)^{-1} T^T BSP$$

Electrophysiological study and catheter ablation

The electrophysiologists (H.R. and V.D.) were blinded to the IPM results. During the electrophysiological study, femoral venous and arterial access was established. In all cases, a hexapolar catheter (Supreme; St. Jude Medical) was placed in the right atrial appendage, and the proximal electrode located in the inferior vena cava served as the

unipolar indifferent electrode. In addition, a screw-in temporary pacing lead (Medtronic) was placed in the right ventricle as a positional reference for the electroanatomic mapping (EAM) system (Ensite Velocity 3.0; St. Jude Medical). An EAM was created using the roving catheter. Respiratory compensation was set to automatic. No field scaling was performed.

If no spontaneous PVCs were present, isoproterenol and/or pacing maneuvers were used to provoke PVCs. After the focus location was identified, targeted ablation was performed using a standard 4-mm nonirrigated ablation catheter with power delivery up to 50W and a temperature limitation of 50°C. Subsequently, the site of ablation was marked on the EAM system.

Comparison of focus localisation

Following the ablation procedure, the ectopic PVC focus location identified on the IPM was compared with the site of ablation specified on the EAM (gold standard). For this purpose, 2 experienced operators (P.B. and H.R.) independently identified the foci on IPM and EAM to provide a measure of interobserver variability.

This approach resulted in 3 different data sets describing the focus localisation as the x, y, and z coordinates: (1) IPM using the homogeneous model (data set 1), (2) IPM using the inhomogeneous model (data set 2), and (3) EAM (data set 3). Subsequently, Pythagoras' theorem for 3-dimensional coordinate vectors, in which the distance between 2 points is equal to the square root of the sum of the squared coordinate differences, was used to calculate the differences between coordinate data sets 1 and 3 and coordinate data sets 2 and 3.

Statistical analysis

Statistical analysis was performed using IBM SPSS Statistics (version 22.0; IBM Corp). Continuous variables were expressed as mean±SD or as median and interquartile range. Localisation errors between the 2 VCMs were compared using the Wilcoxon signed-rank test. The intraclass correlation coefficient was used to analyse interobserver agreement. $P<0.05$ was considered statistically significant.

RESULTS

Study population

Baseline characteristics of the 3 volunteers and 8 patients (N=11) are provided in **table 1**. All volunteers had normal ECGs. In both volunteers and patients, structural heart disease was excluded based on the MRI examination.

Table 1. Characteristics of participants undergoing inverse potential mapping.

	Volunteers	Patients
n	3	8
Age, y	28 ± 3	46 ± 13
BMI	22.1 ± 1.4	25.2 ± 6.7
Female (%)	1 (33)	7 (88)
LVEF (%)	55 ± 2	50 ± 3
RVOT PVCs	-	6 (75%)
Duration of PVCs, months	-	18 ± 12
PVC burden before procedure	-	14 121 (10 432 to 22 373)
PVC burden after procedure	-	17 (1 to 24)

Age, BMI, LVEF, and PVC duration are expressed in mean±SD. PVC burden before and after procedure is expressed using median (interquartile range). PVC burden is expressed in ectopic beats per 24 hours. BMI indicates body mass index; LVEF, left ventricular ejection fraction; PVC, premature ventricular contractions; RVOT, right ventricular outflow tract.

Ablation procedure

The preprocedural median PVC burden was 14 121 ectopic beats per 24 hours (interquartile range 10 432 to 22 373 ectopic beats per 24 hours). Average procedural time, including mapping and ablation, was 129±53 minutes. An average of 4468 points were acquired to construct the EAM. No periprocedural displacements of the EAM were observed.

After catheter ablation, the PVC burden was reduced to a median of 17 ectopic beats per 24 hours (interquartile range 1 to 24 ectopic beats per 24 hours), a reduction of >99%.

IPM in sinus rhythm

During sinus rhythm, the first point of activation on the potential map of healthy volunteers was located anatomically near the transition of the superior vena cava (crista terminalis) into the right atrium (**Figure 1A**, white arrow). Ventricular breakthrough began at the right ventricular free wall (**Figure 1B**), at the site at which the moderator band was attached to the ventricular myocardium.

Comparison between IPM focus and actual ablation site

No pacing maneuvers were required for PVC induction. Five patients required isoproterenol to induce PVCs. Based on invasive mapping, the ablation site was in the right ventricular outflow tract (VOT) in 6 patients and in the left VOT in 2 patients (**Table 2**). One patient had a right bundle branch block, which was reconstructed correctly by IPM (Video S1).

In all 8 cases, IPM located the ectopic focus in the correct cardiac compartment (**Table 2**). IPM identified all right VOT foci in close proximity to the ablation lesion (8.4±3 mm, n=6) defined on the EAM (**Figure 2**; Video S2). A similar difference was found for the left VOT foci (7.9±1.5 mm, n=2). IPM located 1 of the left VOT foci (Case 2) at the right coronary cusp; however, the ablation for this patient was performed successfully in the distal left VOT (**Figure 3**). The other left VOT focus was closely approximated to the actual site of ablation.

Table 2. Comparison of PVC focus identified with IPM and ablation site on electroanatomic mapping.

Case	PVC focus IPM	Ablation site
1	NCC–LCC junction	LCC
2	RVOT-septal	RVOT-septal
3	RVOT-anterior proximal	RVOT-anterior proximal
4	RVOT-anterior	RVOT-anterior
5	RVOT-septal proximal	RVOT-septal proximal
6	RVOT-anteroseptal	RVOT-septal
7	RVOT-posteroseptal	RVOT-septal
8	NCC	NCC

LCC indicates left coronary cusp; LVOT, left ventricular outflow tract; NCC, non-coronary cusp; RCC, right coronary cusp; RVOT, right ventricular outflow tract.

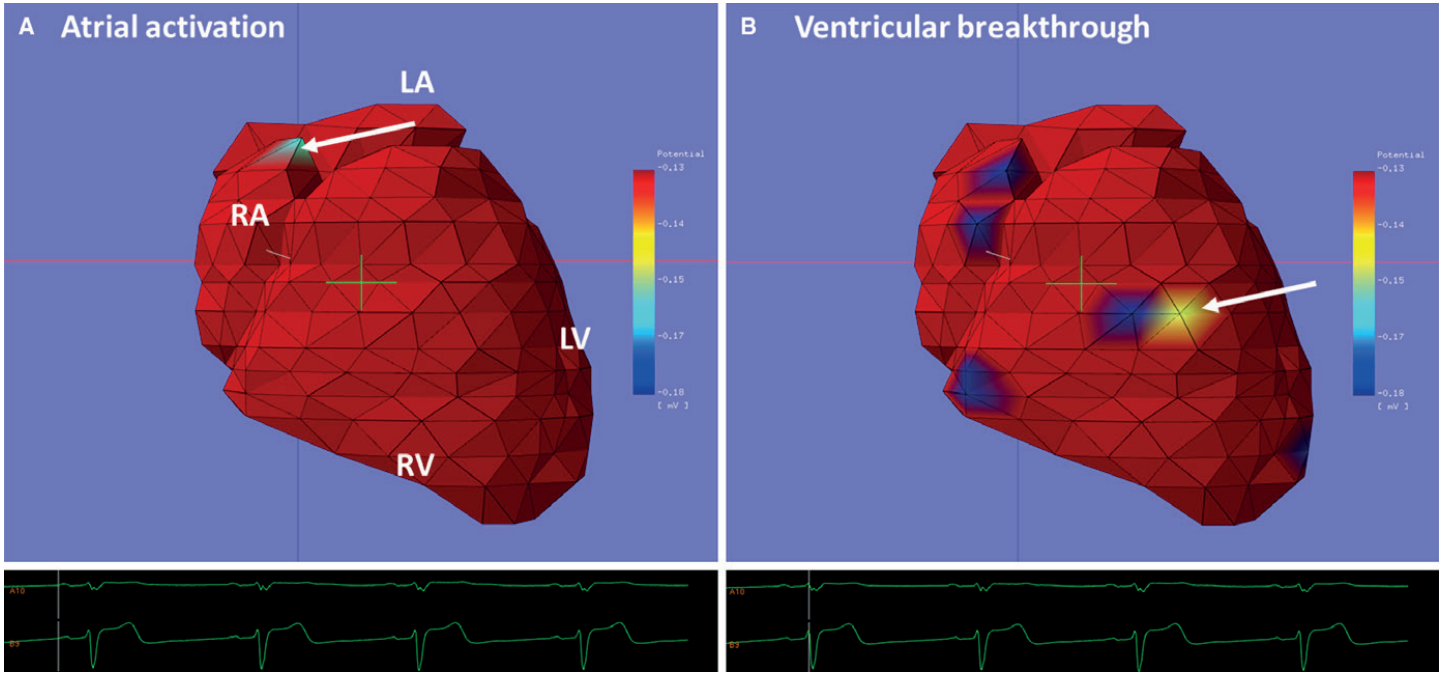

Figure 1. IPM in a healthy volunteer during sinus rhythm. The left panel depicts the IPM at the start of the atrial depolarisation (P wave), and the right panel depicts the IPM at the start of the ventricular depolarisation (QRS). The anterior-posterior view of the 3-dimensional heart model can be observed. The first point of atrial activation is observed near the entrance of the superior vena cava (white arrow) into the right atrium. The first point of ventricular activation is observed at the RV free wall (white arrow), at which the moderator band is attached to the ventricular myocardium. IPM indicates inverse potential mapping; LA, left atrium; LV, left ventricle; RA, right atrium; RV, right ventricle.

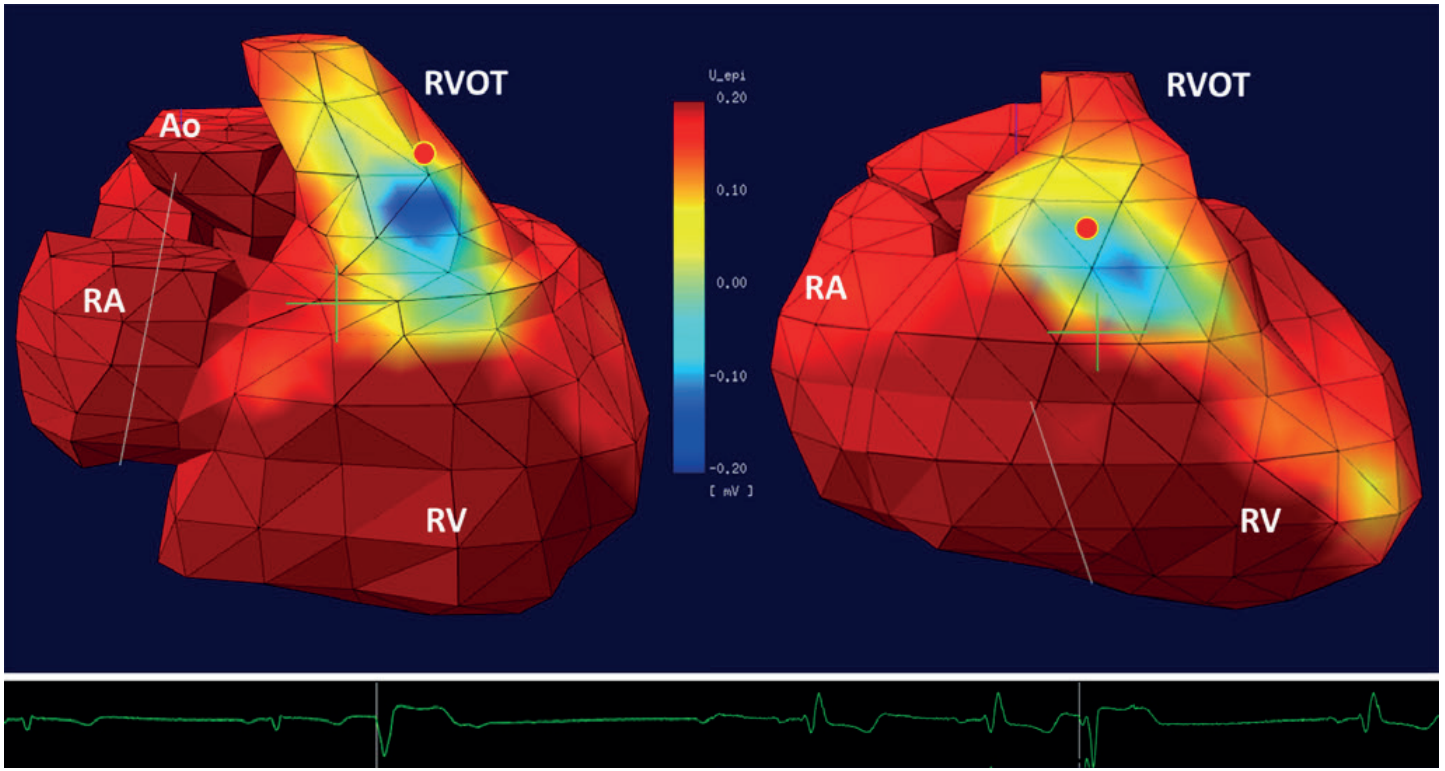

Figure 2. Comparison between inverse potential mapping and electroanatomic mapping for patients with RVOT premature ventricular contractions. Blue indicates the area of epicardial breakthrough. The red dot indicates the site of ablation. ECG is provided underneath each image. Ao indicates the aorta; RA, right atrium; RV, right ventricle; RVOT, right ventricular outflow tract.

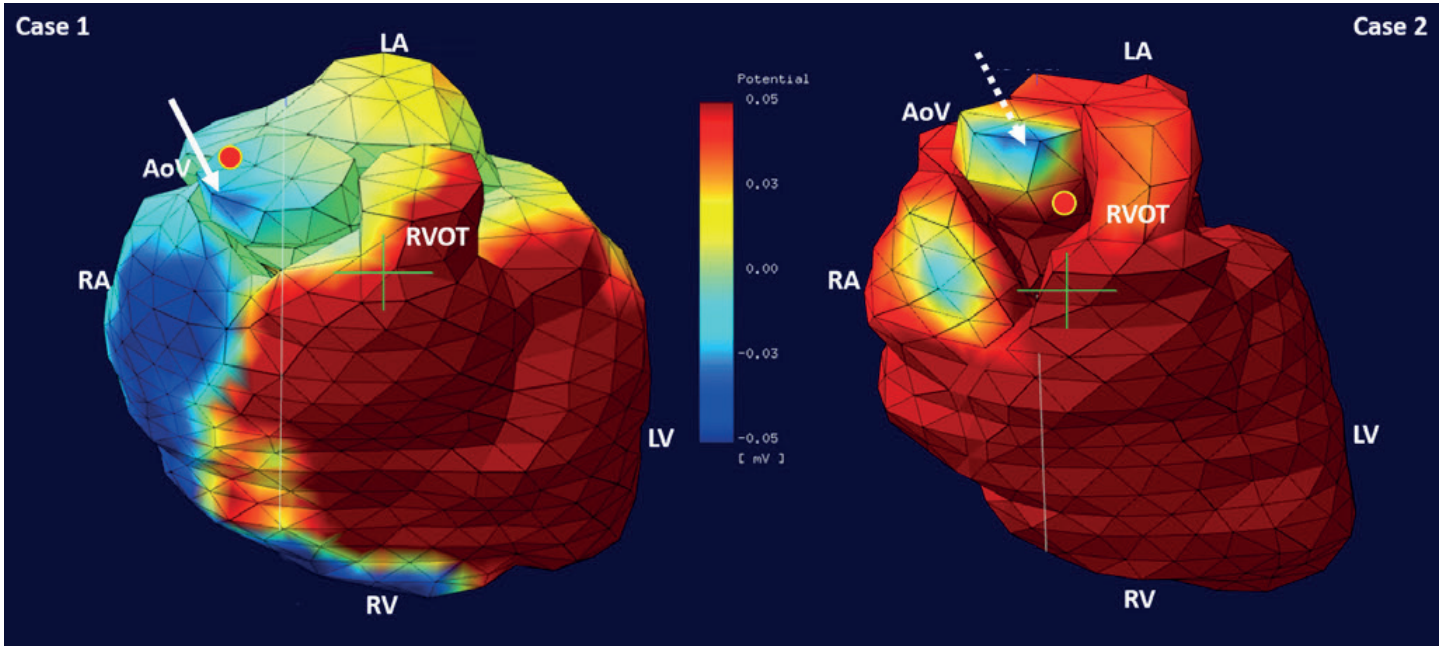

Figure 3. Comparison between inverse potential mapping and electroanatomic mapping for the patients with left ventricle outflow tract premature ventricular contractions. Blue indicates the area of epicardial breakthrough (white arrows). The red dot indicates the site of ablation. ECG is provided underneath each image. AoV indicates the aortic valve; LA, left atrium; LV, left ventricle; RA, right atrium; RV, right ventricle; RVOT, right ventricular outflow tract.

Comparison between homogeneous and inhomogeneous VCMs

The comparison of PVC focus between the inhomogeneous VCM and EAM demonstrated localisation accuracy of 8.3±2.7 mm (observer 1) and 8.2±2.8 mm (observer 2), with high interobserver agreement (intraclass correlation coefficient 0.812, 95% CI 0.318 to 0.959, P=0.004). A similar comparison between the homogeneous VCM and EAM demonstrated accuracy of 10.3±3.1 mm (observer 1) and 9.8±2.9 mm (observer 2) and also showed high interobserver agreement (intraclass correlation coefficient 0.862, 95% CI 0.399 to 0.975, P=0.003).

The focus localisation accuracy showed significant differences between the homogeneous and inhomogeneous VCMs. The homogeneous VCM had a significantly higher localisation error compared with the inhomogeneous VCM for both observers (P=0.043) (**Table 3**). In addition, the homogeneous VCM failed to identify the focus in 1 right VOT case (**Figure 4**, case 6), in which the inhomogeneous model correctly identified the site of ablation.

Table 3. Localisation difference between ectopic focus identified using homogeneous and inhomogeneous volume conductor model compared with the ablation site marked on the electroanatomic mapping.

Case	Homogeneous (mm)	Inhomogeneous (mm)	*P* value
1	11.1	9.3	
2	9.1	9.1	
3	6.4	6.4	
4	14.4	12.1	
5	Focus not identified	7.6	
6	14.9	11.7	
7	7.8	3.6	
8	8.3	6.4	
Median (IQR)	9.1 (7.8 to 14.4)	8.35 (6.4 to 11.1)	*P* = 0.043

IQR indicates interquartile range.

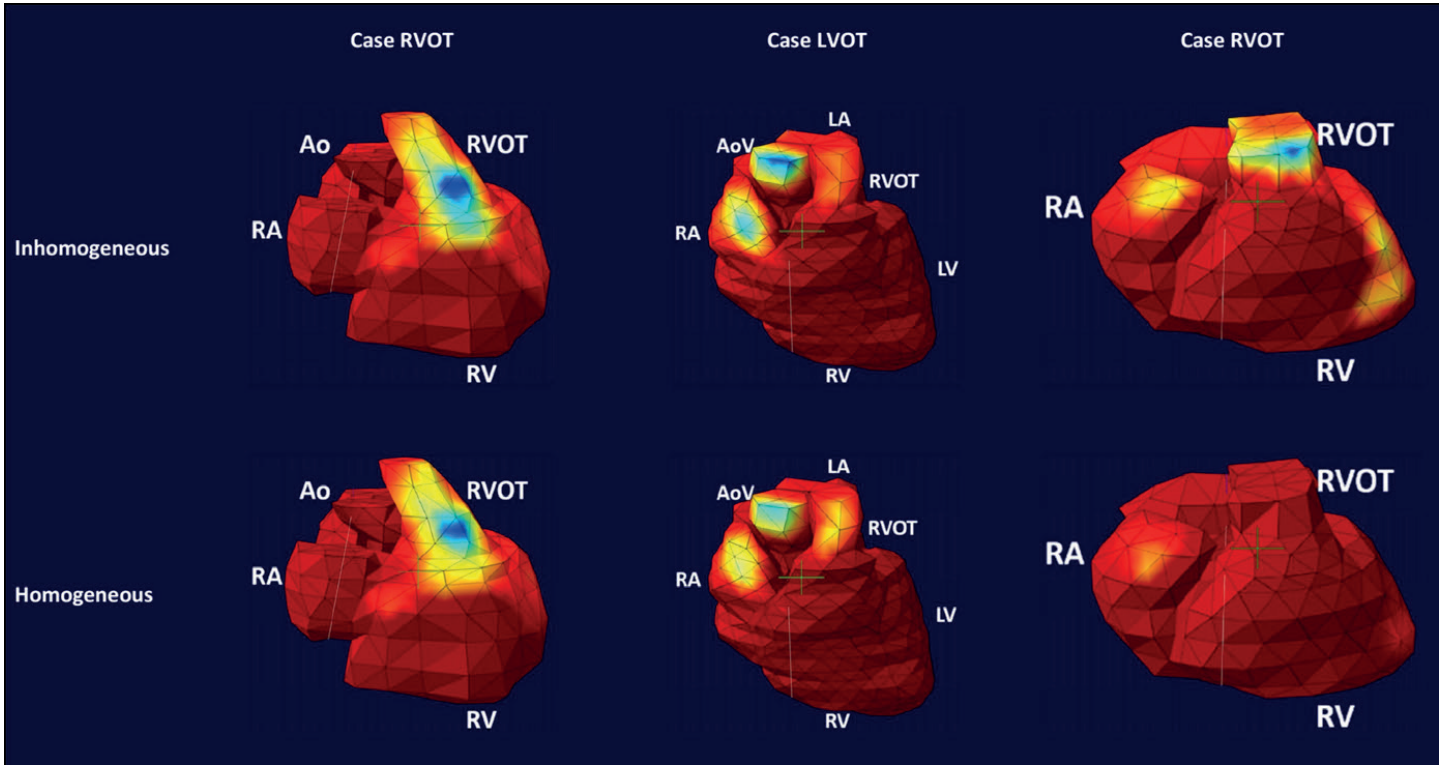

Figure 4. Comparison between homogeneous and inhomogeneous VCMs. Left and center columns depict insignificant and subtle differences between homogeneous and inhomogeneous VCMs, respectively. The right column depicts a clinically significant difference between the 2 VCMs. Ao, indicates the aorta; AoV, aortic valve; LA, left atrium; LV, left ventricle; LVOT indicates left ventricular outflow tract; RA, right atrium; RV, right ventricle; RVOT, right ventricular outflow tract; VCM, volume conductor model.

DISCUSSION

To our knowledge, this study is the first to investigate whole-heart IPM using a 62-lead anterior BSP recording and an MRI-derived inhomogeneous VCM.

The evaluation of this model was performed in healthy volunteers and patients with idiopathic arrhythmias. Using this MRI-based non-invasive method, it was possible to estimate the PVC focus location with clinically sufficient accuracy using BSPs of a single ectopic beat. In addition, a comparison between 2 independent observers demonstrated high reproducibility of the results.

Evaluation in healthy volunteers

IPM localised the origin of atrial activity near the transition of the superior vena cava (crista terminalis) into the right atrium. This location has been described in the literature as the anatomic location of the sinus node [11]. These results suggest that atrial activity may be assessed non-invasively using this combined MRI–IPM method.

The first ventricular epicardial breakthrough was located at the right ventricular free wall and corresponded with descriptions in the literature [1,12]. Furthermore, it was also possible to visualise abnormal ventricular activation patterns such as a right bundle branch block (Video S1).

These findings illustrate the potential sensitivity of IPM to detect minute changes in cardiac activation and demonstrate the ease of combining IPM with MRI acquisitions. This result offers the prospect of using this method for screening purposes.

Clinical impact in idiopathic PVC ablation

IPM successfully approximated the ablation site in 8 of 8 patients, providing a surrogate for the clinical PVC focus. This finding suggests that routine application of this non-invasive technique as part of the clinical workup could have multiple benefits such as improved ablation planning due to accurate preprocedural identification of the PVC focus (target ablation site) and reduction in procedural duration (and accompanying radiation exposure) due to reduced invasive mapping time. This may especially be valid for patients with a low PVC burden and/or multifocal PVCs.

Volume conductor models

The current, most frequently used BSP mapping technique (ECVUE; CardioInsight Technologies Inc) uses a homogeneous torso conductor model. The clinical utility of this method has been demonstrated after extensive investigation [13,14] however,

recent research advocates the integration of the various organs with their own specific impedance [8,15]. This may be the case particularly in patients with high body surface area, pulmonary edema, or myocardial infarction. These circumstances could substantially influence the BSPs due to altered conductivity and resistivity conditions.

The comparison performed in this study indicated a significant difference between homogeneous and inhomogeneous VCMs (**Table 3**). These results suggest that although it is possible to perform IPM using a homogeneous VCM, an inhomogeneous VCM provides more accurate results.

Limitations

Several inherent technical limitations may have led to the observed differences between IPM-identified ectopic focus and site of ablation defined on the EAM.

Although clinically more practical, the limited number of electrodes used in this study and the electrode positioning on the patient thorax may have affected the accuracy of focus localisation. In addition, movement of the ablation catheter may cause spatial displacement of the marked ablation site by ≈10 mm [16]. Furthermore, small and subtle catheter movements can also result in significant shifts within the EAM while using a reference catheter. All of these factors could have contributed to the differences in focus location between IPM and EAM.

Even if these conditions can be optimised, factors still remain that may cause discrepancies. These include image misregistration due to patient respiration, inaccurate cardiac geometry due to image acquisition during different phases of the cardiac cycle, and substantial regional variations in cardiac displacement during contraction and relaxation (ranging between 5 and 25 mm) [17,18]. In particular, the base of the heart moves ≥20 mm toward the apex. This is of particular importance because all ectopic foci were located at the basal part of the heart. Motion-related inaccuracies will probably have less influence on hearts with reduced function (less movement) or when analyzing foci from regions less susceptible to motion. A larger study will be needed to establish the impact of a screening approach prior to routine implementation.

Future directions

This proposed strategy combining IPM and MRI offers the prospect of studying electrical activation in relation to tissue characteristics for complex ventricular or supraventricular tachycardias and scar-based arrhythmias with clinically relevant accuracy.

The design of the computational model allows for instantaneous integration of patient-specific characteristics such as tissue properties and their associated conductivity. These tissue properties can be obtained easily using MRI. Integration of these characteristics will enable the operator to provide more patient-tailored therapy.

CONCLUSION

This study demonstrates the clinical applicability of an MRI-based whole-heart IPM method in patients with idiopathic ventricular foci. There was high localisation accuracy between the focus identified with IPM and the ablation site on the EAM. The interobserver agreement was high for both VCMs. IPM accuracy improved significantly when using an inhomogeneous VCM.

The integration of this IPM technique with EAM systems may facilitate patient-specific catheter-ablation strategies.

REFERENCES

1. Ramanathan C, Ghanem RN, Jia P, Ryu K, Rudy Y. Noninvasive electrocardiographic imaging for cardiac electrophysiology and arrhythmia. Nat Med. 2004;10:422–428.
2. Jamil-Copley S, Bokan R, Kojodjojo P, Qureshi N, Koa-Wing M, Hayat S, Kyriacou A, Sandler B, Sohaib A, Wright I, Davies DW, Whinnett Z, Peters S, Kanagaratnam P, Lim PB. Noninvasive electrocardiographic mapping to guide ablation of outflow tract ventricular arrhythmias. Heart Rhythm. 2014;11:587–594.
3. Erkapic D, Greiss H, Pajitnev D, Zaltsberg S, Deubner N, Berkowitsch A, Mollman S, Sperzel J, Rolf A, Schmitt J, Hamm C, Kuniss M, Neumann T. Clinical impact of a novel three-dimensional electrocardiographic imaging for non-invasive mapping of ventricular arrhythmias-a prospective randomized trial. Europace. 2015;17:591–597.
4. Roguin A. CardioPulse. Radiation in cardiology: can't live without it!: using appropriate shielding, keeping a distance as safely as possible and reducing radiation time are essential principles for radiation reduction. Eur Heart J. 2014;35:599–600.
5. van Dam PM, Tung R, Shivkumar K, Laks M. Quantitative localisation of premature ventricular contractions using myocardial activation ECGI from the standard 12-lead electrocardiogram. J Electrocardiol. 2013;46:574–579.
6. Cochet H, Dubois R, Sacher F, Derval N, Sermesant M, Hocini M, Montaudon M, Haissaguerre M, Laurent F, Jais P. Cardiac arrythmias: multimodal assessment integrating body surface ECG mapping into cardiac imaging. Radiology. 2014;271:239–247.
7. Revishvili AS, Wissner E, Lebedev DS, Lemes C, Deiss S, Metzner A, Kalinin VV, Sopov OV, Labartkava EZ, Kalinin AV, Chmelevsky M, Zubarev SV, Chaykovskaya MK, Tsiklauri MG, Kuck KH. Validation of the mapping accuracy of a novel non-invasive epicardial and endocardial electrophysiology system. Europace. 2015;17:1282–1288.
8. Bear LR, Cheng LK, LeGrice IJ, Sands GB, Lever NA, Paterson DJ, Smaill BH. The forward problem of electrocardiography: is it solved? Circ Arrhythm Electrophysiol. 2015;8:677–684.
9. Marchandise E, Geuzaine C, Remacle JF. Cardiovascular and lung mesh generation based on centerlines. Int J Numer Method Biomed Eng. 2013;29:665–682.
10. Oostendorp T, Nenonen J, Korhonen P. Noninvasive determination of the activation sequence of the heart: application to patients with previous myocardial infarctions. J Electrocardiol. 2002;35(suppl):75–80.
11. Sanchez-Quintana D, Cabrera JA, Farre J, Climent V, Anderson RH, Ho SY. Sinus node revisited in the era of electroanatomical mapping and catheter ablation. Heart. 2005;91:189–194.
12. Arisi G, Macchi E, Baruffi S, Spaggiari S, Taccardi B. Potential fields on the ventricular surface of the exposed dog heart during normal excitation. Circ Res. 1983;52:706–715.
13. Ramanathan C, Rudy Y. Electrocardiographic imaging: I. Effect of torso inhomogeneities on body surface electrocardiographic potentials. J Cardiovasc Electrophysiol. 2001;12:229–240.

14. Ramanathan C, Rudy Y. Electrocardiographic imaging: II. Effect of torso inhomogeneities on noninvasive reconstruction of epicardial potentials, electrograms, and isochrones. J Cardiovasc Electrophysiol. 2001;12:241–252.

15. van Oosterom A. A comparison of electrocardiographic imaging based on two source types. Europace. 2014;16(suppl 4):iv120–iv128.

16. Andreu D, Berruezo A, Fernandez-Armenta J, Herczku C, Borras R, Ortiz-Perez JT, Mont L, Brugada J. Displacement of the target ablation site and ventricles during premature ventricular contractions: relevance for radiofrequency catheter ablation. Heart Rhythm. 2012;9:1050–1057.

17. Zwanenburg JJM, Gotte MJW, Kuijer JPA, Hofman MBM, Knaapen P, Heethaar RM, van Rossum AC, Marcus JT. Regional timing of myocardial shortening is related to prestretch from atrial contraction: assessment by high temporal resolution MRI tagging in humans. Am J Physiol Heart Circ Physiol. 2005;288:H787–H794.

18. ter Keurs HE, Rijnsburger WH, van Heuningen R, Nagelsmit MJ. Tension development and sarcomere length in rat cardiac trabeculae. Evidence of length-dependent activation. Circ Res. 1980;46:703–714.

PART 4
TOWARDS AN INTEGRATED NON-INVASIVE ELECTRO-MECHANICAL APPROACH

11

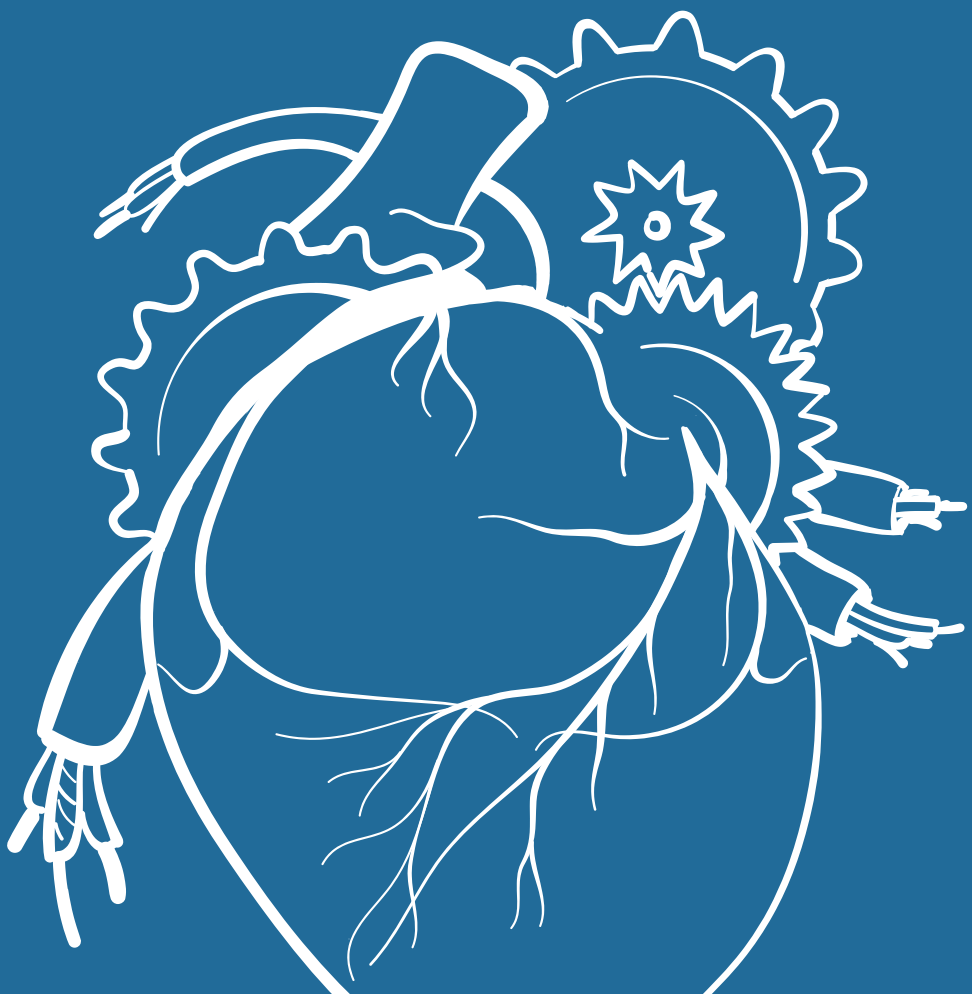

GENERAL DISCUSSION

This thesis focused on the development and subsequent in-vivo application of a novel non-invasive MRI-based inverse potential mapping (IPM) technique. The first part of the thesis discussed the safety and potential risks of using MRI in patients with cardiac pacing devices and investigated the clinical use of MRI in this patient category. In part two of this thesis, the development of a new non-invasive mapping methodology was described. Part three illustrated the initial results after application of the novel mapping technique in volunteers and patients.

In this fourth part, the main findings of the studies will be summarised and discussed. Furthermore, directions for future research will be suggested.

A novel non-invasive MRI-based inverse potential mapping technique

Non-invasive imaging of cardiac electrophysiology is an active field of research and has shown rapid development in recent years. More and more attention has drifted to increasing the amount of information that can be obtained in a non-invasive manner, with the patient at a minimal risk of suffering from adverse events. Non-invasive, detailed imaging of mechanical processes of the heart has been incorporated in clinical routine for years. On the contrary, the time-consuming nature of data acquisition and post-processing has historically hampered detailed non-invasive imaging of the electrical processes of the heart. Post-processing has been accelerated by increased computational power and sophisticated software. Despite these developments, acquisition of multi-electrode body surface potentials remains cumbersome. However, the development of dedicated electrode-vests or electrode-strips may accelerate the acquisition process.

Although several non-invasive mapping techniques have been developed through the years [1-5], a novel variant was developed by our research group, because 1) current techniques were still associated with exposure to radiation since Computed Tomography (CT) was used to obtain anatomical information, 2) a-priori models (consisting of assumptions with regard to physical circumstances) were required to reconstruct cardiac events, 3) surface potentials were reconstructed without having any information about the potential distribution between surfaces of interest, 4) the desire to perform real-life computer simulations that could be used to test various hypothesis concerning the impact of electrode positioning, the effect of inclusion or exclusion of thoracic organs on the end-result, and to investigate whether the sizes of the constituents of the 3D heart model would influence the outcome.

Clinical implications

Since patients with implanted pacemaker systems were the desired patient category, the first chapters of this thesis review and investigate the feasibility and safety of performing MRI in patients with an implanted cardiovascular implantable electronic device (CIED). **Chapter 2** demonstrated that MRI can be safely performed in this patient category with appropriate monitoring and strict adherence to a safety protocol. Besides MRI-conditional pacemaker systems, MRI-conditional internal cardioverter defibrillators (ICD) and biventricular pacing systems have been introduced [6]. Most of these devices have a specific MRI-mode that must be activated before entering the MRI suite. The most important features of this MRI-mode include bipolar stimulation instead of unipolar pacing, increased electrical output, specific filters to prevent sensing of external non-cardiac signals and temporarily disabling the recording of arrhythmic episodes [7].

Apart from MRI examinations in patients with an MRI-conditional CIED, an increasing amount of literature describes the safety of MRI in patients with conventional (i.e. non-MRI-conditional) devices. A landmark study on this topic has been performed by Nazarian et al. [8] demonstrating the safe performance of 555 MRI examinations in 438 patients with non-MRI-conditional devices. Only small changes in programming, sensing and impedance were reported in this study. In patients with conventional pacing devices or patients who are continuously pacing dependent, it must be ascertained that the expected benefits outweigh the potential risks of the examination. The most important MRI-related complications are heating of the tip of the pacing lead (and subsequent loss of capture), unwanted asynchronous pacing or inhibition of pacing, battery depletion or changes to the software of the device. These complications have been reported in technical ex-vivo studies or in case-reports and small observational studies, but have not been observed in humans in more recent studies [9].

In a single-center study, described in **Chapter 3**, the incidence and safety of MRI in patients with an MRI-conditional device was investigated. The majority of post-implant MRI scans (57%) were performed to confirm, exclude or follow-up on neurological disease. No MRI-related adverse events were reported during the follow-up period. It has been calculated that approximately 75% of all patients with an implanted CIED will need an MRI examination during the lifetime of their device [10]. Currently, implantation of an MRI-conditional system is not (yet) the standard of care for all patients. Therefore, identification of suitable patients is mandatory. Patients with a high probability of requiring an MRI scan in the near future are eligible for implantation of an MRI-conditional pacing device. Therefore, patients with neurological disorders constitute a group in which implantation of an MRI-conditional CIED should be strongly considered.

The mechanical function of the heart can be quantified using functional images that can be obtained by echocardiography or MRI. Earlier research demonstrated that global echocardiographic left and right ventricular function measures may be insensitive to early regional dysfunction, as can be observed in patients receiving long-term RV pacing [11]. Therefore, evaluation of myocardial contraction in relation to pacing using MRI may be advantageous. Local myocardial deformation including regional wall thickening can be quantified using a separate MRI sequence named 'myocardial tagging' [12]. A tagging sequence places non-invasive markers on the myocardium that can be traced during the cardiac cycle. In this way, local myocardial deformation can be quantified in three dimensions [13]. Unlike myocardial tagging, MRI-feature tracking does not require the acquisition of additional MRI images [14]. Instead, feature-tracking software can be retrospectively applied on routinely obtained functional MRI images [15]. To demonstrate a potential benefit of performing MRI in patients with implanted devices, **Chapter 4** illustrated the feasibility of performing strain analysis on conventional (non-tagged) MRI function images of patients with implanted MRI-conditional pacing devices.

Non-invasive mapping of cardiac excitation

Chapter 5 provided an overview of the history of body surface potential mapping (BSPM) and the use of mathematical inverse procedures. The use of inverse procedures has augmented the amount of information that can be distilled from the potentials recorded on the body surface. However, a solution to an inverse problem is never unique [16]. For this reason, various assumptions are made regarding the influence of signal noise, bones, thoracic organs, subcutaneous fat and muscle on the potentials recorded on the body surface [17]. The chosen assumptions and strength of the constraint that is imposed on the solution is subject of constant debate [18].

Despite multiple favourable reports and experiences, non-invasive mapping of cardiac excitation has not yet evolved into daily clinical practice. This is most likely due to the time consuming nature of BSPM and the complexity of - and heavy dependence on - the mathematics underlying the inverse procedures. Most experience is gained with reconstructing epicardial potentials. From a clinical perspective, the possibility of reconstructing endocardial potentials would be an important breakthrough. Although this possibility has been claimed [2], this method relies on yet another algorithm, deriving endocardial data from epicardial data. The robustness of this technique and this reproducibility of the data has yet to be determined.

In **Chapter 6**, the possibility of generating volume meshes and body volume potentials (BVP) was demonstrated. Instead of solely reconstructing surface potentials, the use of the Finite Element Method (FEM) allowed reconstructing of volume potentials. Use of the FEM never advanced into clinical practice due to its time consuming and elaborative nature. Increased computational power and the introduction of open source software enabled the calculation of BVP for clinical purposes. This chapter demonstrated that the potential field inside a simple rectangular tank filled with an electrolytic conductor could be visualised. A 3D volume model was reconstructed from MRI images of the rectangular tank. Later, the impact of variable organ conductivity on the reconstructed potentials was investigated using forward simulations in a human torso model. The FEM enables the incorporation of different anisotropies (directional dependence), local tissue characteristics and sigma gradients over different regions [19]. BVP may be used to gain a better insight in the genesis of body surface potentials (BSP) and sources of local inaccuracies.

Chapter 7 described the complete workflow using the developed software. The possibility of performing realistic simulations resulting in body surface potentials (forward procedure) and reconstructing cardiac activation sequences from body surface potentials (inverse procedure) was demonstrated. Investigating the optimal positioning of 62 torso electrodes, the ability to perform realistic simulations was subsequently used to experiment with various electrode positions. **Chapter 8** demonstrated that by concentrating the available electrodes (20 mm inter-electrode distance) in the area directly overlaying the heart, a high-resolution anterior view of the epicardial potentials can be obtained. In order to investigate whether this method could be used for the purpose of non-invasive focus localisation, it was applied in ten patients with implanted pacing devices. Ventricular paced beats were used to simulate ventricular ectopic foci. **Chapter 9** illustrated that for all patients, the site of earliest epicardial depolarisation could be identified. When the tip of the pacing lead was implanted in vicinity to the epicardium, i.e. right ventricular (RV) apex or RV outflow tract, the distance between lead tip position and epicardial breakthrough was 6.0±1.9 mm. In **Chapter 10**, the non-invasive mapping system was used to localise premature ventricular contractions in patients scheduled for ablation. The location of the identified focus was subsequently compared to the ablation site on the electroanatomic maps. The IPM-derived focus was 3-dimensionally located within 8.3±2.7 mm of the invasively determined focus using electroanatomic mapping.

DIRECTIONS FOR FUTURE RESEARCH

Application in patients with pacing devices

This thesis shows that a novel MRI-based inverse potential mapping strategy can be used to non-invasively study cardiac excitation and localise anterior sites of earliest epicardial breakthrough. In this thesis, ventricular paced beats were used to mimic ventricular ectopic foci. Besides focus localisation, the developed non-invasive mapping strategy can be used to investigate depolarisation and repolarisation during the complete cardiac cycle. When sequentially performed in patients with implanted pacing devices, this would allow detailed monitoring of long-term right or left ventricular pacing effects. Preferably, these observations would be combined with detailed regional function analyses performed using MRI. In this way, the electrical and mechanical effects of cardiac pacing could be studied simultaneously and sequentially.

Cardiac resynchronisation therapy

Cardiac resynchronisation therapy (CRT) is still associated with a 30% non- or adverse responders rate [20]. Monitoring and follow-up of electrical and mechanical activation times in CRT patients may increase the understanding of the pathophysiologic mechanisms in non- or adverse responders. In an attempt to improve the response rate to CRT, a more patient-specific implantation strategy has been advocated in recent literature. Proposed measures include the avoidance of regions of transmural scar and implantation of the left ventricular epicardial pacing lead at the site of latest electrical or mechanical activation [21-23]. Cardiac MRI is the current golden standard for the identification and quantification of regions of myocardial scar [24]. Currently, determination of the site of latest electrical activation would require an invasive EPS. This EPS would have to precede the implantation procedure. This would result in additional radiation exposure for the patient. Alternatively, the region of latest electrical activation could be identified using non-invasive IPM [25].

The software developed in this thesis enables the merging of the MRI data on tissue characteristics and mechanical activation with the data on electrical activation obtained using non-invasive IPM. In this way, the optimal site of lead implantation could be determined prior to the implantation procedure. This site could be visualised in a patient-specific 3D heart model that is available during the implantation procedure. Other research groups have demonstrated the feasibility of merging an earlier acquired 3D heart model with the fluoroscopic images used during implantation of a pacing device [26-27]. In this way, the implanting physician would navigate inside the high-resolution 3D heart model.

Leadless pacing

Historically, the fixation site of the pacing leads is restricted to areas that are easily accessible with conventional pacemaker leads. Recently, leadless pacemakers were introduced [28]. In theory, leadless pacing would increase the number of potential pacing sites, since implanters are no longer hampered by the mechanical constraints of the pacing leads. Regions of latest electrical or mechanical activation may be easier to reach. In this way the chance of response to therapy could be increased. However, current leadless pacing devices are too big to be navigated through coronary veins and leadless pacing is limited to the right ventricular apex. A recent study demonstrated that patients with one or multiple leadless pacing devices can safely undergo MRI scans in both 1.5 and 3 Tesla scanners [29]. MRI and IPM will provide a detailed roadmap to guide implantation of cardiac devices in order to optimise patient outcome.

Application in patients with arrhythmias

The technique may be used to localise accessory pathways or the origin of atrial or ventricular tachycardias [30-31]. Accessory pathways or arrhythmogenic sites can be isolated or terminated by local ablation. Currently, ablation is preceded by an invasive electrophysiological study (EPS). During the EPS, the anatomy of the patient's heart is reconstructed and local depolarisation and repolarizing times are registered using intra-cardiac catheters. In this way, an electro-anatomical map is constructed. This procedure is associated with significant exposure to radiation and exposes the patient to risks such as haemorrhage and stroke.

Using non-invasive IPM, a patient-specific electro-anatomical map can be constructed at an earlier instance. The electrophysiological mechanisms of certain arrhythmias may be studied before the ablation procedure. In this way, the actual invasive procedure can be prepared in detail beforehand and the total procedure time may be decreased [32]. This may reduce the risk of complications, increase patient-safety and contribute to a more patient-tailored therapy.

Methodological improvements

The current research was limited to mapping the anterior surface of the heart. Increasing the total number of electrodes and positioning the electrodes around the torso will enable mapping of the complete cardiac surface. This would allow the localisation of ectopic foci from the inferior and posterior wall. The torso electrodes used in this research were organised in an easy-to-apply patch. When the number of electrodes would be increased, a similar strategy is needed to prevent prolonged acquisition times.

It is anticipated that in the near future, patient-specific, 3D heart and thorax models will be used to guide invasive electrophysiological studies. To do so, these models must be as realistic as possible. Therefore, future research will focus on the incorporation of several variables that influence both electrical and mechanical processes in the heart. As mentioned earlier, the incorporation of local tissue characteristics (e.g. edema, scar, hypertrophy) is an important topic. A recently introduced cardiac MRI sequence named diffusion tensor imaging (DTI) enables the visualisation of intra-cardiac fiber orientation [33-34]. By incorporating this information, parameters on directional dependence can be further individualised in attempt to approach upmost realistic computer models.

REFERENCES

1. Rudy Y. Noninvasive electrocardiographic imaging of arrhythmogenic substrates in humans. Circ Res. 2013;112(5):863-74.
2. Revishvili AS, Wissner E, Lebedev DS, et al. Validation of the mapping accuracy of a novel non-invasive epicardial and endocardial electrophysiology system. Europace. 2015;17(8):1282-8.
3. van Dam PM, Gordon JP, Laks MM, et al. Development of new anatomy reconstruction software to localize cardiac isochrones to the cardiac surface from the 12 lead ECG. J Electrocardiol. 2015;48(6):959-65.
4. Zhou Z, Han C, Yang T, et al. Noninvasive imaging of 3-dimensional myocardial infarction from the inverse solution of equivalent current density in pathological hearts. IEEE Trans Biomed Eng. 2015;62(2):468-76.
5. van Dam PM, Oostendorp TF, Linnenbank AC, et al. Non-invasive imaging of cardiac activation and recovery. Ann Biomed Eng. 2009;37(9):1739-56.
6. Nordbeck P, Ertl G, Ritter O. Magnetic resonance imaging safety in pacemaker and implantable cardioverter defibrillator patients: how far have we come? Eur Heart J. 2015;36(24):1505-11.
7. Klein-Wiele O, Garmer M, Urbien R, et al. Feasibility and safety of adenosine cardiovascular magnetic resonance in patients with MR conditional pacemaker systems at 1.5 Tesla. J Cardiovasc Magn Reson. 2015;17:112.
8. Nazarian S, Hansford R, Roguin A, et al. A prospective evaluation of a protocol for magnetic resonance imaging of patients with implanted cardiac devices. Ann Intern Med. 2011;155(7):415-24.
9. Ipek EG, Nazarian S. Safety of implanted cardiac devices in an MRI environment. Curr Cardiol Rep. 2015;17(7):605.
10. Kalin R, Stanton MS. Current clinical issues for MRI scanning of pacemaker and defibrillator patients. Pacing Clin Electrophysiol. 2005;28(4):326-8.
11. Ibrahim el-SH. Myocardial tagging by cardiovascular magnetic resonance: evolution of techniques--pulse sequences, analysis algorithms, and applications. J Cardiovasc Magn Reson. 2011;13:36-42.
12. Lorca MC, Haraldsson H, Ordovas KG. Ventricular mechanics: techniques and applications. Magn Reson Imaging Clin N Am. 2015;23(1):7-13.
13. Götte MJ, Germans T, Rüssel IK, et al. Myocardial strain and torsion quantified by cardiovascular magnetic resonance tissue tagging: studies in normal and impaired left ventricular function. J Am Coll Cardiol. 2006;48(10):2002-11.
14. Khan JN, Singh A, Nazir SA, et al. Comparison of cardiovascular magnetic resonance feature tracking and tagging for the assessment of left ventricular systolic strain in acute myocardial infarction. Eur J Radiol. 2015;84(5):840-8.

15. Schuster A, Hor KN, Kowallick JT, et al. Cardiovascular Magnetic Resonance Myocardial Feature Tracking: Concepts and Clinical Applications. Circ Cardiovasc Imaging. 2016;9(4). pii: e004077.

16. van Oosterom A. The inverse problem of bioelectricity: an evaluation. Med Biol Eng Comput. 2012;50(9):891-902.

17. Gulrajani RM. Models of the electrical activity of the heart and computer simulation of the electrocardiogram. Crit Rev Biomed Eng. 1988;16(1):1-66.

18. Milanič M, Jazbinšek V, Macleod RS, et al. Assessment of regularisation techniques for electrocardiographic imaging. J Electrocardiol. 2014;47(1):20-8.

19. Caiani EG, Colombo A, Pepi M, et al. Three-dimensional left ventricular segmentation from magnetic resonance imaging for patient-specific modelling purposes. Europace. 2014;16 Suppl 4:iv96-iv101.

20. Coppola G, Ciaramitaro G, Stabile G, et al. Magnitude of QRS duration reduction after biventricular pacing identifies responders to cardiac resynchronisation therapy. Int J Cardiol. 2016;221:450-455.

21. Taylor RJ, Umar F, Panting JR, et al. Left ventricular lead position, mechanical activation, and myocardial scar in relation to left ventricular reverse remodeling and clinical outcomes after cardiac resynchronisation therapy: A feature-tracking and contrast-enhanced cardiovascular magnetic resonance study. Heart Rhythm. 2016;13(2):481-9.

22. Daoulah A, Alsheikh-Ali AA, Al-Faifi SM, et al. Cardiac resynchronisation therapy in patients with postero-lateral scar by cardiac magnetic resonance: A systematic review and meta-analysis. J Electrocardiol. 2015;48(5):783-90.

23. Leyva F. Cardiac resynchronisation therapy guided by cardiovascular magnetic resonance. J Cardiovasc Magn Reson. 2010;9;12:64.

24. Abbasi SA, Ertel A, Shah RV, et al. Impact of cardiovascular magnetic resonance on management and clinical decision-making in heart failure patients. J Cardiovasc Magn Reson. 2013;15:89.

25. Dawoud F, Spragg DD, Berger RD, et al. Non-invasive electromechanical activation imaging as a tool to study left ventricular dyssynchronous patients: Implication for CRT therapy. J Electrocardiol. 2016;49(3):375-82.

26. Shetty AK, Duckett SG, Ginks MR, et al. Cardiac magnetic resonance-derived anatomy, scar, and dyssynchrony fused with fluoroscopy to guide LV lead placement in cardiac resynchronisation therapy: a comparison with acute haemodynamic measures and echocardiographic reverse remodelling. Eur Heart J Cardiovasc Imaging. 2013;14(7):692-9.

27. Laksman Z, Yee R, Stirrat J, et al. Model-based navigation of left and right ventricular leads to optimal targets for cardiac resynchronisation therapy: a single-center feasibility study. Circ Arrhythm Electrophysiol. 2014;7(6):1040-7.

28. Rutzen-Lopez H, Silva J, Helm RH. Leadless Cardiac Devices-Pacemakers and Implantable Cardioverter-Defibrillators. Curr Treat Options Cardiovasc Med. 2016;18(8):49.

29. Soejima K, Edmonson J, Ellingson ML, et al. Safety evaluation of a leadless transcatheter pacemaker for magnetic resonance imaging use. Heart Rhythm. 2016. pii: S1547-5271(16)30493-3.

30. Dubois R, Shah AJ, Hocini M, et al. Non-invasive cardiac mapping in clinical practice: Application to the ablation of cardiac arrhythmias. J Electrocardiol. 2015;48(6):966-74.

31. Zhang J, Cooper DH, Desouza KA, et al. Electrophysiologic Scar Substrate in Relation to VT: Noninvasive High-resolution Mapping and Risk Assessment with ECGI. Pacing Clin Electrophysiol. 2016;39(8):781-91.

32. Aryana A, O'Neill PG, d'Avila A. Noninvasive Electrocardiographic Mapping: Are We Ready for Prime Time? J Am Heart Assoc. 2015;4(10):e002655.

33. McGill LA, Ferreira PF, Scott AD, et al. Relationship between cardiac diffusion tensor imaging parameters and anthropometrics in healthy volunteers. J Cardiovasc Magn Reson. 2016;6;18:2.

34. Prakosa A, Malamas P, Zhang S, et al. Methodology for image-based reconstruction of ventricular geometry for patient-specific modeling of cardiac electrophysiology. Prog Biophys Mol Biol. 2014;115(2-3):226-34.

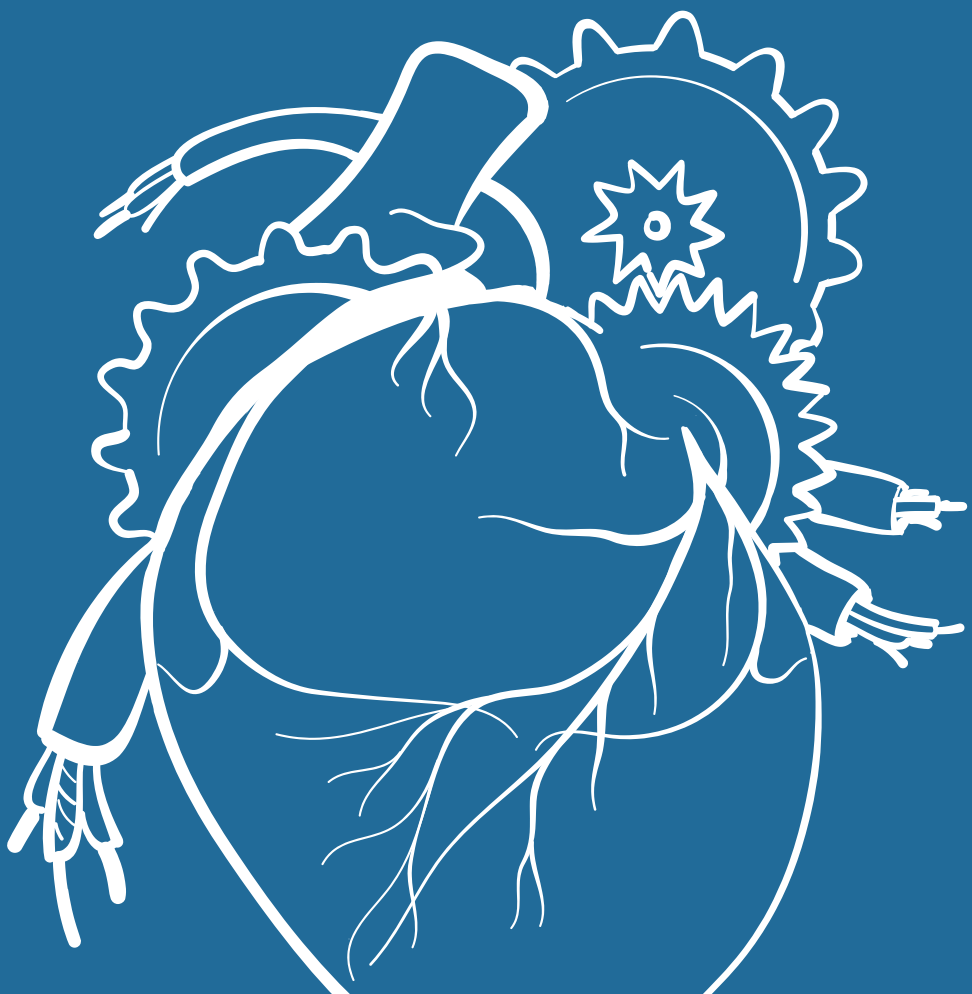

APPENDICES

SUMMARY

Non-invasive imaging of cardiac excitation uses body surface potential mapping (BSPM), non-invasive anatomical imaging and mathematical equations to reconstruct electrophysiological (intra-) cardiac processes. Despite multiple favourable reports, non-invasive imaging of cardiac excitation has not yet evolved into daily clinical practice. This is most likely due to the time consuming nature of BSPM and the complexity of - and heavy dependence on - the mathematics underlying the inverse procedures. It is anticipated that in the near future, patient-specific, 3D heart and thorax models will be used to guide invasive electrophysiological studies. To do so, these models must be as realistic as possible. In the work described in this thesis, a novel non-invasive mapping technique was developed and applied in humans.

The outline of this thesis is provided in **Chapter 1**. In summary, the aims of this thesis were to 1) investigate the safety of using MRI in patients with implanted pacing devices, 2) develop software through which the electrical activity inside the heart and thorax can be realistically modelled, 3) perform simulation studies to investigate the impact on the end-result of using different torso electrode layouts for the recording of body surface potentials, 4) investigate the validity of the simulation studies by performing non-invasive mapping in volunteers using different torso electrode layouts, 5) apply the novel non-invasive mapping technique in patients with an implanted pacing devices and in patients suffering from premature ventricular contractions and 6) investigate the localisation accuracy and reproducibility of the results in these patients.

In the first part of this thesis, the feasibility and safety of using MRI in patients with an implanted cardiovascular implantable electronic device (CIED) was investigated. **Chapter 2** discussed the safety concerns associated with performing MRI in patients with an implanted CIED. An in-house developed safety protocol was proposed to minimise the chance of adverse events. **Chapter 3** evaluated the use of MRI in patients after implantation of an MRI-conditional CIED. In this study, the majority of MRI scans after implantation of a CIED were performed to either follow-up on or investigate neurological disorders. Currently, not all implanted devices are MRI-conditional. Therefore, patients with neurological disorders constitute a group in which implantation of an MRI-conditional CIED should be strongly considered. **Chapter 4** illustrated the feasibility of using MRI-feature tracking in patients with an MRI-conditional CIED to evaluate regional wall motion. Normally, global cardiac function is monitored using transthoracic echocardiography (TTE) in this patient category. However, these global function measures are insensitive to early regional dysfunction. Therefore, it may be of advantage to use MRI in these patients. MRI-feature tracking is a relatively new tool

that can be applied retrospectively on regular functional MRI images. Hence, it does not require the acquisition of additional MRI sequences. In this study, adequate endocardial and epicardial delineation was possible, despite the presence of susceptibility artefacts induced by the CIEDs.

The second part of this thesis discussed the current status of non-invasive imaging of cardiac excitation. **Chapter 5** provided an overview of this active field of research. An inverse procedure uses Body Surface Potential Mapping (BSPM), non-invasive anatomical imaging and mathematical equations to reconstruct electrophysiological (intra-)cardiac excitation. Despite multiple favourable reports and experiences, non-invasive mapping of cardiac excitation has not yet evolved into daily clinical practice. A novel non-invasive mapping technique was developed by our research group, because 1) current techniques were still associated with exposure to radiation since Computed Tomography (CT) was used to obtain anatomical information, 2) a-priori models (consisting of assumptions with regard to physical circumstances) were used to reconstruct intra-cardiac events, 3) surface potentials were reconstructed without having any information about the potential distribution between surfaces of interest, 4) the desire to perform real-life computer simulations that could be used to test various hypothesis concerning the impact of electrode positioning, the effect of inclusion or exclusion of thoracic organs on the end-result and to investigate whether the sizes of the constituents of the 3D heart model would influence the outcome.

Chapter 6 described the first experiments using in-house developed software for the generation of realistic 3D volume models and calculation of volume potentials. The advantage of using the Finite Element Method instead of the Boundary Element Method is illustrated by experiments performed in a plastic tank filled with water. Volume potentials inside a simple rectangular tank filled with an electrolytic conductor were visualised. Volume potentials may be used to gain a better insight in the genesis of body surface potentials and sources of local inaccuracies. The impact of including or excluding organ conductivity parameters on the reconstructed potentials was investigated using forward simulations in a human torso model. **Chapter 7** described the complete workflow using the developed non-invasive mapping software. The impact of including or excluding information on myocardial scar or oedema was investigated.

The third part of this thesis describes the application of the novel non-invasive mapping technique in volunteers and patients. In **Chapter 8**, the possibility of performing realistic simulations resulting in body surface potentials (forward procedure) and reconstructing cardiac activation sequences from body surface potentials (inverse procedure) was demonstrated. Epicardial potentials were calculated using different torso electrode

layouts. After deciding on a definitive electrode layout, it was applied in volunteers and later in patients to record potentials from the body surface. By positioning the available electrodes at a 20 mm inter-electrode distance in the area directly overlaying the heart, a high-resolution anterior view of the epicardial potentials could be obtained. The localisation accuracy of the novel mapping technique was investigated in **Chapter 9**. In ten patients with implanted pacing devices, ventricular paced beats were used to simulate ventricular ectopic foci. The site of earliest activation as identified by the non-invasive mapping system was correlated to the actual location of the tip of the pacing lead on the MRI-images. When the tip of the pacing lead was implanted in vicinity to the epicardium, i.e. right ventricular (RV) apex or RV outflow tract, the distance between lead tip position and epicardial breakthrough was 6.0±1.9 mm. In **Chapter 10**, the non-invasive mapping system was used to localise premature ventricular contractions in patients scheduled for ablation. The IPM-derived focus was 3-dimensionally located within 8.3±2.7 mm of the invasively determined focus using electroanatomic mapping. In **Chapter 11**, the clinical relevance of this thesis was discussed and directions for further research were suggested.

SAMENVATTING

Het op een niet-invasieve manier verkrijgen van zoveel mogelijk informatie over fysiologische processen in het menselijk lichaam heeft de laatste jaren een vlucht genomen. Steeds meer wordt geprobeerd om de patiënt op die manier te behoeden voor risico's die een invasieve methode (waarbij het lichaam wordt binnengedrongen) met zich meebrengt.

Om lokale, elektrische activiteit van het hart nauwkeurig te registreren is het noodzakelijk over te gaan tot een invasief elektrofysiologisch onderzoek. Dit proefschrift beschrijft de totstandkoming van een nieuwe methode die het mogelijk maakt om de elektrische activiteit van het hart op een niet-invasieve manier te onderzoeken. Het ontwikkelen van een dergelijke nieuwe techniek gebeurt met de overtuiging dat invasieve cardiologische procedures steeds meer gestuurd zullen worden door informatie die van tevoren op een niet-invasieve manier is verkregen.

De indeling van dit proefschrift wordt beschreven in **Hoofdstuk 1**. Samenvattend waren de onderzoeksdoelen 1) te onderzoeken in hoeverre Magnetic Resonance Imaging (MRI) veilig kan worden gebruikt bij patiënten met een geïmplanteerde pacemaker of implanteerbare cardioverter defibrillator (ICD), 2) het ontwikkelen van software waarmee de elektrische activiteit in het hart en in de borstkas kan worden nagebootst met behulp van op de borstkas gemeten potentialen, 3) het uitvoeren van simulaties waarbij gevarieerd wordt met het aantal en de plaatsing van de huidelektrodes, 4) het onderzoeken van de validiteit van de simulaties door verschillende elektrodeconfiguraties bij mensen toe te passen en de resultaten van de computer simulaties en de registraties in mensen met elkaar te vergelijken, 5) de nieuw ontwikkelde methode toepassen bij patiënten met geïmplanteerde pacemakers en bij patiënten met ventriculaire extrasystolen, 6) de nauwkeurigheid van de nieuw ontwikkelde methode te testen in deze groepen patiënten.

Het eerste deel van dit proefschrift gaat over het gebruiken van MRI bij patiënten met een geïmplanteerde pacemaker of ICD. Tot niet lang geleden was het maken een MRI-scan bij een patiënt met een geïmplanteerd pacing systeem ondenkbaar. **Hoofdstuk 2** geeft een overzicht van de literatuur met betrekking tot gevaren en mogelijke complicaties die kunnen optreden wanneer een MRI-scan wordt gemaakt bij een patiënt met een pacemaker of ICD. Het gaat hierbij over zowel de nieuwere MRI-conditionele systemen (waarbij MRI veilig gebruikt kan worden mits aan strikte voorwaarden wordt voldaan) als over conventionele systemen (waarvan eigenlijk onduidelijk is in hoeverre MRI veilig kan worden gebruikt). Verder wordt een door ons ontwikkeld

veiligheidsprotocol geïntroduceerd. Door het volgen van dit veiligheidsprotocol kan de kans op complicaties worden geminimaliseerd. Nu er sinds enkele jaren MRI-conditionele systemen worden geïmplanteerd, rijst de vraag hoeveel mensen er profijt van hebben gehad, met andere woorden: werden er bij deze mensen ook MRI-scans gemaakt? En zijn er bepaald groepen patiënten te identificeren waarbij de kans groot is dat zij in de jaren na implantatie een MRI-scan nodig hebben? Momenteel is het namelijk zo dat niet bij iedereen een MRI-conditioneel systeem kan worden geïmplanteerd. Dit werd nader onderzocht in **Hoofdstuk 3**. In ons eigen centrum werd de meerderheid van MRI-scans na implantatie van een pacemaker of ICD verricht in patiënten met een (vermoedelijke) neurologische aandoening. In deze patiëntengroep zou implantatie van een MRI-conditioneel systeem dus zeker te overwegen zijn. **Hoofdstuk 4** toont de mogelijkheid om regionale wandbewegingen te analyseren middels MRI-feature tracking in patiënten met een geïmplanteerde pacemaker of ICD. MRI-feature tracking is een nieuwe techniek waarbij gebruik kan worden gemaakt van standaard MRI functie opnames. Omdat er geen aanvullende opnames nodig zijn, is er geen extra belasting voor de patiënt terwijl er in potentie wel meer informatie uit de beelden kan worden gehaald. In het verleden is gebleken dat echocardiografie onvoldoende in staat is om vroege, regionale wandbewegingsstoornissen, zoals gezien kan worden bij patiënten die langdurig met pacing worden behandeld, te detecteren. Dit zou met MRI-feature tracking wel mogelijk kunnen zijn.

Het tweede deel van dit proefschrift gaat over het ontwikkelen van een nieuwe methode die het mogelijk maakt om de elektrische activiteit in het hart op een niet-invasieve manier te onderzoeken. **Hoofdstuk 5** geeft een literatuuroverzicht. Het maken van uitgebreide elektrocardiogrammen (body surface potential maps) is al oud, maar door deze informatie te combineren met anatomische informatie kan vervolgens door middel van wiskundige differentiaalvergelijkingen meer informatie uit de BSPM signalen worden gedestilleerd. Op deze manier kan informatie die buiten op het lichaam wordt gemeten worden gebruikt om te onderzoeken wat er binnenin het hart gebeurt. In **Hoofdstuk 6** worden de eerste experimenten met de nieuwe software beschreven. Een van de voordelen van de nieuwe software is dat er volume potentialen in plaats van oppervlakte potentialen kunnen worden berekend. Op deze manier kan inzichtelijk worden gemaakt wat zich in een volume afspeelt. Dit wordt geïllustreerd aan de hand van simulaties en experimenten met een blauwe plastic bak gevuld met een zoutwater oplossing. **Hoofdstuk 7** beschrijft vervolgens alle stappen die nodig zijn om van lichaamspotentialen die bij een patiënt gemeten zijn te komen tot een patiënt-specifiek 3-dimensionaal hart model. Tevens wordt er in dit hoofdstuk geëxperimenteerd met het includeren of excluderen van littekenweefsel of oedeem in de hartspier. In **Hoofdstuk 8** wordt geëxperimenteerd met verschillende aantallen

huidelektrodes. Hierbij worden de beschikbare elektrodes ook verschillend verdeeld over het huidoppervlak. Deze experimenten werden eerst met de nieuw ontworpen software uitgevoerd. Nadat er enkele optimale elektrode-configuraties waren gevonden werden deze vervolgens toegepast bij gezonde vrijwilligers. In **Hoofdstuk 9** wordt de nieuwe techniek toegepast bij patiënten met een geïmplanteerde pacemaker. De plek van eerste activatie wordt niet-invasief gelokaliseerd met de nieuw ontworpen software. Vervolgens werd de locatie van eerste activatie vergeleken met de plek waar de ventriculaire pacemakerdraad geïmplanteerd is. Toe nu toe kan alleen epicardiale activatie worden waargenomen. In dit hoofdstuk wordt geïllustreerd dat epicardiale bronnen met een nauwkeurigheid van 6.0±1.9mm kunnen worden gelokaliseerd. In **Hoofdstuk 10** wordt de techniek toegepast bij patienten met ventriculaire extrasystolen die later een ablatieprocedure zouden ondergaan. Voorafgaande aan de ablatie werd het arritmogene focus gelokaliseerd met behulp van het niet-invasieve mapping systeem. Na vergelijken van de locatie van het gevonden focus met de locatie van het ableerde focus werd een gemiddelde afstand van 8.3±2.7 mm gevonden. **Hoofdstuk 11** vat de belangrijkste bevindingen van dit proefschrift samen en plaatst deze in het daglicht van de hedendaagse literatuur. Ook worden er voorstellen gedaan voor verder onderzoek.

LIST OF PUBLICATIONS

Bhagirath P, **van der Graaf AW**, de Hooge J, de Groot NM, Götte MJ. Integrated whole-heart computational workflow for inverse potential mapping and personalised simulations. *J Transl Med.* 2016;14:1-7.

van der Graaf AW, Bhagirath P, Scheffer MG, Robles de Medina R, Götte MJ. MR-feature tracking in patients with implanted MRI-conditional pacing systems: The impact of pacing. *J Magn Reson Imaging.* 2016;44(4):964-71.

van der Graaf AW, Bhagirath P, de Hooge J, Rammana H, van Driel VJ, de Groot NM, Götte MJ. Non-invasive focus localisation, right ventricular epicardial potential mapping in patients with an MRI-conditional pacemaker system - a pilot study. *J Interv Card Electrophysiol.* 2015;44(3):227-234.

Bhagirath P, **van der Graaf AW**, van Dongen E, de Hooge J, van Driel VJ, Ramanna H, de Groot NM, Götte MJ. Feasibility and accuracy of cardiac magnetic resonance imaging-based whole-heart inverse potential mapping of sinus rhythm and idiopathic ventricular foci. *J Am Heart Assoc.* 2015; 14;4(10):e002222.

van der Graaf AW, Bhagirath P, de Hooge J, de Groot NM, Götte MJ. A priori model independent inverse potential mapping: the impact of electrode positioning. *Clin Res Cardiol.* 2016;105(1):79-88.

van der Graaf AW, Bhagirath P, van Driel VJ, Ramanna H, de Hooge J, de Groot NM, Götte MJ. Computing volume potentials for noninvasive imaging of cardiac excitation. *Ann Noninvasive Electrocardiol.* 2015;20(2):132-9.

Bhagirath P, **van der Graaf AW**, Karim R, Rhode K, Piorkowski C, Razavi R, Schwitter J, Götte MJ. Interventional cardiac magnetic resonance imaging in electrophysiology: advances toward clinical translation. *Circ Arrhythm Electrophysiol.* 2015;8(1):203-11.

van der Graaf AW, Bhagirath P, S Ghoerbien, Götte MJ. Cardiac magnetic resonance imaging; artefacts for clinicians. *Neth Heart J.* 2014;22(12):542-549.

Bhagirath P, **van der Graaf AW**, Karim R, van Driel VJ, Ramanna H, Rhode KS, de Groot NM, Götte MJ. Multimodality imaging for patient evaluation and guidance of catheter ablation for atrial fibrillation - Current status and future perspective. *Int J Cardiol.* 2014;20;175(3):400-408.

van der Graaf AW, Bhagirath P, Götte MJ. MRI and cardiac implantable electronic devices; current status and required safety conditions. *Neth Heart J.* 2014;22(6):269-76.

van der Graaf AW, Bhagirath P, Ramanna H, van Driel VJ, de Hooge J, de Groot NM, Götte MJ. Noninvasive imaging of cardiac excitation: current status and future perspective. *Ann Noninvasive Electrocardiol.* 2014;19(2):105-13.

Aziz NA, Pijl H, Frölich M, **van der Graaf AW**, Roelfsema F, Roos RA. Increased hypothalamic-pituitary-adrenal axis activity in Huntington's disease. *J Clin Endocrinol Metab.* 2009; 94 (4):1223-8.

Ahmad Aziz N, Pijl H, Frölich M, **van der Graaf AW**, Roelfsema F, Roos RAC. Leptin secretion rate increases with higher CAG repeat number in Huntington's disease patients. *Clin Endocrinol (Oxf).* 2010; 73 (2):206-11.

PHD PORTFOLIO

PhD portfolio - summary of PhD training and teaching activities

Name PhD student:	Abraham Willem Maurits van der Graaf
Erasmus MC department:	Cardiology, Department of Translational Electrophysiology
Research school:	Cardiovascular Research School (COEUR), Erasmus MC
PhD period:	July 2011 – July 2015
Promotor:	prof. dr. F. Zijlstra
Copromotoren:	dr. N.M.S. de Groot, dr. M.J.W. Götte

Education and degrees:

2011-2015 PhD Translational Electrophysiology, COEUR, Erasmus Medical Center, Rotterdam, The Netherlands & Haga Teaching Hospital, The Hague, The Netherlands
2004-2011 Doctorate in Medicine, Leiden University Medical Center, Leiden, The Netherlands

Extra-curricular activities:

Clinical Business Administration, TIAS school for Business and Society, The Netherlands
Co-founder of WikiCMR, online educational platform on cardiac MRI for residents.
Co-director CMR dagen, on-site cardiac MRI training for residents

PhD training

2011	**ECTS**
Haga Wetenschapsdag	1
2012	
Netherlands Society of Cardiology Congress (NVVC)	2
EuroCMR Vienna	3
European Society of Cardiology Congress (ESC)	5
Netherlands Heart Rhythm Association	2
Pacemaker course, Brummen	2
American Heart Association Congress	5
Netherlands Society of Cardiology Congress (NVVC)	2
Cardiac MRI course VUMC	3
Cardiac MRI Symposium, The Hague	1
PhD course Papendal 'Vascular Biology'	2
Haga Wetenschapsdag	1

2013	
Society of Cardiovascular MRI Congress	5
Netherlands Society of Cardiology Congress (NVVC)	2
Biotronik Electrophysiology course	2
EuroCMR Florence	3
Netherlands Heart Rhythm Association	2
Netherlands Society of Cardiology Congress (NVVC)	2
Biotronik Electrophysiology course	1
Cardiac MRI Symposium, The Hague	1
Haga Wetenschapsdag	1
2014	
Netherlands Society of Cardiology Congress (NVVC)	2
Society of Cardiovascular MRI Congress	5
Coeur Erasmus MC Symposium	2
Netherlands Society of Cardiology Congress (NVVC)	2
Haga Wetenschapsdag	1
Total	**60**

Oral presentations

- 2017 CMR dagen, level 1 CMR course for residents, Amsterdam, The Netherlands
- 2015 Netherlands Society of Cardiology Congress (NVVC), Noordwijkerhout. NL
- 2014 Coeur Erasmus MC Symposium, Rotterdam, The Netherlands
- 2014 Cardiac MRI Symposium, The Hague, The Netherlands
- 2014 Society of Cardiovascular MRI Congress, New Orleans, USA
- 2014 Netherlands Society of Cardiology Congress (NVVC) Arnhem, The Netherlands
- 2014 Medtronic Evera MRI-ICD launch event, Eindhoven, The Netherlands
- 2013 Cardiac MRI Symposium, The Hague, The Netherlands
- 2013 Society of Cardiovascular MRI Congress, San Fransisco, USA
- 2012 Haga Teaching Hospital Wetenschapsdag, The Hague, The Netherlands
- 2012 American Heart Association Congress, Los Angeles, USA
- 2012 Netherlands Society of Cardiology Congress (NVVC) Arnhem, The Netherlands
- 2012 Pacemaker Course, Brummen, The Netherlands
- 2012 Netherlands Heart Rhythm Association, Ermelo, The Netherlands
- 2012 European Society of Cardiology Congress, München, Germany
- 2012 Netherlands Society of Cardiology Congress (NVVC), Noordwijkerhout, NL

Poster presentations

- 2012 Haga Teaching Hospital Wetenschapsdag, The Hague, The Netherlands
- 2011 Haga Teaching Hospital Wetenschapsdag, The Hague, The Netherlands

ABOUT THE AUTHOR

Abraham Willem Maurits van der Graaf was born on January 15th 1986 in Voorburg, The Netherlands. He finished secondary school at the Stedelijk Lyceum Schubertrode in Zoetermeer. In 2004, he started medical school at the Leiden University Medical Center (LUMC) in Leiden. In 2007, he completed an elective surgery internship at the Dhulikhel Hospital in Nepal. In 2008, he spent five months in Ethiopia and participated in a clinical research team from the University of Addis Ababa concentrating on lymphatic filariasis (professor A. Hailu, professor A.M. Poldermans). In 2009, he travelled through South-America. In 2010, he completed an internship gynaecology at the Diaconessenhuis in Paramaribo, Suriname (dr. M. Sietaram). His interest in cardiology increased during his internship pediatrics in Gouda, where he was introduced to the world of echocardiography in newborns by dr. J.S. Starreveld. He received his medical degree in 2011. He started working on the research described in this thesis in a collaboration between the department of cardiology of the Haga Teaching Hospital (dr. M.J.W. Götte) and the department of translational electrophysiology of the Erasmus Medical Center (dr. N.M.S. de Groot). In July 2017, he completed his residency in internal medicine (dr. E.F.M. Posthuma, dr. H. Boom) at the Reinier de Graaf Gasthuis in Delft. He will continue his cardiology training at the VU medical center in Amsterdam (dr. G. Veen, dr. R.B. van Loon). His hobbies are playing guitar and cycling. He lives happily together with Emily in The Hague.

DANKWOORD

Door de toch wat gekke en overcomplete mix van kliniek, fysica, ICT, MRI, pacemakers, elektrofysiologie, programmeren, wiskunde en handvaardigheid zijn er nogal wat mensen die hebben bijgedragen aan de totstandkoming van dit proefschrift. Ik wil dan ook iedereen bedanken die mij op wat voor manier dan ook heeft geholpen gedurende de vier jaren in het HagaZiekenhuis en het Erasmus MC. Enkele mensen wil ik in het bijzonder even noemen.

Mijn promotor, professor Felix Zijlstra, zeer veel dank voor de gelegenheid bij u te promoveren. Graag dank ik prof. dr. A.C. van Rossum, prof. dr. H.J.G.M. Crijns en dr. R.P.J. Budde voor het lezen en beoordelen van mijn proefschrift.

Mijn copromotor Natasja de Groot, je hebt mij erg geholpen bij het schrijven van artikelen en bij het afronden van dit proefschrift. Na een avondje schrijven in het Reinier de Graaf Ziekenhuis in Delft stuurde ik je de laatste versie van de tekst. Wanneer ik, na een fietsrit van ongeveer 30 minuten, in Den Haag thuiskwam had ik vaak al jouw commentaar in mijn inbox. Enorm inspirerend!

Alle cardiologen, arts-assistenten en verpleegkundigen in het HagaZiekenhuis bedankt voor jullie medewerking en steun.

Alle MRI laboranten en pacemakertechnici in het HagaZiekenhuis enorm bedankt. Het moet vermoeiend voor jullie zijn geweest met twee van die jonge honden in je nek waarvoor het nooit goed genoeg was.

Jacques, voor Pranav en mij was jij een reddende engel. Wij kwamen met jou in contact op een moment dat wij het echt niet meer wisten. De samenwerking met jou was bijzonder. Enorm bedankt voor je geduld.

Mijn andere copromotor Marco Götte, what a ride…. Ik herinner mij goed dat jij mij benaderde voor het onderzoek. Iets over de jungle, met een kapmes en niet weten waar je uitkomt. Zo voelde het soms zeker. Ik heb veel van je geleerd. Door jou zal ik nooit meer rustig naar een niet strak uitgelijnde presentatie kunnen kijken.

Suresh, onze MRI goeroe en goede vriend. In Delft hebben wij enkele avonden, nachten en weekenden met jou gescand. Je hebt zelfs mij een keer gescand. Ik zal nooit weten of, toen ik vastgebonden in de scanner lag met een koptelefoon op, het programmeren

van de sequentie nou echt zo lang duurde of dat jullie toch gewoon buiten zijn gaan roken. Wij waren als kinderen zo blij toen jij naar het Haga kwam. Ik hoop in de toekomst nog veel met je te mogen werken.

Pranav, behalve een boekje en een titel houd ik aan deze promotietijd een vriend voor het leven over. Daarvoor ben ik zeer dankbaar. In het begin was het soms moeilijk en botsten wij geregeld. Hoewel soms moeilijk, denk ik dat dit er mede voor gezorgd heeft dat onze band nu zo diep is. Wij hebben in vier jaar tijd zo ongelofelijk veel meegemaakt. Van jou heb ik geleerd wat echt doorzetten is. Maar wat is nu precies het verschil tussen stroom en spanning?

Lieve mama, ik mis je nog iedere dag. Het zou zo heerlijk zijn om je nog één keer bij ons te hebben….

Lieve papa, bedankt dat je er altijd voor mij bent. Een luisterend oor, iemand om mee te sparren als ik het even niet meer weet of om mij 's nachts op te halen als ik met een lekke band in de polder sta…. Mooi om te zien hoe je de draad hebt opgepakt na het overlijden van mama en nu volop geniet van jouw leven, als opa van Flynn en Zoë, als onze vader en als molenaar!

Lieve Guisou, wat een leuk gezin heb jij samen met Jorn. Ik ben ongelofelijk trots op jou en de ontwikkeling die jij hebt doorgemaakt.

Lieve Leon en Marion, bedankt voor jullie interesse, aanmoediging en het welkome gevoel. En bedankt dat jullie zo'n leuke dochter hebben!

Lieve Emily, love of my life, dank voor al je steun, kritiek en aanmoediging. Wat een heerlijk leven hebben wij samen! Ik verheug mij op de rest!

Financial support for the publication of this thesis was provided by: Biosemi, Biotronik, Chipsoft, Guerbet, Haga Teaching Hospital, Servier and Stichting Cardiovascular.